Degradation of Epoxy Composite Coating Using Corrosion and Fracture Mechanics Framework

Ngasoh Fayen Odette
(70116)

A THESIS PRESENTED TO FACULTY OF THE AFRICAN UNIVERSITY OF SCIENCE AND TECHNOLOGY, ABUJA, IN CANDIDACY FOR THE DEGREE OF DOCTOR OF PHILOSOPHY

RECOMMENDED FOR ACCEPTANCE BY THE DEPARTMENT OF MATERIALS SCIENCE AND ENGINEERING

ADVISOR:_____
PROFESSOR WOLE SOBOYEJO

2021

© Copyright 2021 by Ngasoh Fayen Odette.

All right reserved

ABSTRACT

This work presents the results of a combined analytical and experimental study of the effect of reinforcement on the corrosion and adhesion ability of epoxy coatings. Firstly the corrosion behavior of 5-hydroxytryptophan (HTP), and clay particulate reinforced epoxy coatings is studied on a steel substrate that is used widely in pipelines and tanks. The corrosion behavior was studied in sodium chloride (3.5 wt. % NaCl) solutions that simulate potential seawater exposure at pH 3 and 7. X-ray diffraction (XRD) and Scanning Electron Microscopy (SEM) were used for microstructural characterization of the samples. The thermal stability was characterized using Thermogravimetric Analysis (TGA). The underlying corrosion reactions and reaction products were also elucidated via Fourier Transform Infrared Spectroscopy (FTIR). Electrochemical impedance spectroscopy (EIS) and in-situ observations of interfacial blisters were used to study the underlying degradation mechanisms. Electrochemical impedance spectroscopy revealed that for prolonged exposure of about 90 days and above, the composite materials exhibited better corrosion resistance at a pH of 3 as seen by the higher diameter of the Nyquist plot. Fewer corrosion products were observed on the scribed areas of the HTP samples in the scribe test in pH of 3 corroding environments. This signifies improved adhesion of the coatings in that environment for the HTP/epoxy coatings. The results obtained also show that a 1 mm blister size was observed in the pristine epoxy sample while no blisters were observed in the clay/epoxy and HTP/epoxy samples exposed at pH of 3. In the pH 7 environment, the EIS experiment revealed the presence of blisters with diameters in the range of 1–4 mm, after exposure for 90 days. The implications of the results are discussed for the corrosion protection of steel surfaces with composite coatings. Secondly, the nano-indentation and Brazil Disk techniques is use to determine the Young's moduli, hardness values and mode mixity

characteristics of the composite coatings. The Young's moduli of the reinforced composites comprising 1, 3, and 5 wt. % of montmorillonite clay particles are shown to improve respectively by about 23 %, 58 %, and 50 % while the respective hardness values increased by about 46 %, 80 %, and 88 %, relative to those of pristine epoxy. The interfacial toughness between X65 steel and the epoxy/clay coatings increases with increasing mode mixity. This is associated with crack-tip shielding by crack deflection and crack bridging. The trends in the measured mode-mixity dependence of the interfacial fracture toughness values are consistent with predictions from the simplified zone, normal zone, and row models (at lower mode mixity). The insights from the observations and the measured crack profiles are incorporated into zone and row models for the estimation of crack-tip shielding. The implications of the results are discussed for the design of epoxy/clay composites with attractive combinations of mechanical properties. Thirdly, the tribological properties of epoxy composite coatings reinforced with montmorillonite clay particles are studied using nano-indentation and nano-scratch techniques. These are used to determine the nano-wear characteristics of the composite coatings. The plastic indentation resistance of the composites decreases with increasing particle loading, while the wear rates also drops with increase in re-enforcement from 1 and 3 wt.% and again the scratching experiments revealed a slight decrease in the surface damage of the coating with increasing clay loading. However, in all of the composites, the friction coefficients varied from 0.63 to 0.015. The section groove profile of each sample showed that the scratch depth reduced as clay reinforcement increased. The scratch depth of pristine epoxy was the highest ~ 150 nm followed by a depth of 100 nm for the 1% clay reinforced epoxy and 90 nm depth for 3% reinforced epoxy reinforced epoxy. There was also a general decrease with the wear coefficient, K, with hardness and increase in clay reinforcement up to 3%. The measured mechanical and tribological

properties have also shown to compare favorably with predictions from composite theories of wear performance criteria. The implications of the results are discussed for the design of epoxy/clay composites with attractive combinations of mechanical and tribological properties.

Keywords: Keywords: epoxy composite coatings; steel substrate; corrosion degradation behavior, Mechanical properties, interfacial fracture, toughening mechanisms, epoxy/clay composites, coating/interfacial design, nano-scratch, nano-wear, tribological

LIST OF PUBLICATIONS

1. Textbook Chapters

- **Ngasoh Fayen. Odette**, Wole Soboyejo, Failure Mechanisms in Pipeline Epoxy Coatings, Advanced Materials Research Online: 2015-12-22, ISSN: 1662-8985, Vol. 1132, pp 366-384 doi:10.4028/www.scientific.net/AMR.1132.366 © 2016 Trans Tech Publications, Switzerland

2. Peer-Review Journal Articles

a. Articles from the PhD Research Work:

i. **O. F. Ngasoh**, V. C. Anye, B. Agyei-tuffour, O. K. Oyewole, P. A. Onwualu, and W. O. Soboyejo, "Corrosion behavior of 5-hydroxytryptophan (HTP)/ epoxy and clay particle-reinforced epoxy composite steel coatings Corrosion behavior of 5-hydroxytryptophan (HTP)/ epoxy and clay particle-reinforced epoxy," *Cogent Eng.*, vol. 7, no. 1, 2020.

ii. **O. F. Ngasoh**, V. C. Anye, Emeso B. Ojo, Tido T. Stanislas, Abdulhakeem Bello, Benjamin Agyei-Tuffour, Kingsley Orisekeh, Oluwaseun K. Oyewole, NimaRahbar and Winston O. Soboyejo``Mechanical Properties of Epoxy/Clay Composite Coatings on an X65 Steel Substrate", Cogent Eng., (Accepted)

In Preparation:

iii. **Odette. F. Ngasoh**, V. C. Anye, Emeso B. Ojo, Tido T. Stanislas, Abdulhakeem Bello, Oluwaseun K. Oyewole, and Winston O. Soboyejo, "Tribological Study of Epoxy Composite coatings"

b. Other Peer-Review Article Published:

i. Emeso B. Ojo, Kabirat O. Bello, **Odette F. Ngasoh**, Tido T. Stanislas, Kabiru Mustapha, Holmer Savastano Jr, Wole O. Soboyejo. "Mechanical performance of fiber-reinforced alkali activated un-calcined earth-based composites*," Constr. Build. Mater., vol. 247, 2020.*

ii. TidoTiwaStanislas, Gbétoglo Charles Komadja, **Odette Fayen Ngasoh**, IfeyinwaIjeomaObianyo, Josepha FobaTendo, Peter,AzikiweOnwualu, HolmerSavastano Junior "Production and Characterization of Pulp and Nanofibrillated Cellulose from Selected Tropical Plants" July 2020*Journal of Natural Fibers DOI: 10.1080/15440478.2020.1787915*

iii. TidoTiwaStanislas, Gbétoglo Charles Komadja, **Odette FayenNgasoh**, IfeyinwaIjeomaObianyo, Josepha FobaTendo, Peter AzikiweOnwualu&HolmerSavastano Junior "Performance and Durability of Cellulose Pulp-Reinforced Extruded Earth-based Composites"*Arabian Journal for Science and Engineering (2021)doi.org/10.1007/s13369-021-05698-1*

iv. F.O. Kolawole, S.A. Adeniji, A. T. Idowu, T.A. Owoseni, **O.F. Ngasoh** and W.O. Soboyejo, Corrugated Laterite Based Ceramic Roof Tile Stabilized with Cement, International Journal of Engineering and Technology Volume 4 No. 3, March, 2014.

3. Peer-Review Conference Papers

i. **O.F. Ngasoh** and W.O. Soboyejo, Failure Mechanisms of Steel Pipelines, African Materials Research Society (AMRS) Conference, Addis Ababa, Ethopia, December 2013**.**

ii. **Odette F. Ngasoh**, VitalisAnye, Emeso B. Ojo, Tido.T. Stanislas, NimaRahbar and Winston O. Soboyejo, "Mechanical Performance of a Novel Epoxy

Nanocomposite for Coating Applications”10th International Conference of the African Materials Research Society (AMRS2019) 10th - 13th December 2019

LIST OF CONFERENCE PRESENTATIONS

- African Materials Research Society (AMRS) Conference, Addis Ababa, Ethiopia (2019)
- Materials Society of Nigeria Congress, Abuja, Nigeria (2018)
- African Materials Research Society (AMRS) Conference, Addis Ababa, Ethiopia (2013)

DEDICATION

This Thesis is dedicated to my family:

My parents, Mr. Gambar Ngasoh Martin and Mrs. Jeannett Bongaah

and

My dearest husband, Vitalis Chioh Anye and my wonderful children Daniel Nkah'nwi Chioh-Anye, David Nzahnwi Chioh-Anye and Dasia Akwa Chioh-Anye

ACKNOWLEDGEMENTS

All glory and adoration be unto God, the creator of the universe. My acknowledgement goes to God for He has shown His faithfulness to me throughout this journey of my PhD program at African University of Science and Technology (AUST), Abuja. He is the Alpha and the Omega, the beginning and the ending of my life. He is the God who has showered me with wisdom that is beyond human imagination. Who am I not to appreciate Him for the unmerited blessings He has endowed me. His name shall be praised forever and ever.

I want to sincerely acknowledge my supervisor, mentor and father, Professor Winston Oluwole Soboyejo. Your selflessness and commitment toward my success cannot be undermined. Please accept the appreciation that comes from the deepest of my heart. I also want to appreciate your loving family, your wife, Mrs. Morenike Soboyejo and children: Timmy, Deji, Junior and Kanyinsola. You were the very first family I knew during my stay here in Nigeria and I am so glad I have met you. May all your time and investments in making me who I am becoming not go in vain.

I also want to appreciate Prof. Peter Azikiwe Onwualu, the head of department of the materials science and engineering in the African University of Science and Technology, for his unending care, guidance and support throughout my studies. I would also like to thank Dr. Shola Odusanya of Advanced Biotechnology Laboratory, Sheda Science and Technology Complex, Abuja for his advice and guidance. I want to say a big thank you to Dr. Oyewole Kehinde Oluwaseun of the Department of Mechanical Engineering, the Worcester Polytechnic Institute, Massachusetts, United State of America for his technical contributions to my work. I am also grateful to Dr. Abdulhakeem Bello for the technical assistance and discussions they were truly helpful. May God richly bless you all.

My unending gratitude goes to my parents: Parent Mr. Gambar Ngasoh Martin and mother, Mrs. Gambar Jeannett Bongaah, for their care, advice, and prayers. It would have been difficult without my siblings: Flaviours, Gregory, Angela and Catherine. You have all blessed me in care, support and prayers. May Almighty God be with all of you.

I also acknowledge the financial support of African University of Science and Technology; Nelson Mandela Institute; African Development Bank; The Pan African Materials Institute (PAMI) through the World Bank center of excellence. I am also to AUST staff and AUST professors especially Mrs. Victoria Ogechi Agbo you all made my stay a memorable one. Almighty God will bless all of you in return.

I wish to appreciate finally and specially my dearest husband, Vitalis Chioh Anye and the children for your unending support and understanding. Thank you for your patience and endurance throughout the period of my program. To those I could not mention their names I say thank you.

TABLE OF CONTENTS

Contents

LIST OF TABLEs

LIST OF FIGURES

Chapter 1

1.1 Introduction

The durability of infrastructural materials and pipelines depends on the robustness of their protective coating layers. Coatings also provide physical barriers between steel structures and their surrounding environments. However, a coated steel structure exposed directly to the harsh sea water can be hit or bombarded by floating objects that leaves impact defects on the coating surface which can influence corrosion of a neatly coated area of a steel substrate [1]. The pores at the cross linked junctions in a cured epoxy coating can also assist in migration of absorbed water and other species such as chlorides and hydroxide ions into the epoxy/metal interface. This leads to the initiation of corrosion in the metallic substrate, and ultimately to the delamination of the coating from the substrate [2] [3]. Blistering is the most common mode of failure which is caused by the migration of liquid through the coatings, as a result of the induced osmotic effect [3] [4]. Prior studies have shown that the service lives of epoxy-based coatings can be decreased due to the degradation of epoxy matrices in different working environments (temperature, moisture and corrosive elements) [2], [5].

Epoxy coatings are also prone to damage by surface stresses and indentation/wear phenomena service [6], [7] Nano-indentation and nano-scratch testing can, therefore, be used to evaluate coating resistance and durability. There is therefore a strong interest in the development of novel coatings that can extend the service lives of pipelines, storage tanks and offshore structures in the oil and gas industry [8], where billions of Dollars are lost annually due to corrosion degradation phenomena [9]. The above challenges have stimulated researchers to explore alternative coatings that can be used for the protection of steels that are used extensively in the pipeline industry and structural applications [10].

Recent discoveries indicate that the inclusion of inorganic fillers effectively enhances the corrosion protection of pristine polymers such as conductive, thermoplastic and thermosetting polymers on cold rolled steel [11]. Epoxy coatings that contain fillers have also been shown to enhance corrosion protection [10]. They may also reduce the tendency of coatings to blister or delaminate [12]. Montmorillonite, which has a plate-like structure, is often used as a filler to increase the diffusion pathways, and thus reduce the permeability of corrosive agents within the coating material. 5-hydroxyltriptophan (5-HTP) has also proven to be an effective corrosion inhibitor on bare steel, as shown in the work by Ituen et al, (2015) [13]. Developed organically as a food supplement (to fight depression in humans), 5-HTP is gradually being considered as an anti-corrosion filler due to its stability in acidic environments [13].

However, under damage mode and interfacial failure and cracking [14]. Scratch testing has been used to study resistance to surface coatings to abrasion and wear [14]. Prior studies of the wear properties of epoxy/clay composites have focused on microscale wear using pin-on-disk experiments [15]. Furthermore, the application of contact or multi-axial loads can give rise to interfacial cracking between steel substrates and epoxy-based coatings [16]. There is therefore, a need to use interfacial fracture mechanics methods to study interfacial cracking phenomena between steels and epoxy-based coatings.

1.2 Statement of the Problem

There have been great studies and research in the corrosion and fracture mechanics of epoxy composite coatings. Less attention has been given to the study combination of strength, Young's moduli and interfacial fracture toughness between steels and epoxy/clay composite coatings. The problem addressed in this study is the degradation of epoxy composite coating through a fracture mechanic framework and corrosion study which is relevant to pipelines, storage tanks and

infrastructural applications. It is estimated that this can save millions of dollars when these mechanisms are understood and applied.

1.3 Scope of work

This thesis presents the results of a combined experimental and analytical/computational study of the study mechanism of corrosion in epoxy and epoxy composites using EIS. This links mechanistic understanding of potential failure mechanisms to fracture mechanics framework or approach. The study is divided into 6 sections. Following the background and introduction, the literature review is presented in section 2. This is followed by section 3 in which the processing, characterization and corrosion behavior of the coated and uncoated steel structures are presented. The adhesion and interfacial fracture behavior of the nanocomposite coated steels are then explored in Section 4. The tribological behavior of the composite coatings is presented in section 6. Finally, salient conclusions arising from the research are elucidated.

Chapter 2

2.1 Fundamentals of Interfacial Fracture Mechanics

Fracture toughness is the ability of a material containing a crack to resist fracture and is the most vital steps to consider for every material when in use. A large value signifies that fracture follows a ductile path. The fracture toughness is obtained from K, the stress intensity factor regarded as the point where an existing crack in a material begins to propagate [14]. It also measures the resistance of a material to crack propagation. The adhesion, the corrosion resistance and longevity of coatings are controlled by the joint at the coating/substrate composite [17]. The liquid form of epoxy diamine constitutes one of the most outstanding coatings used [14]. Most coatings shrink upon application inducing residual stresses which reduces adhesion and may cause interfacial delamination as well [14]. The fracture mechanic approach creates a balance amid the elastic energy caused by an outside force and an interfacial crack growth at the coating/substrate interface. From this the strain energy is given as;

$$G = \frac{\partial(W-U)}{\partial u}, \quad (1)$$

Where W is given as work done by outside load, U is the stored elastic energy, and A is the crack area. It has been observed that when G is greater than the critical value G_c, the crack begins to grow causing delamination at interface [18]. The total energy required is given as;

$$G_T = G_I + G_{II} = \frac{1}{E^*}(K_I^2 + K_{II}^2) \quad (2)$$

Where $E^* = E$=*young's modulus* for plane stress and $E^* = E/(1 - v^2)$ for plane strain, and K is the stress intensity factor. K is calculated independently for each fracture mode and is used to find the mode mixity, ψ. The schematics of the different failure modes are given in **Figure 2:1**. Atkinson [19] has shown that the mode I and mode II stress intensity factors, K_I and K_{II}, for the Brazil disk specimen are given by:

$$K_I = f_I \frac{F}{\pi t r} \sqrt{\pi a} \quad (3)$$

$$K_{II} = \mp f_{II} \frac{F}{\pi t r} \sqrt{\pi a} \quad (4)$$

where a is half of the crack length, the positive and negative signs correspond to the two tips, F is the applied load, t is the specimen thickness and r is the radius of the disk, while $f_I \, and \, f_{II}$ are the respective dimensionless factors for mode I and mode II. It is important to note here that the two dimensionless factors are functions of loading angle and crack size $(\frac{a}{r})$ [20]. The mode mixity/phase angle is given by [21]:

$$\Psi = \left(\frac{K_I}{K_{II}}\right) + \omega + \in ln \, ln \left(\frac{L}{h}\right) \quad (5)$$

where L is the length for the loading mode, h is the combined thickness of the sandwich materials, ω is the phase shift due to elastic mismatch and ∈ is the Dundur parameter. The phase shift, ω, is a function of the Dundurs parameters α, β, and ∈, which are given in **Table 2.1**, [21]:

Table 2.1 Elastic mismatched parameters as adapted from **[22]**

Bimaterial	α	β	ϵ
Aluminum/epoxy	0.90	0.218	-0.071
Brass/epoxy	0.94	0.228	-0.074
Steel/epoxy	0.96	0.232	-0.075
Plexiglass/epoxy	-0.15	-0.029	0.009

$$\alpha = \frac{\frac{1-\vartheta_2}{\mu_2} - \frac{1-\vartheta_1}{\mu_1}}{\frac{1-\vartheta_2}{\mu_2} + \frac{1-\vartheta_1}{\mu_1}} \quad (6)$$

$$\beta = \frac{1}{2}\frac{\frac{1-2\vartheta_2}{\mu_2} - \frac{1-2\vartheta_1}{\mu_1}}{\frac{1-\vartheta_2}{\mu_2} + \frac{1-\vartheta_1}{\mu_1}} \quad (7)$$

$$\epsilon = \frac{1}{2\pi} ln \frac{1-\beta}{1+\beta} \quad (8)$$

Where, μ_1 and μ_2 are the shear moduli of materials 1 and 2 respectfully. Note that in the case of the epoxy/steel system, $\omega = -13^0$ which falls within the range of $\omega = -14^0$ to -8^0 expected for metal/epoxy systems [22].

The interfacial fracture toughness between the two dissimilar materials can be estimated as the energy release rate at the tip of the interfacial crack between the bilayers. The mode I and mode II energy release rates are given by [9]:

$$G_I = \frac{K_I^2}{E^*} \quad (9)$$

$$G_{II} = \frac{K_{II}^2}{E^*} \quad (10)$$

Where the total energy release rate (G_T) is given by:

$$G_T = G_I + G_{II} = \frac{1}{E^*}(K_I^2 + K_{II}^2) \quad (11)$$

WhereE^* is the Young's modulus, E, for plane stress. In the case of plane strain, $E^*$is given by,

$$E^* = \frac{E}{1-\vartheta^2} \quad (12)$$

Finally an effective E^* can be determined relative to the thickness of the bilayer material structure. This is given by [23]:

$$\frac{1}{E^*} = \frac{\Gamma_1}{E_1} + \frac{\Gamma_2}{E_2} \quad (13)$$

Where

$$\Gamma_1 = \frac{t_1}{t_1+t_2}, and\ \Gamma_2 = \frac{t_2}{t_1+t_2} \quad (14)$$

Given as [24];

$$\Psi = \left(\frac{K_I}{K_{II}}\right) + \omega + \varepsilon \, ln \, ln \left(\frac{L}{h}\right) \quad (15)$$

L= reference length and h= thickness of the sandwich material layer in case of a sandwich structure. The stress intensity factor K_I and $K_{II,}$ greatly affects the mode mixity or loading phase which is not the case with the loading angle. The loading phase is also influenced by ω, which is the shift due to elastic modulus mismatch and it is also a function of the Dundurs parameters α, β and ε given as [25] [23], [24]

$$\alpha = \frac{\frac{1-\vartheta_2}{\mu_2} - \frac{1-\vartheta_1}{\mu_1}}{\frac{1-\vartheta_2}{\mu_2} + \frac{1-\vartheta_1}{\mu_1}} \quad (16)$$

$$\beta = \frac{1}{2} \frac{\frac{1-2\vartheta_2}{\mu_2} - \frac{1-2\vartheta_1}{\mu_1}}{\frac{1-\vartheta_2}{\mu_2} + \frac{1-\vartheta_1}{\mu_1}} \quad (17)$$

$$\epsilon = \frac{1}{2\pi} ln \frac{1-\beta}{1+\beta} \quad (18)$$

μ_1 and μ_2 are the shear moduli of material 1 and 2 respectfully. K_I and K_{II} are the mode I and mode II stress intensity factors.

For fracture to occur, $G_i = G_{ic}$, where G_i is the interfacial fracture toughness or the critical energy release rate [26]. The fracture criterion can be written as,

$$G_{ic} = G_{ic} = (1 + tan^2\varphi)(1 + tan^2\emptyset) \quad (19)$$

G_{ic} is the average mode I critical energy release rate. In 2 dimensions, Ø = 0 implying that the roughness is symmetric with respect to the phase angle ψ and Ø.

For an epoxy and steel composite ω = -13^0, the loading phase, L is equal to the sandwiched material layer, h which is equal to 100um and ϵ = -0.075 [23].

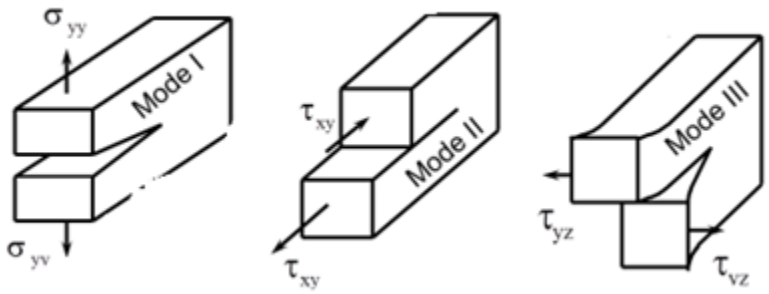

Figure 2.1 Schematic of the different loading mode of fracture mechanics

2.2 Theory of Coating adhesion

Adhesion is the tendency of dissimilar or similar surfaces to cling to one another. In other words is the force that holds surfaces together in contrast to stress exerted to pull the substrates apart. It can also be defined as the attractive force between dissimilar surfaces. This is summarized in F**igure 2.2.** Adhesion can either be studied in terms of adhesive strength using simple experimental methods like the pull-of-test or fracture mechanical analysis by the measurement of interfacial fracture toughness [27].

2.2.1 Adhesive Strength

The adhesive strength is the maximum tensile stress possible at the interface. It is affected by the coating thickness and the solvent retention, when solvent-containing coatings are used [28] [29]. Adhesion can be classified in three basic categories which are; specific adhesion which is the molecular attraction between contacting surfaces; mechanical adhesion which occurs when adhesives flows into the microstructure of the surfaces to be bonded and effective adhesion that involves a combination between specific and mechanical adhesion for optimum joining strength [30]. The intermolecular forces that bring about adhesion in stickers and sticky tapes can be classified as chemical adhesion, dispersion adhesion, and diffusion adhesion.

2.2.2 Mechanisms of adhesion

Mechanisms of adhesion tell of the different inherent forces existing at the coating substrate joint. Some suggested mechanisms are listed below. There is no single theory that gives a complete explanation to adhesion hence so many mechanisms are suggested to give reasons why objects stick to one another. The bonding of molecules at the coating substrate interface determines the molecular forces which are what brings about the adhesion mechanism [30] [29].

2.2.3 Mechanical Interlocking Adhesion

This happens when adhesives flows and fill the voids or pores of the surfaces and hold the surfaces together by interlocking. This is regarded as the major form of adhesion which increases the longevity of a coated surface to about seven to ten years [28] [30]. The adhesive must have the right properties to enable it flow, and the surface of the substrate must be roughened with peaks and valleys. The roughened surface increases the contact angle between the adhesive and the substrate; it provides mechanical interlocking and becomes more valuable if there is adequate wetting of the coating on the substrate surface. The structure of the substrate and the wetting ability of the coating is an important factor regarding mechanical interlocking.

2.2.4 Diffusion Mechanism.

Diffusion is the shared solubility and mobility of molecules at the coating/substrate joint.

Work done on the diffusion theory indicates the existence of macromolecular diffusion [28] [30], [31]. Diffusion can be forced at the metal/polymer joint and an interface area created. Diffusion is considered as the most productive mode of adhesion. Some of the factors that can influence diffusion include the operating temperature; the period of contact time, molecular weight of the polymer material, the solubility between the coating and the substrate and also the physical form of the surfaces in contact. It is important to also note that polarity influences diffusion.

2.2.5 Chemical bonding Mechanism

Chemical bonds are created during diffusion reactions where the coating through a chemical reaction creates a chemical bond or primary valence bond. These bonds can be ionic, covalent or metallic bonds [28] [32]. In the case of epoxy coating, a metal hydroxide is formed between the coating and the steel through a condensation reaction. There are other types of bonds responsible for adhesion such as polar and secondary valence bonds.

2.2.6 Electrostatic Mechanism

Electrostatic adhesion mechanism involves the movement of electrons in the coating/substrate joint producing charges that act on each other. An organic polymer receives electrons from a metallic substrate when coated producing an attractive force known as the electrical double layer (EDL). This force is known to be responsible for coating delamination. Scientists such as Deryagin and Krotova worked with the electrostatic mechanism as far back as the 1940s [29] [32]. This theory relies on the fact that there is usually an electrochemical potential difference at the joint of coating/substrate surfaces in contact.

2.2.7 Adsorption Mechanism

The mechanism of absorption seeks to give reasons to adhesion on basis of angle of contact and the ability to flow and wet [29] [30]. Adhesion is said to be experience at molecular joints of the surface and coating as a result of attractive forces between them. These attractive forces are considered the Van Del Waal forces and the hydrogen bonding [30]. It has been reported in literature that there is the presence of hydrogen bonding, ionic bonding and ion dipole interaction when an oxidized metal surface was coated with polymethylmethacrylate (PMMA) [33] [30].

Some of the factors that affect adhesion include; Polarity between substrate and coating, the extern of roughening of the substrate i.e the extent of peak and valleys produced on the substrate and the level of substrate contamination.

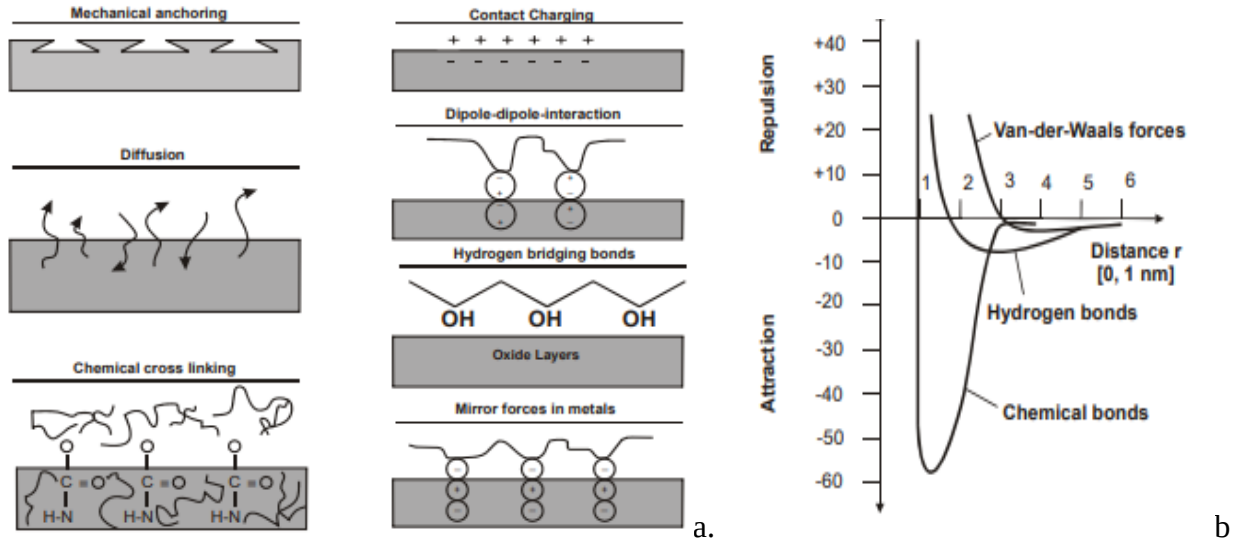

Figure 2.2 Schematic on the different modes of adhesion (a.) and the curves and numbers of the potential energies of van-der-Waals forces as well as hydrogen bonds as causes for adhesion (b.) [118].

2.3 Different methods to evaluate coating adhesion

Coating adhesion can be studied firstly as bond strength which is the ultimate load a coating/substrate can attain before separation. Test techniques used are the pull-off test and tape test [27]. Secondly adhesion can also be presented using fracture mechanic approach by studying the interfacial fracture toughness of coating/substrate interface [34]. This largely depends on the phase, ψ, angle hence making it difficult to be evaluated as a sole unit. Different evaluation techniques have been established to evaluate the interfacial toughness of coating/substrate frameworks such as the double cantilever beam fracture toughness test methods (DCB) [35], four point bend test [36] [37] and Brazil disc specimen [2] [23] [38]. There is also the indentation test which functions by determining the hardness of a solid by making an indentation in a sample under standard conditions and measuring the size of the indentation or the distance moved by the indentation [39]. The indentation test method has transcended the investigation of just hardness, young's modulus, and fracture toughness to the evaluation of coating and films with high adhesion strength [40] [41]. There is also the scratch test whose performance is easy to set up

and is applicable for thin, hard coatings on soft and flexible substrate [42]. Each of these test methods can be classified as either the rigid/flexible/rigid or a flexible/rigid structure. The initiation phase simply involves bond separation at the atomic level between coating and substrate creating defects. While the propagation phase involves the application of load either directly or parallel to the specimen or by an external force such as the indenter. Rigid/flexible/rigid samples were developed to investigate coating adhesion while the theoretical framework was suggested by Suo and Hutchinson [22]. In such a design the coating thickness is expected to be very small relative to the crack length and other dimensions of the sample.

2.4 Fundamental principles of Corrosion

Corrosion is the slow failure of a material through a chemical reaction with it surrounding [43]. Corrosion comprises an anodic and a cathodic reactions, to the acidic reaction in which metals are oxidized to yield metal ion as shown in the equations below [43].

$$M \rightarrow M^{n+} + ne \quad \text{----------} \quad 1$$

Several cathodic reactions exist to support/drive the corrosion process. Some of these reactions are

Hydrogen evolution:

$$2H^{+} + 2e^{-} \rightarrow H_{2(g)} \uparrow \quad \text{----------} \quad 3$$

$$Fe \rightarrow Fe^{2+} + 2e^{-} \quad \text{----------} \quad 4$$

Anodic reactions

$$Fe^{2+} + 2OH^{-} \rightarrow Fe(OH)_2 \quad \text{----------} \quad 5$$

$$2Fe(OH)_2 + H_2O + {}_{1/2}O_2 \rightarrow Fe(OH)_3 \quad \text{----------} \quad 6$$

According to the world corrosion organization (WCO), the annual cost of corrosion worldwide is $2.5trillion which is about 3% the world GDP (IMPACT 2016)

Corrosion can be classified into different groups' namely as uniform corrosion, localized corrosion, and corrosion-erosion as shown in **Figure 2:3**.

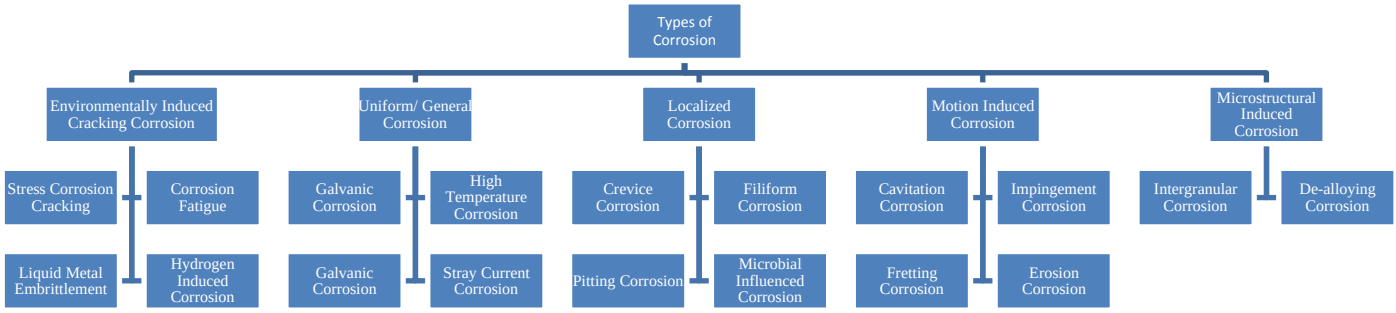

Figure 2.3 Different Types of Corrosion

2.5 Organic Coatings

Coatings consist of lacquer (binders with bulky organic molecules which often are completely polymerized prior to application) and enamel (resin molecules which are completely or incompletely polymerized). Other components of coatings include pigments to provide color, denseness and brightness; solvents for application of the coating; additives [5]. We can also improve the beauty of an object by designing the coating or by covering them up [34].

2.6 Characterization of Organic Coatings

2.6.1 Fourier transforms infrared spectroscopy (FTIR)

They used recorded molecular bond vibrations at various infra-red frequencies for the identification of chemical bonds in a solid or liquid sample by producing an infrared absorption spectrum that is like a molecular fingerprint [44]. FTIR is much simpler for the identification of different functional groups in a molecule since chemical functional groups are known to absorb infrared light at specific frequencies.

2.6.2 Scanning Electron Microscope (SEM)

The scanning electron microscope (SEM) uses high-energy electrons to produce signals at the surface of a sample corresponding to different elements that are used for elemental characterization of polymeric samples [45].

2.6.3 Energy Dispersion Spectroscopy (EDS)

Can also be referred to as EDS, EDX or XEDS, with the help of an X-ray, provides chemical analysis for element/samples for an element with atomic number >3. It gives a fast result and it is easy to use [45].

2.7 Problems Associated with Organic Coatings

Despite the exceptional properties of coated surfaces, they still suffer from so many corrosion prevention setbacks. Most coatings experience residual stress on curing which introduces cracks in the coating, and corrosive substances pass through. In the case of epoxy coatings, the pores at the cross linked junctions in a cured epoxy coating can also assist in migration of absorbed water and other species such as chlorides and hydroxide ions onto the epoxy/metal interface, leading to the initiation of corrosion of the metallic substrate and delamination of the coating [2] [3]. Majority of the different types of coating corrosion such as cathodic delamination, blistering in the case where organic coatings absorb up to 0.1 to 3% of liquid water [46], filiform corrosion where threadlike filaments are seen as evidence of corrosion, results into the development of pits on the substrate. It has been revealed that the durability of epoxy coatings drops due to the degradation of the matrix caused by the working environment which includes fluctuations in climate conditions, dampness and corrosive elements. [47] [32]. They are often susceptible to destruction by surface abrasion and wear [48] [49] [50]. Additionally, they demonstrate poor protection from the initiation and propagation of cracks [48] [49]. Such processes introduce localized defects in the coating and impair their appearance and mechanical strength.

Imperfections can likewise give rise to localize corrosion. Curing of epoxy-based coatings is often accompanied by enormous volume shrinkage and can absorb water from the environment due to its hydrophobicity. Resins act as nutrients to some bacteria and in other cases bacteria may produce an acidic environment to which coatings such as polyamides and epoxies cannot resist [51]. Detailed work of Saha et al [52] showed that polymeric coatings used on steel structures for the marine application were resistant to salt water corrosion by 77% with a decrease in the corrosion rate of about 0.8mm/year for HEMPALIN ENAMEL 52140 for 54hrs. But visual micrographs still showed dominance in pitting corrosion. The work presented by McCafferty et al indicated that corrosion under an organic coating can only exist when an electrolyte exists at the organic coating/substrate interface, either through diffusion, osmosis or by capillary action through voids or cracks [43]. Discoveries are made where ions go through the coating and a localized cathodic site is generated at various areas at the interface causing debonding also known as cathodic delamination forming blisters which eventually fails [53]. Jayanta investigated the tendency of pit formation on a substrate of some organic coated panels on steel substrate and found out that the pit nature of the steel with different primer coatings to be the same when exposed with the same time/period [54].

Evaluation of epoxy coatings for protecting aluminum alloy 2024 from corrosion caused by *Aspergillus niger* was done by Raaman et al [53]. They found out that epoxy does not serve as an effective protection against A. niger confirming the work done by Al et al, [55] where they indicated that epoxy serves as an easy carbon source for fungus [56]. The above illustrations are to point to the fact that there is always evidence of some form of corrosion underneath coatings after some time hence the need to study coating corrosion becomes a necessity.

2.8 Advances in the Evaluation of Corrosion Resistance of Coating

Polymer coating permeability has been widely studied over the years using various techniques. It has been observed that corrosion causing ions and elements such as oxygen, water, and chlorides ions penetrate through polymer coating when exposed to such environments. These corrosive elements and ions that go through the coating enhance corrosion rate at the coating substrate joint thereby weakening the coating adhesion [57] [58]. Polymer coating being able to prevent corrosion, usually impacts directly on the durability or service life of the part under protection. It is of necessity to put in place ways on how to check the functionality of the coating. Besides the short term exposure electrochemical tests or accelerated test and long term field exposure for evaluating coating corrosion resistance, conscious efforts are made nowadays to develop more realistic models for corrosion so as to be able to account for the gaps of the accelerated and dynamic test. Some corrosion testing methods are illustrated as seen in **Figure 2:4**

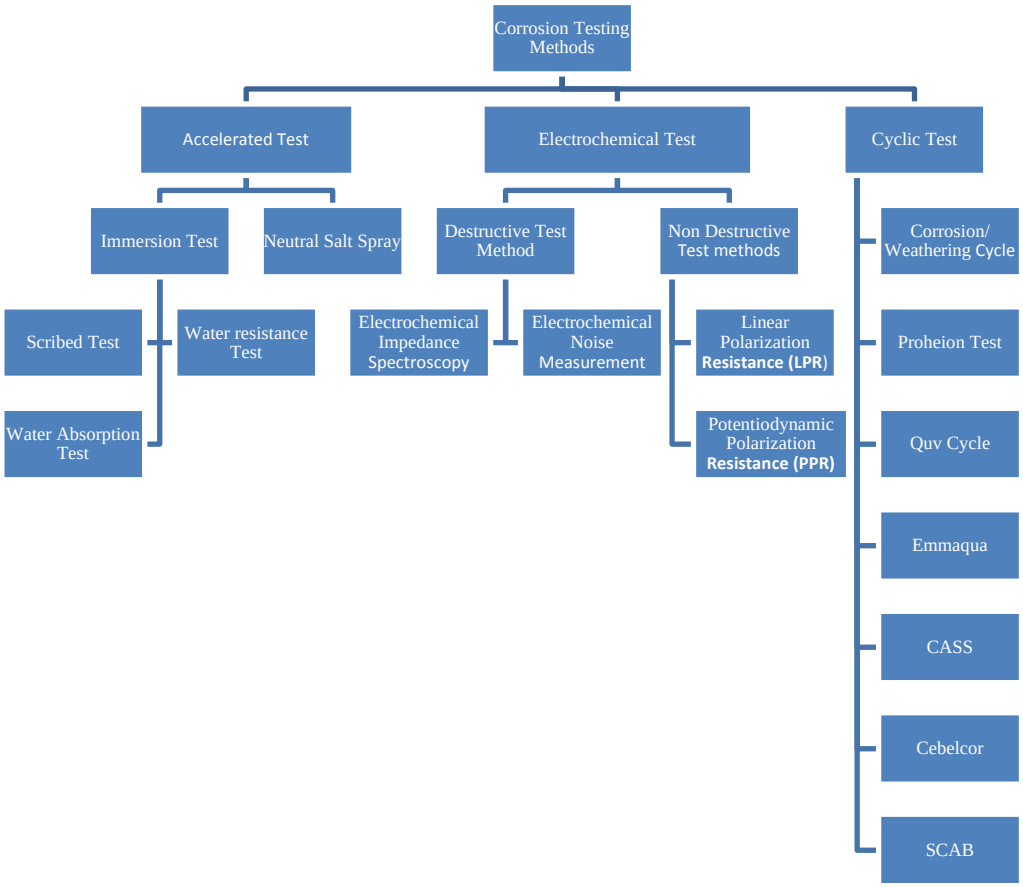

Figure 2.4 Classification of test methods

2.9 ACCELERATING TEST METHODS FOR COATINGS

Accelerated exposure tests procedures have been used to validate organic coatings. These tests can either be a long term field procedure or a short term laboratory test. Because the time expected for novel coatings to start giving clues to deterioration under natural environments is too long, faster test procedures are used. Fasts tests are done with the aim of getting quick information and reproducible data. It always involves the use of many test samples and adds natural circumstances such as temperature, humidity, UV and salt into a guarded chamber [59]. These accelerated tests are either static or cyclic salt spray. The fast testing method has seen a lot of criticism because it is believed that it changes the deterioration pattern of the coating hence is not a true representation of the actual deterioration in life [60] [61]. Accelerated test methods are used to reduce the duration to ascertain the durability of the coating material. Basiru et al 2018

carried out experiments in static, ultraviolet and dynamic conditions [59] and were able to establish the importance of the function of silicon resin and nanoparticles in improving organic coatings against UV degradation in a static mode but the outcome in dynamic mode was not too good.

2.9.1 Neutral Salt Spray (NSS)

The salt spray was invented in the 20^{th} century. It is the most available means to classify the behavior of polymer coatings [52] based on the ASTM standards [62] [63]. A classical salt spray capacity includes the following parts; a saturated air column to pacify the salt concentration, a solution and specimen holder, a heat distributing technique and a temperature controller.

An example of the salt spray (fog) test with ASTM B117 operates by atomizing salt solution with 5% NaCl onto specimens suspended at $15\text{-}30^0$ at an upright position as uniform droplets. Hall et al used techniques such as the neutral salt spray and electrochemical pitting test, to compare the corrosion resistance of coatings and concluded that if pitting formation is what determines the quality of the coating, then the electrochemical pitting test will be the best method to use because of the accuracy and ease of use [57]. Other combinations of accelerated test by Nguyen et al where a combination of cyclic salt fog, SO^2 salt fog at 35^0 to evaluate coating failure immersed in an electrolyte [64]; another method was also suggested by Adam Blakeley [65] where they employed a novel rapid assessment technique known as the thermal cycling test. This test involved 3 days of heating and cooling proceeds by 3 days of room temperature immersion. There is also the constant accelerated voltage test that has been used in a number of ways. The oxygen concentration cell mechanism is employed to speed up corrosion durability evaluation on different specimens and coatings [66]. Salt spray test was also carried out by Ismail et al on fusion bonded epoxy in a fog chamber which revealed that it is a promising

material for internal coating on steel water pipes [30]. One of the most fundamental limitations to accelerated test is stated by Townsend et al as "there is seldom a direct relationship between resistance to the action of salt sprayed and resistance to corrosion in other media because several factors influencing the progress of corrosion such as the formation of protective films vary greatly with the conditions encountered" [67]. Therefore considering this test to evaluate corrosion resistance for a metallic substrate is not valid [68]. Another limitation is the fact that there is no exposure to ultraviolet light in the salt spray chamber which is the core root to coating disintegration [68].

2.9.2 Immersion test

This involves the complete soaking of samples either in distilled or deionized water, salt water, acidic or alkaline solutions either in the presence or absence of heat. Immersion tests include water absorption tests, water resistance tests and the scribe test [69] Water absorption is the ability of a material to hold water when exposed to a moist environment or immersed in water. This can be evaluated in terms of specific absorption of quality and specific absorption of volume [69]. M. Al-Qadhi et al, 2013 used the water absorption test according to ASTM D570 on neat epoxy and epoxy clay nanocomposite for a period of 299 days in tap water [70]. They found out that within the first 40 days, the absorption process was diffusion controlled and the diffusion constant was calculated using Fick's law and the absorption process further asymptote toward saturation. Secondly, the test is affordable and can be done using just a glass beaker or larger vessels for bigger specimens [71]. G.DeSchutter et al also used the water absorption test to measure the resistance of concrete against carbonate and chloride migration [69]. The major advantage of this test method is that, firstly, it can be applied to all shapes of specimens if the

test focuses on the finished product. Secondly, it gives a guide to which type of coating to be used for which application based on the coating's ability to retain or resist moisture.

Water resistance test is done in accordance with ASTM D870-02; the coated samples are sucked in water in a corrosion resistance vessel [72]. This is performed either by varying the temperature and the operation time of the experiment. The importance of this test is to find out how coatings will curb degradation while in water because ideas on this will tell the durability of the coating. There are so many factors that accelerate the degradation of organic coatings such as the coating matrix, defects, impurities at the substrate and lack of adhesion.

2.9.3 Scribe Test

The scribe test is performed according to the ASTM 1654-08 with a scribe or knife [72]. The scribe is expected to penetrate all organic coating layers on the samples and is carried out at room temperature and pressure. This test predicts fundamental behavior of coating, substrate and coating/substrate interface. The quantity of rust at the scribed area and underneath the coatings close to the scribe is measured. The number of and shape of blister is also evaluated [73].

2.9.4 Some General Limitations to Accelerated Tests

Moisture test is very necessary but an intermittent drying cycle is also of great importance.

Varying global locations may possess varying climate, stresses and aging mechanisms on the coating [74]. The more corrosion is forced in the laboratory, the less accurate we are to predict field performance. According to research done by Glueckert, six coated samples were studied for gloss retention in Colton with the highest heat, more intense sun and adequate sandblast, East Chicago which had moderate weather of temperature ranging from -23^0 C to 38^0 C and Indiana [75]. This can be seen in **Table 2:2** below. This confirms the fact that varying global locations may possess varying climate, stresses and aging mechanisms on the coating [74].

Table 2.2 Exposure Results from Colton, California, East Chicago and Indiana.

Coating	**Gloss loss (%), East Chicago**	**Gloss loss (%), Colton**	**Ranking, East Chicago**	**Ranking, Colton**
Epox-Urethane	3	0	1	1
Urethane	38	31	2	3
Waterborne alkyd	56	6	3	2
Epoxy B	65	83	4	5
Acrylic Alkyd	68	77	5	4
Epoxy A	98	98	6	6

***Source*: Data from Guekert, Aj., Correlation of accelerated test to outdoor exposure for railcar exterior coatings, presented at corrosion/1004, NACE International, Houston, 1994, paper 596**

2.10 ELECTROCHEMICAL TEST METHOD

Corrosion mostly happens through a chemical process at the metal steel interface. An electrochemical test method predicts the potential and current during an oxidation and reduction process.

2.10.1 Non- Destructive Test Methods

The nondestructive test method is the process of investigating or testing substances for defects or flaws without the component, that is to say, the part can still be used after the test. Nondestructive tests are classified as follows;

2.10.1.1 Electrochemical Impedance Spectroscopy (EIS)

Electrochemical Impedance Spectroscopy (EIS) is regarded as one of the most recent methods to evaluate polymer coatings on the basis of electrical and adhesion properties to the metal[57]. EIS is the method in which the impedance of a coated sample is evaluated in regard to the frequency of an alternating current wave[57]. EIS can predict developments within the coating before it breaks down. It can also process the alterations of coatings as a result of the presence of moisture or ions [76]. EIS is very friendly to handle and its generated data is non-complicated to interpret. EIS can be used to evaluate the quantity of moisture that has penetrated the coating and is trapped in it which gives us an idea of the solubility of the coating [76]. EIS data gives information relating to the blistering formation, water sorption, swelling of the coating, adhesion properties, which involves debonding/delamination and the process of corrosion [57]. Modeling the equivalent circuit of EIS allows comparison between charge transfer/diffusion responses of the Nyquist curve that provide a reasonable indication of the effectiveness of a coating. Capacitance measurements predict water uptake in a coating. This is because the least amount of moisture absorbed has a huge influence on the capacitance of the film which can be seen in the expression below. The dielectric constants of organic coatings are generally small [57].

$$C = \varepsilon\varepsilon_0 \frac{A}{d} \quad (20)$$

Were c, is the capacitance ε is the dielectric constant of the coating; $\varepsilon\varepsilon_0$is the dielectric constant of a vacuum, d is the thickness of the dielectric and A is the surface area.

Figure 2:5 gives a summary of the processes involved in an electrochemical process. Step one indicates the start of the water sorption process of the coating which leads to the fast growth of water penetration in the coating, at phase two the coating is soaked up and saturates turning into a plateau with a constant capacitance. Phase three, however, reveals delamination at the metal-

polymer joint due to increased inflow of water and can also be considered as the beginning of corrosion [57].

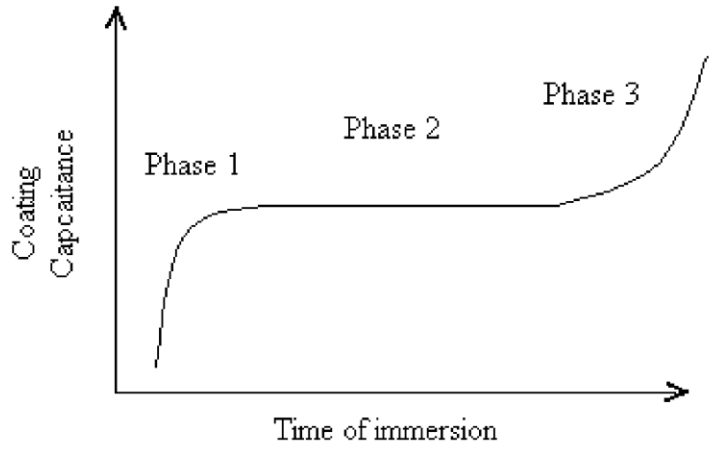

Figure 2.5 Capacitance variation in an organic coating as a function of immersion time adapted from **[57]**.

EIS is also used to classify coatings based on their ability to function [77]. Other researchers have used EIS to compare the deterioration procedures of polyurethane coatings on carbon steel and galvanized steel revealing that polyurethane has a better adhesion and corrosion safety as a coating on carbon steel [78]. Computer devices such as VersaSTAT (Princeton Applied Research software), the Camry Instrument and Biologic lab can be used to perform EIS.

2.10.1.2 Electrochemical Noise Measurement (ENM)

The electrochemical noise measurement functions by measuring the signal perturbations which are low-level signals of the corrosion potential amidst electrodes that are used to examine the speed and manner of corrosion. It is considered as the measure of the rate of diffusion across organic coatings [79]. ENM came to light when Eden, Hoffman, and Skerry used it to evaluate the corrosion resistance of two similar painted steel panels during an immersion test [55]. The initial application of this technique on an organically coated metal was performed by Jamali et al [51] [56]. Homburg et al. used ENM to investigate pitting caused by microbes [79]. The ENM

signals of cell of Sulphur reducing bacteria developed toward a consistent instantaneous frequency decomposition in the Hilbert spectral that is typical for a fast pitting corrosion process after 13 days of observation, these signals actually approved the microscopic view of a pit underneath the attached biofilms at the working electrodes [79].

2.10.2 Destructive Electrochemical Test

Destructive tests involve the complete destruction of the test sample to define the physical properties of that test sample. Since it involves destroying the sample, only limited samples are used.

2.10.2.1 Polarization tests

This is also known as the polarization resistance test which comprises the potentiodynamic polarization. It relies on the Tafel equation. On the other hand, linear polarization resistance (+/- 10mVvs open circuit potential) represents the equilibrium conditions, where the electrochemical reaction only depends on the exchange current density. **Figure 2:6** shows a Tafel plot used to identify different forms of pit development due to current where a low current pit initiation stage and a high current pit growth stage can be clearly identified [80]. Stage I signifies the electrolyte permeation and beginning of the pit in the metal [80]. Stage II signifies vigorous growth of the pit at the metal surface at the interface resulting in cracking within the coating and delamination due to the buildup of corrosion products. Potentiodynamic polarization resistance (PPR) does higher damage on test samples than linear polarization resistance (LPR) [80]. Hence high relative coatings cannot be evaluated by this method.

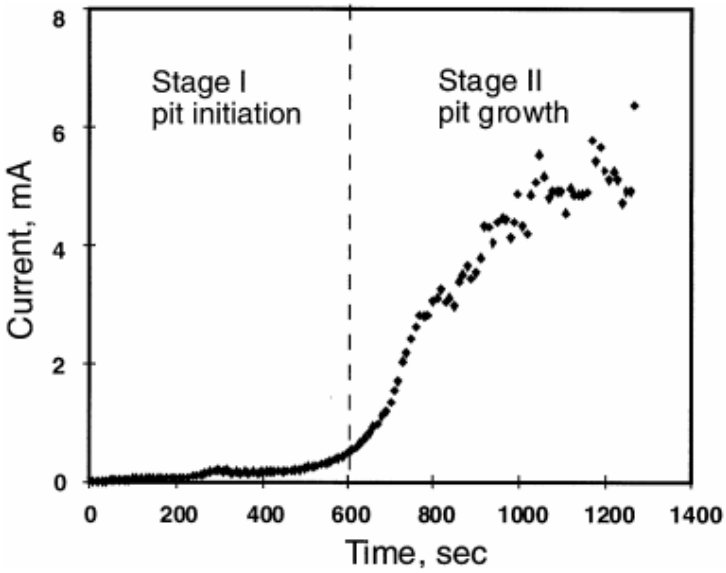

Figure 2.6 Potentiostatic polarization, showing increasing current demand, of a sol-gel, coated Al 2024-T3 **[80]. .**

2.10.3 CYCLIC TEST METHODS

Presently the different corrosion tests being done are not enough to finalize on what happens in an outdoor experience. A combination of the present corrosion testing methods and an outdoor experimental set up is necessary for a more realistic expectation. Cyclic corrosion test (CCT) expose test samples to different atmospheres in a repetitive series. Some examples of cyclic corrosion tests include;

2.10.3.1 Prohesion Test

This test method was invented in England to evaluate coating that was produced for use in the industry. Prohesion test involved the use of a dilute electrolyte cyclic fog/dry test which is considered to be mild compared to the traditional salt spray test [81]. This is because it gives a better result relative to the outdoor environment. It can be used to test filiform corrosion [78]. This test method has the standard ASTM 85-A5 which belongs to the ASTM 85 standard. Many research outcomes on prohesion stipulate that it simulates a marine atmospheric environment [81].

2.10.3.2 Corrosion/Weathering Cycle (ASTM D5894-5)

This test takes advantage of the fact that coatings are exposed to UV radiation which is detrimental to the coatings and makes it susceptible to corrosion. This test involves one week of QUV and one week of Prohesion where the specimens are wet and dry periodically in the presence of UV. This relates more to an outdoor experiment. The QPanel Company was the first to use this test method in 1969 according to work done by Deflorian et al [82] where they simply combined the Corrosion/Weathering Cycle that was established by Skerry in 1988 and his group at the Sherwin Williams Company in the USA. They basically combined prohesion and QUV.

2.10.3.3 QUV cyclic corrosion test

QUV is an accelerated weathering test specifically for long term outdoor experiments. This involves placing the specimens to very adverse conditions such as UV radiations, for sunlight, moisture, and heat. It includes ASTM G154, 4329, 4587, ISO4892, and SAEJ2020. This technique gives the direct correlation between gloss retention and mechanical properties of organic coatings [83]. This is because when sunlight shines on organic coatings, they can crack; peel; lose gloss or chalk which in the presence of moisture causes the coating to deteriorate. The limitation is that mimicking the outdoor experience in the laboratory is not realistic because every location has its own damaging causes such as pollution and biological attack which are unique [84]. Researchers have over the years use the QUV test to validate different weathering effects on coating such as gloss retention [85]. Some of the drawbacks of QUV test is that coatings are exposed to just a given wavelength of light while the natural light has a wider range.

2.10.3.4 EMMAQUA Test

This is the test standard ASTM G90. EMMAQUA stands for equatorial mount with mirrors for acceleration with water. It is the most widely used outdoor fast test [50]. What makes it special is that sunlight is gotten from ten specially designed mirrors targeting the samples with an intensity

of about eight suns [86]. This design tracks the sun with its entire wavelength onto the sample thereby becoming the most realistic cycle test which can be representative to a long term outdoor test [86]. The test specimens are wet with a sprayer at a given interval to create a rainfall scenario. The outcome is presented in the total amount of energy in a given unit area of coating exposed [85] [87].

2.10.3.5 CEBELCOR Cyclic test

Belgian center for corrosion study as far back as 1966 came up with a chemical test term as the CEBELCOR test. It has the standard ASTM G85. This test method is done in an environment that depicts good rural and urban conditions [88] [86].

2.10.3.6 COPPER-ACCELERATED ACETIC ACID SALT SPRAY (CASS)

CASS has the ASTM B368. It is mainly used to test the performance of coatings. It originated as far back as 1945 where acetic acid was introduced into a salt solution for salt spray. This makes the procedure more aggressive than normal salt spray. The test procedures are well recognized to validate corrosion resistance of coatings because it is fast, cheap and can be reproduced. According to Garfias et al [51], CASS was used in combination with other conditions to mimic natural weathering conditions through an accelerated test.

2.10.3.7 SCAB (GM9511P)

SCAB is a cyclic corrosion resistance test for coated metals. This test evaluates the adhesion behavior and corrosion of coated metal that leads to delamination [89]. The test usually runs for a long time of about 12 months with daily exposure of neutral salt and thermal shock weekly at a temperature of about -25^{o} C.

This write up gives a brief of some common test methods ranging from the accelerated, electrochemical and cyclic test used for organic coatings. These tests are chosen and performed

on the specimen on the basis of urgency, area of application and expected durability. Having knowledge of the different testing methods is very important. They are unique for specific applications.

Reference

[1] M. S. Madlangbayan, N. Otsuki, and T. Nishida, "Investigation on the Corrosion of Coated Steel Plates with Impact Defect using Investigation on the Corrosion of Coated Steel Plates with Impact Defect using Divided Steel Plates," no. May 2019, 2018.

[2] Z. T. Khodair, A. A. Khadom, and H. A. Jasim, "Corrosion protection of mild steel in different aqueous media via epoxy/nanomaterial coating: Preparation, characterization and mathematical views," *J. Mater. Res. Technol.*, no. x x, pp. 1–12, 2018.

[3] R. J. Rathish, R. Dorothy, R. M. Joany, M. Pandiarajan, and S. Rajendran, "Corrosion Resistance of Nanoparticle - Incorporated Nano Coatings," *Chem. Bull*, vol. 2, no. 12, pp. 965–970, 2013.

[4] H. R. Dana, A. Perronnet, S. Fréour, P. Casari, and F. Jacquemin, "Identification of moisture diffusion parameters in organic matrix composites," *J. Compos. Mater.*, vol. 47, no. 9, pp. 1081–1092, 2013.

[5] A. Turkiewicz, J. Brzeszcz, and P. Kapusta, "The application of biocides in the oil and gas industry," *Nafta-Gaz*, pp. 103–111, 2013.

[6] N. Saba, M. Jawaid, and M. T. H. Sultan, *An overview of mechanical and physical testing of composite materials*. Elsevier Ltd, 2019.

[7] R. S. R. Kalidindi and R. Subasri, *Sol-gel nanocomposite hard coatings*. Elsevier Ltd, 2014.

[8] G. L. Se, "Rules for Classification and Construction Additional Rules and Guidelines," 2010.

[9] N. Rahbar, Y. Yang, and W. Soboyejo, "Mixed mode fracture of dental interfaces," vol. 488, pp. 381–388, 2008.

[10] D. Zaarei, A. A. Sarabi, F. Sharif, S. M. Kassiriha, and M. M. Gudarzi, "Preparation and Evaluation of Epoxy-Clay Nanocomposite Coatings for Corrosion Protection," *Int. J. Nanosci. Nanotechnol*, vol. 7, no. 2, pp. 126–136, 2010.

[11] H. Huang, J. Yeh, and Y. Yu, "POLYMER Effect of clay on the corrosion protection efficiency of PMMA / Na + -MMT clay nanocomposite coatings evaluated by electrochemical measurements," vol. 44, pp. 13–23, 2008.

[12] M. Ates, "A review on conducting polymer coatings for corrosion protection," vol. 4243,

no. February, 2016.

[13] E. B. Ituen, O. Akaranta, and O. A. James, “5-hydroxytryptophan: A novel eco-friendly corrosion and oilfield microbial inhibitor,” *Soc. Pet. Eng. - SPE Niger. Annu. Int. Conf. Exhib. NAICE 2015*, 2015.

[14] G. Wypych, “Scratch and Mar Resistance,” *Handb. Surf. Improv. Modif.*, pp. 3–41, 2018.

[15] Rashmi, N. M. Renukappa, B. Suresha, R. M. Devarajaiah, and K. N. Shivakumar, “Dry sliding wear behaviour of organo-modified montmorillonite filled epoxy nanocomposites using Taguchi’s techniques,” *Mater. Des.*, vol. 32, no. 8–9, pp. 4528–4536, 2011.

[16] A. U. Malik, S. Ahmad, I. Andijani, F. Al-muaili, T. L. Prakash, and J. O. Hara, “Corrosion Protection Evaluation of Some Organic Coatings in Water Transmission Lines 1,” no. November 1999, pp. 1966–1827, 1999.

[17] M. Niknahad, S. Moradian, and S. M. Mirabedini, “The adhesion properties and corrosion performance of differently pretreated epoxy coatings on an aluminium alloy,” *Corros. Sci.*, vol. 52, no. 6, pp. 1948–1957, 2010.

[18] N. W. Klingbeil and J. L. Beuth, “Interfacial fracture testing of deposited metal layers under four-point bending,” *Eng. Fract. Mech.*, vol. 56, no. 1, pp. 113–126, 1997.

[19] “Atkinson_82 (1).pdf.” .

[20] M. Hoerantner, T. Leijtens, G. Eperon, N. Renewable, and M. D. Mcgehee, “The Potential of Multijunction Perovskite Solar,” no. October, 2017.

[21] E. D. Orthogonal, E. Wedges, U. Normal, and S. Loading, “1 B | I discussion,” vol. 31, pp. 650–652, 2016.

[22] J. S. Wang and Z. Suo, “Experimental determination of interfacial toughness curves using Brazil-nut-sandwiches,” *Acta Metall. Mater.*, vol. 38, no. 7, pp. 1279–1290, 1990.

[23] N. Rahbar *et al.*, “Adhesion and interfacial fracture toughness between hard and soft materials,” *J. Appl. Phys.*, vol. 104, no. 10, 2008.

[24] T. M. Tong, T. Tan, N. Rahbar, and W. O. Soboyejo, “Mode Mixity Dependence of Interfacial Fracture Toughness in Organic Electronic Structures (September 2012),” vol. 14, no. September 2012, pp. 291–299, 2013.

[25] “5-Hydroxytryptophan | C11H12N2O3 - PubChem.” [Online]. Available: https://pubchem.ncbi.nlm.nih.gov/compound/5-Hydroxytryptophan. [Accessed: 27-Jun-2019].

[26] “Methods of Calculating Stress Intensity Factors – Delaminations,” pp. 67–75, 2018.

[27] J. Valli and J. Valli, “A review of adhesion test methods for thin hard coatings,” vol. 3007, no. 1986, 2014.

[28] R. A. Gledhill, A. J. Kinloch, S. Yamini, and R. J. Young, “Relationship between

mechanical properties of and crack progogation in epoxy resin adhesives," *Polymer (Guildf).*, vol. 19, no. 5, pp. 574–582, 1978.

[29] A. G. Evans, M. Rühle, B. J. Dalgleish, and P. G. Charalambides, "The fracture energy of bimaterial interfaces," *Metall. Trans. A*, vol. 21, no. 9, pp. 2419–2429, 1990.

[30] "Theory of Adhesion."

[31] S.-R. Kim and J. A. Nairn, "Fracture mechanics analysis of coating/substrate systems: Part II: Experiments in bending," *Eng. Fract. Mech.*, vol. 65, no. 5, pp. 595–607, 2000.

[32] A. Abdel-samad, Y. Soud, and M. Zaki, "Influence of Paint on Steel Corrosion for Marine Applications," no. July, pp. 189–195, 2014.

[33] K. W. Allen, "Theories of adhesion," *Handb. Adhes. Second Ed.*, pp. 535–538, 2005.

[34] Z. Chen, K. Zhou, X. Lu, and Y. C. Lam, "A review on the mechanical methods for evaluating coating adhesion," *Acta Mech.*, vol. 225, no. 2, pp. 431–452, 2014.

[35] J. W. Hutchinson, *Mixed Mode Cracking in Layered Materials*, vol. 29. 1992.

[36] I. Hofinger, M. Oechsner, H. Bahr, and M. V Swain, "Modified four-point bending specimen for determining the interface fracture energy for thin , brittle layers," pp. 213–220, 1998.

[37] Y. Yin, Y. Qiao, and S. Hu, "Four-point bending tests for the fracture properties of concrete," *Eng. Fract. Mech.*, vol. 211, no. March, pp. 371–381, 2019.

[38] L. Banks-Sills and J. Schwartz, "Fracture testing of Brazilian disk sandwich specimens," *Int. J. Fract.*, vol. 118, no. 3, pp. 191–209, 2002.

[39] H. Chakraborty, A. Sinha, N. Mukherjee, D. Ray, and P. Protim, "A study on nanoindentation and tribological behaviour of multifunctional ZnO / PMMA nanocomposite," *Mater. Lett.*, vol. 93, pp. 137–140, 2013.

[40] D. Tzetzis and G. Mansour, "Nanoindentation , compression and fractural characterization of highly dispersed epoxy silica nanocomposites," 2015.

[41] L. Shen, L. Wang, T. Liu, and C. He, "Nanoindentation and Morphological Studies of Epoxy Nanocomposites," pp. 1358–1366, 2006.

[42] D. Beegan, S. Chowdhury, and M. T. Laugier, "Comparison between nanoindentation and scratch test hardness (scratch hardness) values of copper thin films on oxidised silicon substrates," *Surf. Coatings Technol.*, vol. 201, no. 12, pp. 5804–5808, 2007.

[43] E. E. Stansbury and R. A. Buchanan, *Electrochemical*. .

[44] E. Techniques, "Physico-chemical techniques for analysing the ageing of polymer modified bitumen 12," 2011.

[45] *Physical Principles of Electron Microscopy*. .

[46] “Corrosion Under Organic Coatings,” 2010.

[47] J. J. Ritter and M. J. Rodriguez, “Corrosion Phenomena for Iron Covered with a Cellulose Nitrate Coating *,” vol. 111, no. 4, pp. 223–226, 1982.

[48] O. Becker, R. Varley, and G. Simon, “Morphology , thermal relaxations and mechanical properties of layered silicate nanocomposites based upon high-functionality epoxy resins,” vol. 43, pp. 4365–4373, 2002.

[49] A. Crosky and D. Kelly, “Improvement of bearing strength of laminated composites,” vol. 76, pp. 260–271, 2006.

[50] B. D. Davidson, “A single leg bending test for interracial fracture toughness determination,” pp. 193–210, 1996.

[51] L. Garfias and W. G. Kenny, “Characterization of internal and external coatings used on steel pipelines,” no. January 2010, 2014.

[52] J. K. Saha, P. K. Mitra, S. Paul, and D. D. N. Singh, “Performance of different organic coatings on steel substrate by accelerated and in atmospheric exposure tests,” vol. 17, no. March, pp. 102–110, 2010.

[53] N. Raaman, N. Rajitha, A. Jayshree, and R. Jegadeesh, “Biodegradation of plastic by Aspergillus spp . isolated from polythene polluted sites around Chennai,” vol. 1, no. November, pp. 313–316, 2012.

[54] G. S. Frankel and N. Sridhar, “Understanding localized,” vol. 11, no. 10, pp. 38–44, 2008.

[55] E. E. T. Al, “Application of Electrochemical Noise Measurements,” pp. 36–47, 1986.

[56] S. S. Jamali, D. J. Mills, R. A. Cottis, and T. Y. Lan, “coated metal,” *Prog. Org. Coatings*, pp. 1–6, 2016.

[57] A. Amirudin and D. Thierry, “IN ORGANIC Application of electrochemical impedance spectroscopy to study the degradation of polymer-coated metals,” vol. 9440, no. 95, 1995.

[58] D. P. Bentz, “A Method for Measuring Water Diffusion in a Coating Applied to a Substrate,” no. May, 2014.

[59] Y. A. Basiru, S. Ammar, K. Ramesh, B. Vengadaesvaran, S. Ramesh, and A. K. Arof, “Corrosion protection performance of nanocomposite coatings under static , UV , and dynamic conditions,” *J. Coatings Technol. Res.*, 2018.

[60] T. R. Hull, J. S. Colligon, and A. E. Hill, “of thin film,” vol. 37, pp. 327–330.

[61] M. Mellali, P. Fauchais, and A. Grimaud, “Influence of substrate roughness and temperature on the adhesion / cohesion of alumina coatings,” vol. 81, 1996.

[62] J. Takadoum and H. H. Bennani, “COATIN6S Influence of substrate roughness and coating thickness on adhesion ,” vol. i, pp. 272–282, 1997.

[63] T. Edition, *FRACTURE*. .

[64] X. Shi, T. A. Nguyen, Z. Suo, Y. Liu, and R. Avci, “Effect of nanoparticles on the anticorrosion and mechanical properties of epoxy coating,” *Surf. Coatings Technol.*, vol. 204, no. 3, pp. 237–245, 2009.

[65] Adam Blakeley, “Understanding Corrosion and Salt Spray.” Zalilah, p. 7, 2016.

[66] A. U. Ma, I. Andijani, S. Ahmed, and F. Al-muaili, “Corrosion and mechanical behavior of fusion bonded epoxy (FBE) in aqueous meala,” vol. 150, pp. 247–254, 2002.

[67] C. R. Shastry and H. E. Townsend, “Mechanisms of Cosmetic Corrosion in Painted Zinc and Zinc-Alloy-Coated Sheet Steels *,” vol. 45, no. 2, 1989.

[68] B. S. Skerry, C. H. Simpson, and G. R. Wilson, “Combined CorrosionIWeathering Testing of Coated Steel Products for Automotive Applications,” 2018.

[69] G. De Schutter and K. Audenaert, “Evaluation of water absorption of concrete as a measure for resistance against carbonation and chloride migration,” vol. 37, no. November, pp. 591–596, 2004.

[70] M. Al-Qadhi, N. Merah, and Z. M. Gasem, “Mechanical properties and water uptake of epoxy-clay nanocomposites containing different clay loadings,” *J. Mater. Sci.*, vol. 48, no. 10, pp. 3798–3804, 2013.

[71] C. Coatings *et al.*, “Standard Practice for Testing Water Resistance of Coatings Using Water,” vol. 06, pp. 6–8, 2002.

[72] S. Surfaces *et al.*, “Standard Test Method for,” vol. 08, no. Reapproved 2016, pp. 2016–2019, 2018.

[73] R. Coatings, “Standard Test Method for Evaluating Degree of Blistering of Paints 1,” vol. 02, no. Reapproved 2017, pp. 1–6, 2018.

[74] D. D. Macdonald, “Some Advantages and Pitfails of Electrochemical Impedance Spectroscopy,” vol. 46, no. 3, pp. 229–242, 1990.

[75] D. Tarjan and C. October, “Accelerated Testing,” 2014.

[76] L. Angeles, “Use of electrochemical impedance spectroscopy for the study of corrosion protection by polymer coatings I ---I I,” vol. 25, pp. 187–202, 1995.

[77] J. Titz, G. H. Wagner, H. Spáhn, M. Ebert, K. Jüttner, and W. J. Lorenz, “Characterization of Organic Coatings on Metal Substrates by Electrochemical Impedance Spectroscopy,” vol. 46, no. 3, pp. 221–229, 1990.

[78] E. A. Oriaifo, N. Perera, A. Guy, P. S. Leung, and K. T. Tan, “A Review of Test Protocols for Assessing Coating Performance of Water Ballast Tank Coatings,” no. September, 2014.

[79] A. M. Homborg, C. F. L. Morales, T. Tinga, J. H. W. De Wit, and J. M. C. Mol,

"Electrochimica Acta Detection of microbiologically influenced corrosion by electrochemical noise transients," *Electrochim. Acta*, vol. 136, pp. 223–232, 2014.

[80] N. Voevodin, C. Jeffcoate, L. Simon, M. Khobaib, and M. Donley, "Characterization of pitting corrosion in bare and sol ▪ gel coated aluminum 2024-T3 alloy," pp. 29–34, 2001.

[81] "HistoricBridges." .

[82] F. Deflorian, L. Fedrizzi, and S. Rossi, "Electrochemical Impedance Spectroscopy and Fourier Transform Infrared Spectroscopy of Natural and Accelerated Weathering of Organic Coatings," no. August, pp. 598–605, 1998.

[83] H. Leidheiser, "Corrosion of Painted Metals — A Review *," pp. 374–383.

[84] "16-0712: Toward a 100-Year Bridge Coating System: Bridge Topcoats in Japan," pp. 1–13, 2016.

[85] H. Tanabe and W. Darden, "The Progress of Newly Developed Fluoro-polymer Topcoat Systems ― Weathering performance and track records since the 1980 ' s ―," 1980.

[86] P. Montoya, I. Díaz, N. Granizo, D. De Fuente, and M. Morcillo, "An study on accelerated corrosion testing of weathering steel," *Mater. Chem. Phys.*, pp. 1–9, 2013.

[87] A. Matinmanesh, O. Rodriguez, M. R. Towler, P. Zalzal, E. H. Schemitsch, and M. Papini, "Quantitative evaluation of the adhesion of bioactive glasses onto Ti6Al4V substrates," *Mater. Des.*, vol. 97, pp. 213–221, 2016.

[88] A. Saeed, A. Khan, and M. H. Nazir, "Time dependent surface corrosion analysis and modelling of automotive steel under a simplistic model of variations in environmental parameters," vol. 178, 2016.

[89] F. Mansfeld, M. W. Kendig, and S. Tsai, "Evaluation of Corrosion Behavior of Coated Metals with AC Impedance Measurements *," pp. 478–485, 1982.

Chapter 3

3.1 Introduction

Coatings provide an effective method for the protection of surfaces, especially pipelines, and storage tanks that are used extensively in the infrastructure, oil and gas industry [8]. Coatings also provide physical barriers between steel structures and their surrounding environments. There is therefore a strong interest in the development of novel coatings that can extend the service lives of pipelines, storage tanks and offshore structures in the oil and gas industry [8], where billions of Dollars are lost annually due to corrosion degradation phenomena [9]. However, a coated steel structure exposed directly to the harsh sea water can be hit or bombarded by floating objects that leave impact defects on the coating surface which can influence corrosion of a neatly coated area of a steel substrate [1]. Hence it is necessary to perform a scribe test to evaluate the behavior of the coating at the coating/metal interface near the scribe. According to [90], when a coating surface is damaged, the exposed coating/metal interface should be subject to investigation and the passivating or anticorrosive effect of the coating is investigated to ascertain the extent of the corrosion-induced delamination of the coating near the damaged area.

The pores at the cross linked junctions in a cured epoxy coating can also assist in migration of absorbed water and other species such as chlorides and hydroxide ions into the epoxy/metal interface. This leads to the initiation of corrosion in the metallic substrate, and ultimately to the delamination of the coating from the substrate [2] [3]. Blistering is the most common mode of failure which is caused by the migration of liquid through the coatings, as a result of the induced osmotic effect [3] [4]. Microbes can also attack the hydrocarbon and non-hydrocarbon fuel molecules, leading directly to a change in chemical properties and performance [91]. Tank venting, which is essential for preventing tanks from collapsing under atmospheric pressure, is a major entry route for contaminating microbes [91][5]. Microbes can also be transported from

refinery tanks or barges, through pipelines and terminal tanks, throughout the fuel distribution system. In any case, relatively small volumes of water can support localized pockets or niches of microbial growth that lead ultimately to microbial corrosion.

Furthermore, internal corrosion can occur when the pipeline walls, and storage tank walls are exposed to water and contaminants such as oxygen, hydrogen cyanide, carbon dioxide and chlorides [2]. Prior studies have shown that the service lives of epoxy-based coatings can be decreased due to the degradation of epoxy matrices in different working environments (temperature, moisture and corrosive elements) [2] [5]. Their applications are also limited by their susceptibility to damage by surface abrasion and wear [92] [28] as well as the initiation and propagation of cracks [4]. Such processes can introduce localized defects into coatings, which accelerate the ingress of water, oxygen and chemical species into the metallic substrates, thus resulting in their localized corrosion [3]. The above challenges have stimulated researchers to explore alternative coatings that can be used for the protection of steels that are used extensively in the pipeline industry and structural applications [10]. Some other researchers have used alternative methods such as surface nano-crystalizaion of steels by nano-structuring the surface layer [93] observed enhanced corrosion resistance and the micro-hardness of the treated samples improved from 215 to 310 HV [93]. Recent discoveries indicate that the inclusion of inorganic fillers effectively enhances the corrosion protection of pristine polymers such as conductive, thermoplastic and thermosetting polymers on cold rolled steel [11]. Epoxy coatings that contain fillers have also been shown to enhance corrosion protection [10]. They may also reduce the tendency of coatings to blister or delaminate [12]. Montmorillonite, which has a plate-like structure, is often used as a filler to increase the diffusion pathways, and thus reduce the permeability of corrosive agents within the coating material.5-hydroxyltriptophan (5-HTP) have

also proven to be an effective corrosion inhibitor on bare steel, as shown in the work by Ituen et al, (2015)[13]. Developed organically as a food supplement (to fight depression in humans), 5-HTP is gradually being considered as an anti-corrosion filler due to its stability in acidic environments [13].

This paper therefore presents the results of the corrosion behavior of epoxy-based composite coatings with two different fillers (clay particles and 5-hydroxyltriptophan (5-HTP)). Corrosion phenomena are studied in environments that simulate potential seawater environments (3.5wt% NaCl). A combination of *ex-situ* and *in-situ* microscopic observations is used to study the underlying corrosion behavior. From the literature, it is known that corrosion resistance of a coated metal is dependent on some key factors including the ability of the top coating to resist salt intrusion, to resist the inflow of water and other corrosive chemicals in a corroding environment, the effects of passivating elements, the extent of coating adhesion to the metal, and how oxidized the coating surface is [90]. This study seeks to evaluate the ability of the produced composite coatings to resist the inflow of water and other corrosive chemicals in a corroding environment, the effect of passivating elements, and the extent of coating adhesion to the metal. Electrochemical impedance spectroscopy (EIS) and scribe tests are used to evaluate the blistering and creepage of the coated samples. The underlying corrosion reactions and reaction products are also elucidated via Fourier Transform Infrared Spectroscopy (FTIR) and X-Ray Diffraction (XRD). Finally, the thermal stability of the coatings is evaluated to ascertain the weight loss patterns in the different composites. The implications of the results are discussed for the corrosion protection of steels. This research would potentially find application in the infrastructure, biotechnological and above all the oil and gas industry where the corrosion resistance and good adhesion of coatings is of great importance.

3.2 Materials and Experimental Methods

3.2.1 Materials

Sigmaline 523 (Sigma Lining SF 23) hardener and base obtained from Sigmakalon Belgium N.V Tweemontstraat 104, 2100 Deume-Antwerpen was used to produce the epoxy. The epoxy had a molecular weight of ≤700 g/mol and a specific density of 1.48 g/cm^3. The clay particles, Cloisite 30B (C30 B), were naturally montmorillonite modified with methyl-tallow-bis-3-hydroxyethyl quaternary ammonium salt (procured from Southern Clay Products Inc, Texas., USA). The cation exchange capacity (CEC), which determines the amount of the alkylammonium ions present between the clay-clay layers of C30B, was 90 meq/100 g. The d-spacing of the (001) plane was 1.85 nm, and the density was 1.98 g/cm^3. The average particle size was about 5μm. The 5-Hydroxyltriptophan (obtained from Sigma Aldrich EMD Millipore Corp, Billerica, MA, USA) with an average particle size of ~ 17 μm had a molecular weight (M_w) of 220.22 g/mol and a density of 1.484 g/cm^3. **Figure 3.1** presents the Scanning Electron Microscope, SEM micrographs of the two fillers. The X65 low carbon steel was obtained from the Schiabit Construction Company, SCC, Bwari, Abuja, Nigeria. The actual chemical composition of the low carbon steel is presented in **Table 3.1.**

3.2.2 Experimental Methods

The steel samples were cut into 40 mm by 20 mm by 3 mm with mark V series machines. This was done using a size 64 silicon carbide blade. A cooling fluid was used to cool the samples during the cutting process, in an effort to prevent work hardening of the samples during specimen fabrication. The steel substrate had a Rockwell C hardness of about 10.

Table 3.1 Elemental composition of as-received X65 mild steels

Steel Samples	Composition

	(wt%)								
	C	Si	Mn	P	S	V	Nb	Ti	Fe
Low Carbon Steel	0.12	0.45	1.60	0.025	0.015	0.15	0.15	0.15	97.36

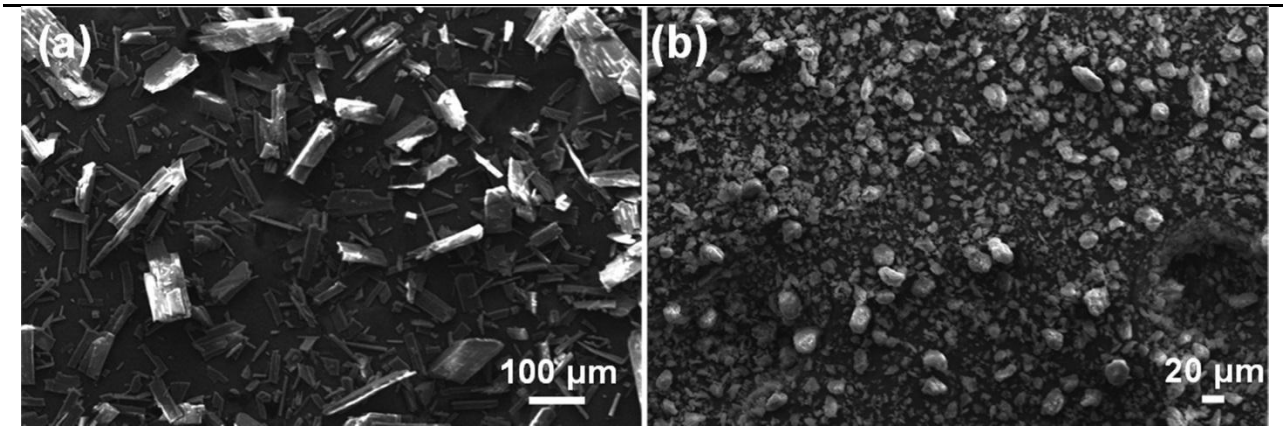

Figure 3.1 SEM image of (a) 5-Hydroxyltryptophane and (b) Cloisite 30B

3.2.3 Epoxy Composite Processing

Epoxy composites with 3 wt. % C30B and 5-HTP were used. It has been found in literature that clay fillers give their optimum protection at 3 wt.% [94] [95] [96]. The 3 wt.% of cloisite 30B clay was added to the epoxy base and stirred with a magnetic stirrer for 2.5 hours at a rate of 1500 rpm. This was done at 50 ^{o}C to enable a uniform dispersion of the clay particles. The resulting mixture was then degassed in a vacuum oven for 2 minutes, before adding a stoichiometric quantity of the curing agent and mixing with a spatula. A final degassing was then carried out in the vacuum oven at 50 ^{o}C for a period of 1 minute. The stoichiometric mixture of epoxy resin and base was 2:1. The same procedure was repeated for 5-Hydroxyltriptophan (5-HTP). The preparatory process is illustrated in **Figure 3.2**.

According to ASTM D823-17 [97], a hand-held spray gun (Devil bis Finishline 4FLG-670 solvent based 4VLP Gravity Feed paint Gun, Worcester, MA, USA) was used to apply the coatings. The coating thickness of ~ 0.5 mm was controlled by: the transverse speed of the gun; the number of passes of the gun; the fluid delivery rate of the gun; the viscosity of the material. The coating mixtures were diluted by adding 20 wt.% of thinner to increase the flow rate. The mixtures were then sprayed for durations of about 10 seconds during each pass. The total of 5 transverse passes was used in spraying at a pressure of ~ 0.1034 MPa /15 psi.

The microstructures of the pristine epoxy, epoxy/clay and 5-HTP/epoxy composites were characterized in a scanning electron microscope (Carl ZEISS model evo10LS-EDAX) that was operated at 20 kV. Optimal Fourier Transform Infra-Red (FTIR) spectra were obtained in the region in the region of 4000-500cm^{-1} (Thermo-Scientific FTIR (Model: Nicolet IS5, USA) to identify the functional groups of the coatings [98]. The structure of the composites was characterized using a Rigaku X-Ray diffractometer using Cu K_{alpha} radiation, measured at 30 kV and 15 mA. The data was recorded within a 2θ range of 5-10 ^{o}, with step size of 0.03 ^{o} and a count speed of ~0.5 ^{o}/min.

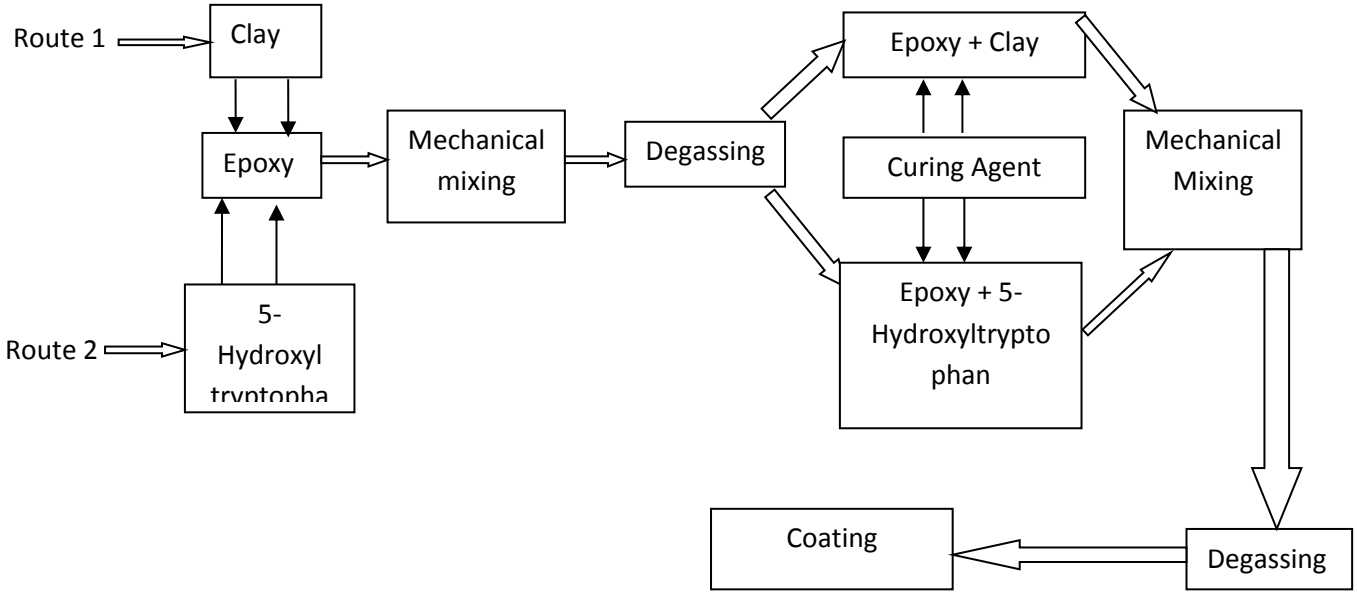

Figure 3.2 Preparation methods of epoxy composites

3.2.4 Scribe /Knife Tests Corrosion Experiments

The susceptibility of the coatings to blistering or adhesion was characterized using scribe testing. The scribe tests were performed in accordance with ASTM 870-02 [71] and ASTM 1654 procedures (Surfaces et al., 2018), [32]. A knife with a width of 0.58 mm was used to conduct the test at room temperature (~25 ^{0}C). The scribe penetrated all the organic coating layers on the samples. After scribe testing, samples were immersed in acidic and neutral 3.5 wt. % NaCl solutions in deionized water. The pH of the solution was controlled by adding 1M HCL into the NaCl solution until the pH of the solution was adjusted to pH of 3. Photographs of each sample were obtained at different time intervals up to a period of 90 days of exposure to 3.5 wt. % NaCl acidified to a pH of 3 and a neutral solution. These were used to characterize the extent of blistering on the scribed and exposed surfaces. The scribed samples were also investigated for creepage and blistering around the scribed and un-scribed areas of the coated samples. This was done in accordance with the ASTM 1654-08 code. The samples were each rinsed at the end of each experiment, using a gentle stream of water at room temperature (25 ^{o}C). The loose coatings along the scribed area were then removed with a knife (within 15 minutes of exposure) prior to the investigation of creepage. The discolored areas of the samples, due to corrosion, were characterized in accordance with the ASTM 1654-08 code. Six measurements of the widths of the corrosion zone were obtained at uniform distances along the scribed area, in accordance with the ASTM standard 1654-08. The arithmetic mean of the measured zone (for each sample) was also computed. This was used to calculate the rust creepage (C) given by equation (1):

$$C = \frac{w_c - w}{2} C = \frac{w_c - w}{2} \qquad (3.1)$$

where w_c w_c is the mean overall width of the corrosion zone and w is the width of the original scribe.

3.2.5 Electrochemical Impedance Spectroscopy (EIS)

In order to prepare the epoxy-coated mild steel panels for electrochemical testing, an electrochemical masking tape (SKU 990-00254, by Gamry Instruments, Worcester, MA, USA) was used to define the working area of the coated metal substrates during the tests. Microstructures of the coated samples are presented in **Figure 3.5.** Electrochemical measurements were carried out using a Versa STAT 3 studio (Princeton Applied Research software). The Versa STAT studio was equipped with a 3 electrode system in a K047 corrosion kit. The epoxy coated steel coupons served as the working electrode. Ag/AgCl was used as the reference electrode, while a graphite rod served as the counter electrode with an exposed area of 1 cm^2 that defined the working electrodes. EIS was used to study the corrosion resistance of the coated panels in which the barrier properties of all the different composite coatings were investigated. EIS was performed in electrolytes that contained 3.5 wt. % NaCl with pH values of 3 and 7. The EIS measurements were obtained from the coated immersed steel samples using the Versa STAT studio system. The steel was polarized at 10 mV. An open circuit potential (E_{oc}) was applied with an alternating current (AC) signal with frequencies between 100 kHz to 10 mHz (10 points per decade).

3.3. Results and Discussion

3.3.1 Fourier Transform Infrared Spectroscopy (FTIR)

Functional group analysis was carried out using Fourier Transform Infrared Spectroscopy (FTIR). This was used to examine possible interactions between the composites and the epoxy. The FTIR peaks of 1507, 1559, 1636, 1653, 1654, and 1400-1000 cm^{-1} were associated with

aromatic rings for pristine epoxy, clay/epoxy, and HTP/epoxy, as shown in **Figure 3.3**. The peak at 3481 cm^{-1} (in the 5-HTP/epoxy spectra) indicated the presence of 5-HTP in HTP/epoxy. The absorption band 668 cm^{-1} indicated the presence of aromatic C-H bending. The peaks observed at 2343 and 2360 cm^{-1} indicate the presence of CO_2. HTP/epoxy and clay/epoxy had similar functional groups with similar absorbance signifying a similar adhesion behavior of the two composites due the presence of O-H bonds for bonding with steel.

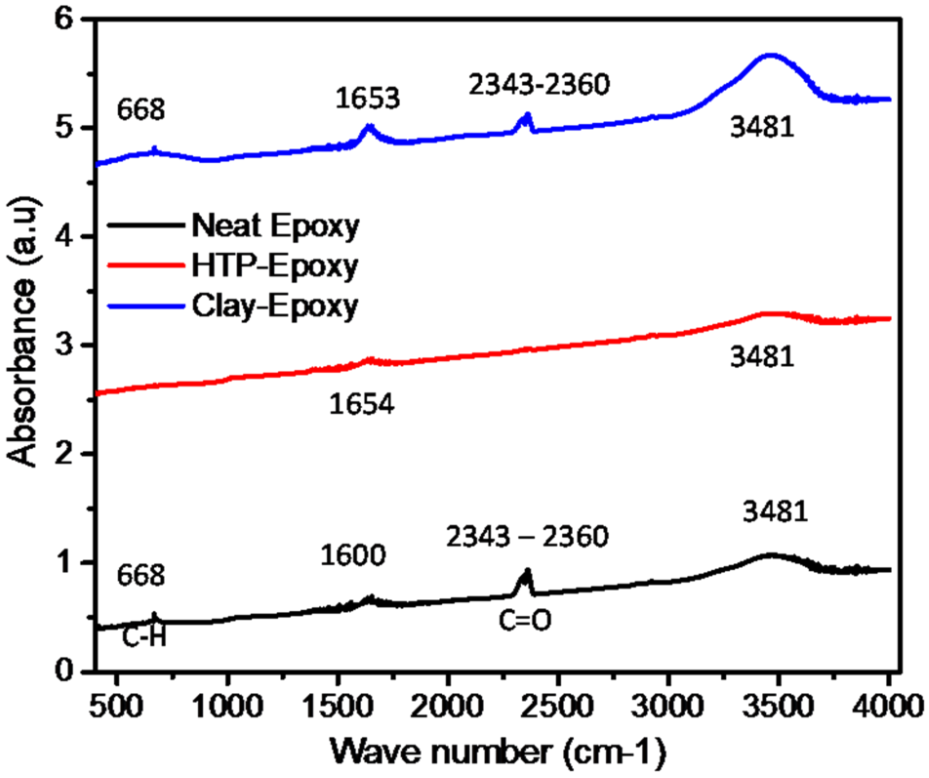

Figure 3.3 FTIR plots of pristine epoxy, clay/epoxy and HTP/epoxy

3.3.2 Electrochemical Impedance Spectroscopy (EIS)

The results of the EIS are presented in **Figure 3.4** in which the Nyquist plots are presented for the three types of coated steel surfaces. The Nyquist plots are characterized by semicircles with inductive loops. This is attributed to the adsorption of an intermediate product during corrosion reaction. In general, the higher the diameter of the semicircle (the charge transfer resistance), the lower the corrosion rate. The radii of the plots decreased with increasing immersion time. This is

consistent with the decrease in the corrosion resistance of the coated steel surface. All the samples were found to exhibit semicircular loops at different impedance values. However, the HTP/epoxy coatings exhibited the highest charge transfer resistance during the first 12 days of environmental exposure. The impedance plots also revealed the dominance of coating capacitance in the high frequency regime and coating resistance in the low frequency regime of about $2x10^5\ \Omega m^2$. This is attributed to the thickness of the coatings, which were about 0.5 mm thick. The second semicircles (observed at the low frequency regime in some of the samples) suggest that the electrochemical reactions occur at the metal/coating interfaces. At this stage, the diffusion of electrolytes into the coating is complete. The electrolyte phase also reaches the metal/coating interface, prior to the growth of the blisters as shown in **Figure 3.7** (interfacial cracking and delamination), and the corrosion of the steel substrate (**Figures 3.4 (a, b, c, d, e, and f**)). The fitted plots for 97 days of exposure are presented in **Figures 3.4 (e) and (f).** A 1 mm size of blister was observed for epoxy samples exposed at pH of 3 while all other samples blistered at different sizes ranging from 1 mm, 2 mm to 4 mm in the corroding environment of pH=7 after 90 days of experiment. The result showed that the composite's corrosion protection generally depends on the pH of the corroding environment. The Nyquist plots were fitted using a non-linear regression analysis

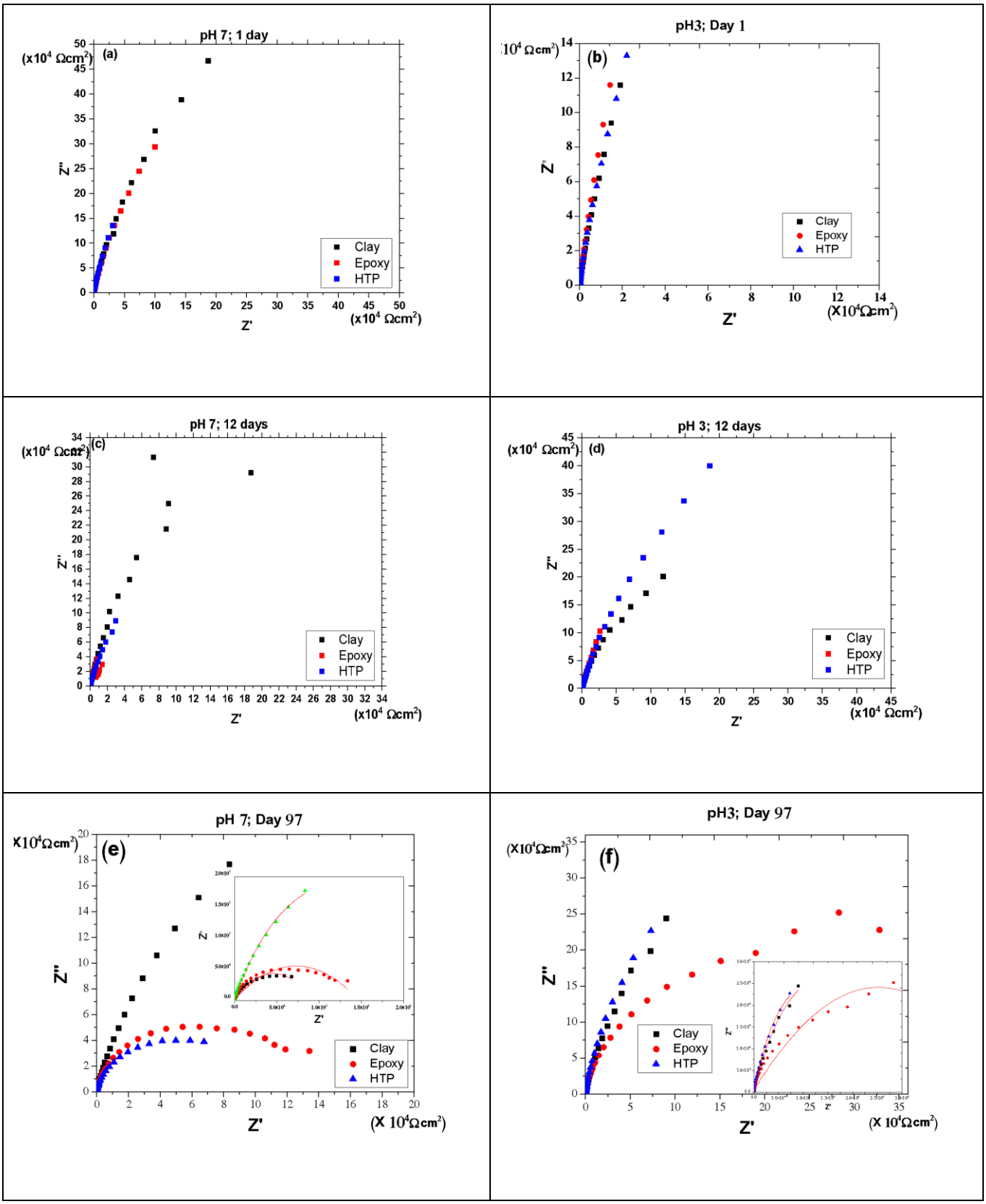

Figure 3.4 Typical Nyquist plots for Pristine Epoxy, HTP/Epoxy and Clay/epoxy for 1, 12 and 97 days of exposure

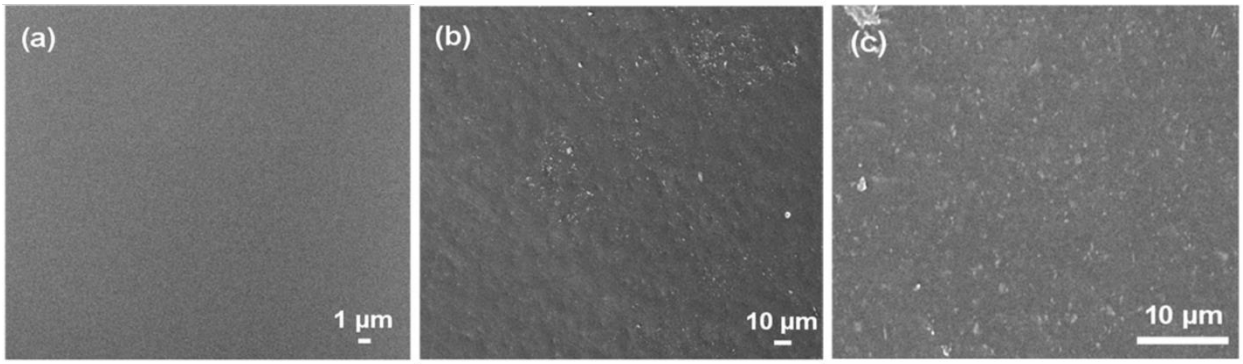

Figure 3.5 Scanning Electron Microscopy (SEM) images of epoxy (a), epoxy/clay composites (b) and epoxy/HTP composites (c)

3.3.3 Scribe Testing

The creepage and ratings data obtained from scribed areas on samples exposed for 90 days are summarized in Table 2 (for pH of 7) and Table 3 (for pH of 3). The HTP samples exhibited good creepage/ratings. The best ratings were obtained for the acidic environment with a pH of 3, with no blistering occurring at the scribed areas as shown in **Figure 3.6**. Furthermore, pristine epoxy and epoxy/clay samples exhibited the lowest creepage/ratings, with no blistering in the scribed areas. These results reveal that HTP/epoxy coatings exhibited better adhesion [90] which is a very important parameter of corrosion resistance of a coated metal.

Table 3.2 Mean creepage from scribe areas on samples observed for 90 days for pH of 7 (E, pristine epoxy sample, C, epoxy/clay samples and HTP, 5-Hydroxyltriptophane samples.)

Coatings	**Duration (days)**	**Creepage**	**Rating**
E1	90	0.91	8
E2	90	0.30	9
C1	90	1.10	7
C2	90	0.86	8

HTP 1	90	0.41	9
HTP 2	90	0.36	9

Table 3.3: Mean creepage from scribed areas on samples immersed at pH of 3 for 90 days

According to the ASTM 714-02 Standard, the scribed areas of the all the samples had no blisters

Coatings	**Duration (days)**	**Creepage**	**Rating**
E1	90	0.42	9
E2	90	0.20	9
C1	90	0.30	9
C2	90	0.10	9
HTP1	90	0.50	9
HTP 2	90	0.06	9

According to the ASTM 714-02 Standard, the scribed areas of all the samples had no blisters. (**Tables 2 and 3**). Interestingly, the corrosion products of samples in the corrosion environment with a pH of 3 had less corrosion products at the scribe area which is reflected by the creepage rating in T**able 2** and the image in **Figure 3.6.** It can also be deduced that the interface at HTP/epoxy had a better adhesion and possibly offered a passivating effect on the metal than clay/epoxy and pristine epoxy. Prior work by [90] on the corrosion inhibition of 5-HTP in acidic environments, and the effect of scribe test on coated metal had similar results. According to [90], as soon as a sample is scribed, the coating/metal interface becomes an area of investigation.

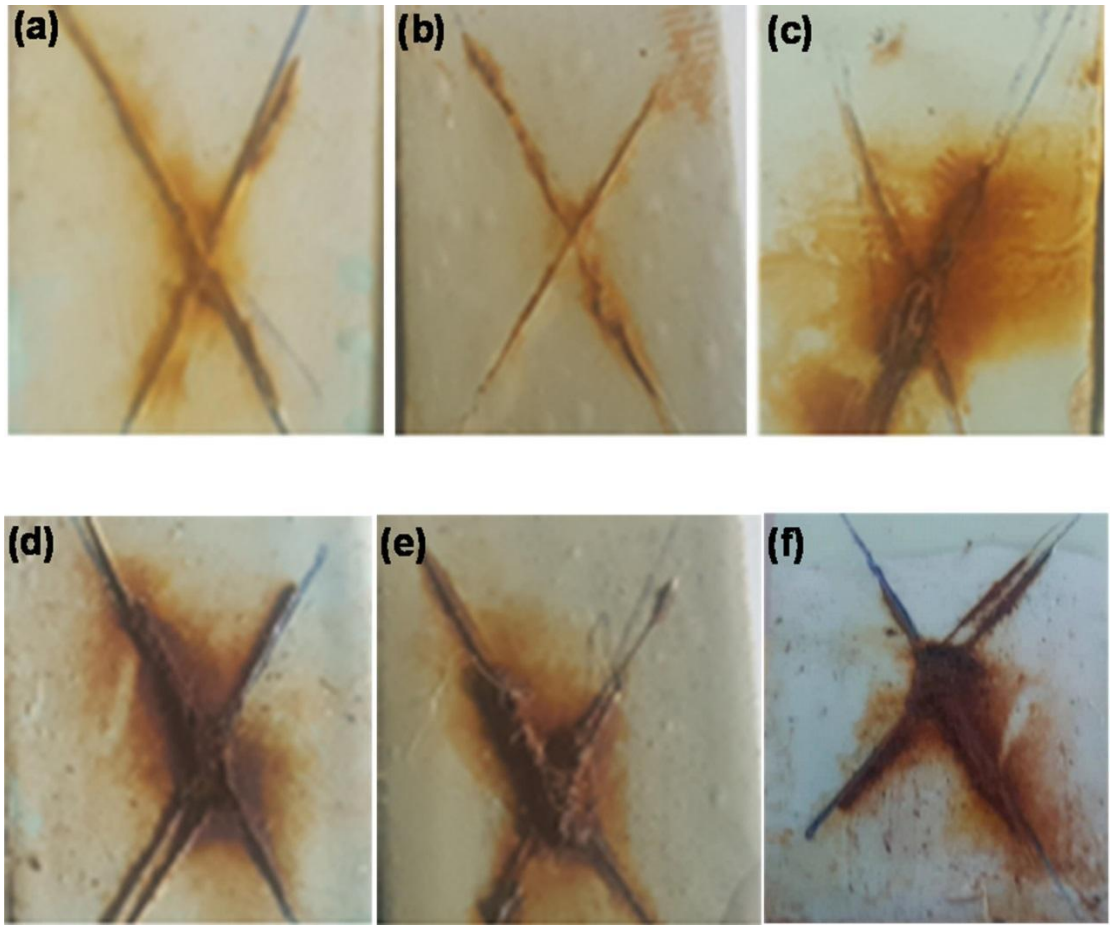

Figure 3.6 Photographs of scribed samples exposed to acid (pH=3: (a), (b), (c)) and neutral (pH=7: (d), (e), (f)) NaCl solutions for 90 days; Neat epoxy (a, d); HTP-Epoxy (b, e) and Clay-Epoxy (c, f).

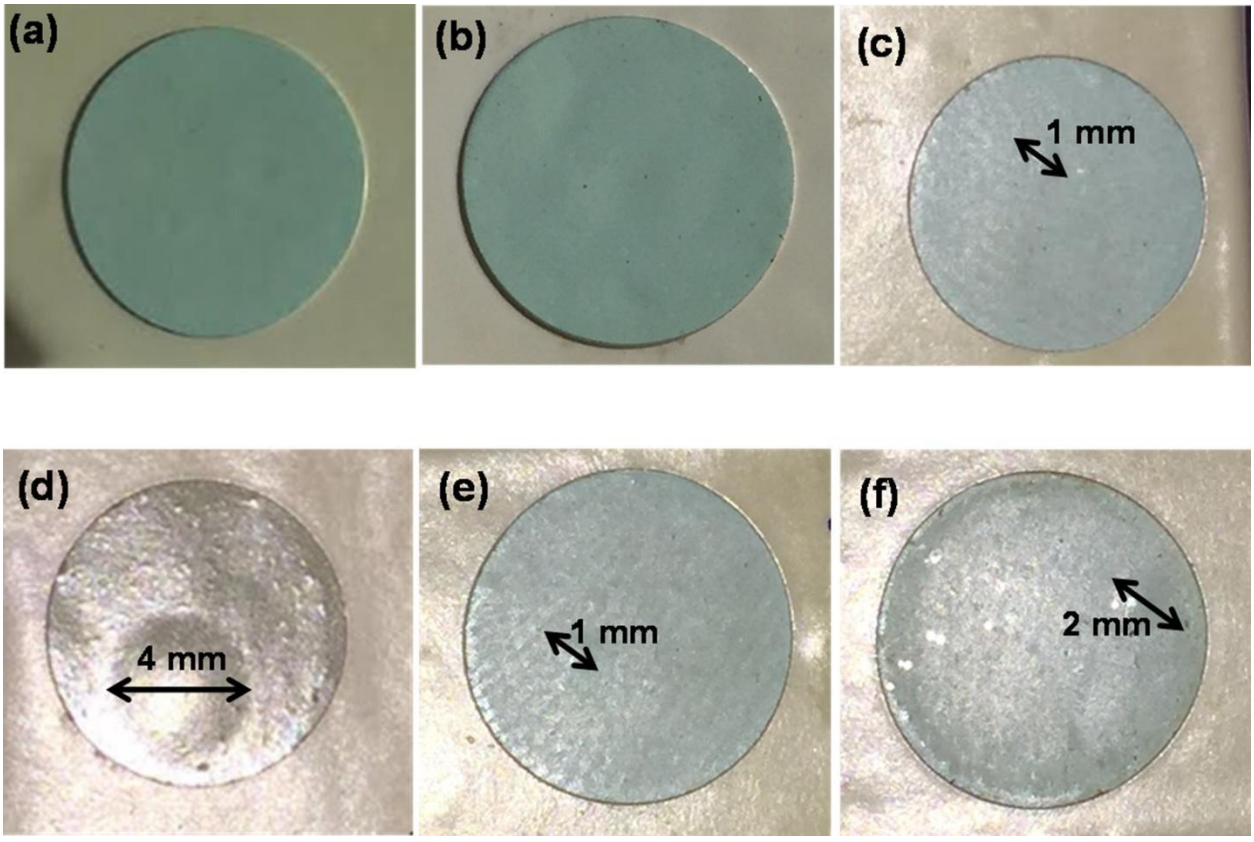

Figure 3.7 Blister formation after 97 days of exposure at different pH during EIS: (a) HTP coating (pH=3); (b) clay coating (pH=3); (c) epoxy coating (pH=3); (d) HTP coating (pH=7); (e) clay coating (pH=7), and (f) epoxy coating (pH=7)

3.3.4 X-Ray Diffraction (XRD) Analysis

Typical XRD peaks obtained for the HTP Epoxy, clay epoxy and pristine epoxy structures are presented in **Figure 3.8**. The results are consistent with prior reports in the literature [10]. The interlayer d-spacing (d_{001}) of pure C30B as reported by Zaarei et al [10], estimated that the position of the intense diffraction peak of the (100) plane, is 1.88 nm. In addition, the weak peak of the (200) plane is placed at higher diffraction angles, corresponding to a d-spacing (d_{002}) of 0.94 nm. There is also a shift to lower 2θ, from 10^{0} in pristine epoxy to 9.9^{0} in HTP/epoxy and clay/epoxy, which had a higher intensity.

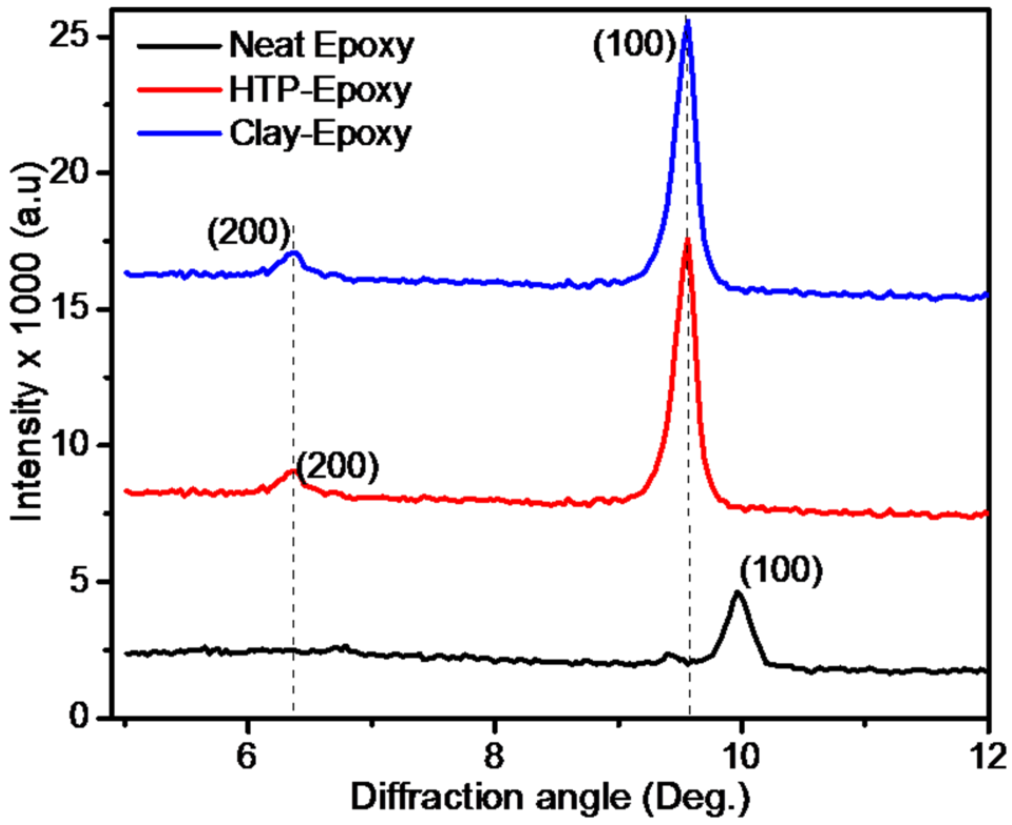

Figure 3.8 XRD patterns obtained from HTP/epoxy, Clay/epoxy and pristine epoxy samples

3.3.5. Thermo-Gravimetric Analysis (TGA)

Figure 3.9 presents the thermogravimetric analyses of the pristine epoxy, epoxy/clay and epoxy/HTP and their decomposition temperature. Pristine epoxy was used as a reference. This was carried out in nitrogen at room temperature (25^{o}C) at a heating rate of 10^{0}C/min. The corresponding mass loss of moisture was seen to be about 3.5% HTP/epoxy, 4% for clay/epoxy and 6% for pristine epoxy. The initial degradation temperatures, cited as the characteristic temperature for assessing the thermal stability, were measured by determining the temperature at which 5% degradation occurs [100]. Pristine epoxy polymer matrix decomposed at 366.6^{o}C, epoxy/clay at 368.6^{0}C and HTP/epoxy at $370.1\ ^{o}$C at a heating rate of 10^{o}C/min.

It has been established in the literature that the inclusion of fillers increases the thermal stability of the composite system [100] [101]. The results revealed that the inclusion of montmorillonite and 5-hydroxyltryptophan improved the thermal degradation of the composites.

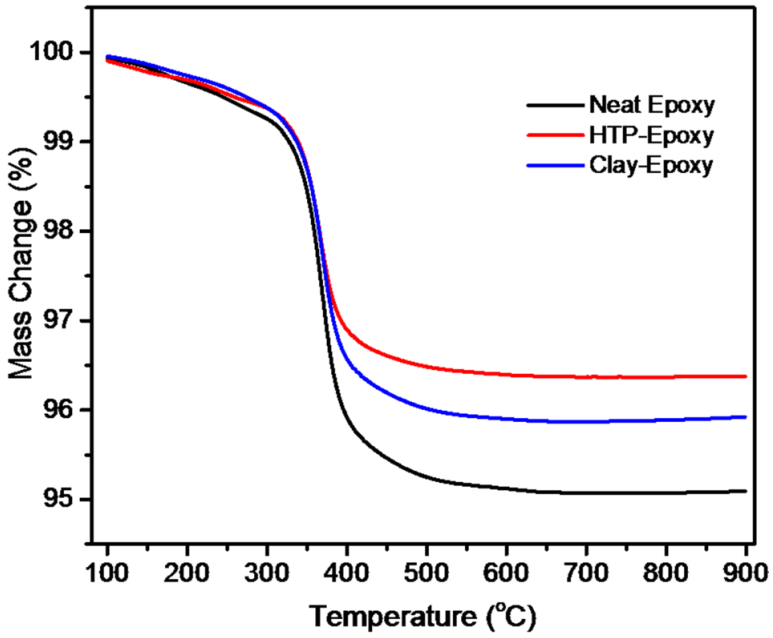

Figure 3.9 TGA plots obtained from pristine epoxy, clay/epoxy and HTP/epoxy

3.4 Implications

The implications of the current work are quite significant. First, the results show that fillers such as 5-HTP and cloisite clay particles can be used to enhance the corrosion resistance of epoxy-based coatings in acidic or neutral environments. However, the enhancements depend on the pH, as shown in the current work. Similar improvements have been reported by other researchers [10] that have used fillers to enhance the corrosion resistance of epoxy-based coatings. The improvements are attributed to the interactions between the filler materials and aqueous species. In the case of the cloisite clay particles and the 5-HTP particles, the fillers behave in ways that can delay the transport of aqueous species to the steel substrate. *In-situ* reactions and chemisorption processes can also occur in ways that reduce the transport of aqueous species to

the substrate. Further work is clearly needed to provide mechanistic insights into such phenomena. In any case, the results of the current study suggest that cloisite clay particles and the 5-HTP fillers can be used to enhance the corrosion resistance of epoxy coatings on mild steel substrate that was used in this study.

3.5 Conclusions

This paper presents the results of an experimental study of corrosion inhibition of mild steel that was coated with epoxy and epoxy composites that contained 5-HTP and cloisite 30B clay micro-particles. Salient conclusions arising from this study are summarized below. The electrochemical impedance spectroscopy and the scribe test revealed that corrosion is pH- dependent. Furthermore, less corrosion products were seen on the scribe areas of the HTP samples in the scribe test in the pH of 3 corroding environments. This signifies a better adhesion of coating in that environment for HTP/epoxy coatings. This was also confirmed by Figure 6 where just 1 mm size of blister was observed for epoxy sample exposed at pH of 3 while all the other sample blistered at different sizes ranging from 1mm, 2mm and 4mm in the corroding environment of pH=7 after 90 days of EIS experiments.

The TGA results reveal that the HTP/epoxy samples had the least mass loss due to moisture content compared to clay/epoxy and pristine epoxy. This possibly might be due to the fact that the blockage of the polymer gallery by the fillers was more evident in HTP in the polymer coating. Hence, the HTP/epoxy composite coating has a better heat resistance than the clay/epoxy and pristine epoxy. The FTIR spectra reveal the presence of O-H bonds in HTP/epoxy which acts as the bonding site of the coating just like in clay/epoxy. Hence, HTP could be a potential filler for epoxy coatings for use in coating steel pipes and tanks. It is recommended that further work should be done on the char yield to determine the flame

resistance of the HTP composite. One of the limitations of this work was that the TGA test was performed only in a nitrogen environment. Further work needs to be done to perform TGA in air for better comparisons. The enhanced thermal stability of HTP/epoxy nanocomposites, in combination with the high corrosion protection, makes them attractive candidates for various coating applications

3.6 REFERENCES

[1] Z. T. Khodair, A. A. Khadom, and H. A. Jasim, "Corrosion protection of mild steel in different aqueous media via epoxy/nanomaterial coating: Preparation, characterization and mathematical views," *J. Mater. Res. Technol.*, no. x x, pp. 1–12, 2018.

[2] "The Evolution of Pipeline Coatings [Gas Exploration]KTA University." [Online]. Available: https://ktauniversity.com/evolution-pipeline-coatings/. [Accessed: 19-Jun-2019].

[3] "Epoxy Resin Market Analysis and Industry Forecast 2022." [Online]. Available: https://www.alliedmarketresearch.com/epoxy-resins-market. [Accessed: 19-Jun-2019].

[4] A. U. Malik, S. Ahmad, I. Andijani, F. Al-muaili, T. L. Prakash, and J. O. Hara, "Corrosion Protection Evaluation of Some Organic Coatings in Water Transmission Lines 1," no. November 1999, pp. 1966–1827, 1999.

[5] Z. Chen, K. Zhou, X. Lu, and Y. C. Lam, "A review on the mechanical methods for evaluating coating adhesion," *Acta Mech.*, vol. 225, no. 2, pp. 431–452, 2014.

[6] A. Jumahat, C. Soutis, N. Ahmad, and W. M. Wan Mohamed, "Fracture toughness of nanomodified-epoxy systems," *Appl. Mech. Mater.*, vol. 393, pp. 206–211, 2013.

[7] A. Jumahat, C. Soutis, F. R. Jones, and A. Hodzic, "Compressive behaviour of nanoclay modified aerospace grade epoxy polymer," *Plast. Rubber Compos.*, vol. 41, no. 6, pp. 225–232, 2012.

[8] N. Saba, M. Jawaid, and M. T. H. Sultan, *An overview of mechanical and physical testing of composite materials*. Elsevier Ltd, 2019.

[9] R. S. R. Kalidindi and R. Subasri, *Sol-gel nanocomposite hard coatings*. Elsevier Ltd, 2014.

[10] O. F. Ngasoh, V. C. Anye, B. Agyei-Tuffour, O. K. Oyewole, P. A. Onwualu, and W. O. Soboyejo, "Corrosion behavior of 5-hydroxytryptophan (HTP)/epoxy and clay particle-reinforced epoxy composite steel coatings," *Cogent Eng.*, vol. 7, no. 1, 2020.

[11] R. A. Gledhill, A. J. Kinloch, S. Yamini, and R. J. Young, "Relationship between mechanical properties of and crack progogation in epoxy resin adhesives," *Polymer (Guildf).*, vol. 19, no. 5, pp. 574–582, 1978.

[12] S.-R. Kim and J. A. Nairn, "Fracture mechanics analysis of coating/substrate systems: Part II: Experiments in bending," *Eng. Fract. Mech.*, vol. 65, no. 5, pp. 595–607, 2000.

[13] L. Banks-sills and J. Schwartz, "Crack paths in adhesive bonds," pp. 225–234, 2002.

[14] N. Rahbar *et al.*, "Adhesion and interfacial fracture toughness between hard and soft materials," *J. Appl. Phys.*, vol. 104, no. 10, 2008.

[15] J. S. Wang and Z. Suo, "Experimental determination of interfacial toughness curves using Brazil-nut-sandwiches," *Acta Metall. Mater.*, vol. 38, no. 7, pp. 1279–1290, 1990.

[16] T. M. Tong, T. Tan, N. Rahbar, and W. O. Soboyejo, "Mode Mixity Dependence of Interfacial Fracture Toughness in Organic Electronic Structures (September 2012)," vol. 14, no. September 2012, pp. 291–299, 2013.

[17] N. Rahbar, Y. Yang, and W. Soboyejo, "Mixed mode fracture of dental interfaces," vol. 488, pp. 381–388, 2008.

[18] J. W. Hutchinson, *Mixed Mode Cracking in Layered Materials*, vol. 29. 1992.

[19] Atkinson. C, Smelser. R.E et al. "Combined Mode Fracture Via the cracked Brazillian Disk Test, Vol. 18, No. 4, pp. 279-2921, April 1982.

[20] M. Hoerantner, T. Leijtens, G. Eperon, N. Renewable, and M. D. Mcgehee, "The Potential of Multijunction Perovskite Solar," no. October, 2017.

[21] E. D. Orthogonal, E. Wedges, U. Normal, and S. Loading, “1 B | I discussion,” vol. 31, pp. 650–652, 2016.

[22] L. Shen, L. Wang, T. Liu, and C. He, “Nanoindentation and Morphological Studies of Epoxy Nanocomposites,” pp. 1358–1366, 2006.

[23] W. C. Oliver and G. M. Pharr, “An Improved Technique for Determining Hardness and Elastic Modulus Using Load and Displacement Sensing Indentation Experiments,” Journal of Biomedical Meterials Research, Vol. 7, No. 6, 1992, pp. 1564-1583. doi:10.1557/JMR.1992.1564

[24] C. P. Systems, F. Corrosion, and F. Perspectives, “Corrosion Protection Systems and Fatigue Corrosion Future Perspectives,” pp. 1–51, 2017.

[25] Kusmono, M. W. Wildan, and Z. A. Mohd Ishak, “Preparation and properties of clay-reinforced epoxy nanocomposites,” *Int. J. Polym. Sci.*, vol. 2013, 2013.

[26] G. Khanbabaei, J. Aalaie, A. Rahmatpour, A. Khoshniyat, and M. A. Gharabadian, “Preparation and properties of epoxy-clay nanocomposites,” *J. Macromol. Sci. Part B Phys.*, vol. 46, no. 5, pp. 975–986, 2007.

[27] A. A. Azeez, K. Y. Rhee, S. J. Park, and D. Hui, “Epoxy clay nanocomposites - Processing, properties and applications: A review,” *Compos. Part B Eng.*, vol. 45, no. 1, pp. 308–320, 2013.

[28] W. O. Soboyejo, R. J. Lederich, and S. M. L. Sastry, “Mechanical behavior of damage tolerant TiB whisker-reinforced in situ titanium matrix composites,” *Acta Metall. Mater.*, vol. 42, no. 8, pp. 2579–2591, 1994.

[29] BYK Additives &Instruments, “Technical Information B-RI 10 Cloisite Nanocomposite Additive for Halogan free Flame Retardants,” pp. 1–4, 2013.

[30] D. Brabazon, *Chapter 16. Nanocharacterization techniques for dental implant development*. Elsevier Inc., 2018.

[31] F. O. Square, “Determination of Stress-Strain Curve through Berkovich Indentation

Testing A.M.S. Dias, 1," vol. 637, pp. 1186–1193, 2010.

[32] "Strong Adhesives for Bonding Metal, Glass & Plastic | Permabond." .

[33] A. Kepstan and S. A. Polymers, *10 High-Temperature Polymers*. 2015.

[34] A. Arciniegas and L. E. Amaya, "Poisson's ratio," *New Trends in Ophthalmology*, vol. 4, no. 1. pp. 25–46, 1989.

[35] A. G. Evans, "Effects of Non-Planarity on the Mixed Mode Fracture Resistance of Bimaterial Interfaces," vol. 37, no. 3, pp. 909–916, 1989.

[36] Bernard Budiansky, John C. Amazigo and Anthony G. Evans, "Small-Scale Bridging and the Fracture Toughness of Particulate-Reinforced Ceramics, Journal of the Mechanics and Physics of Solids, vol. 36, no. 2, 167-187, 1988.

[37] M. R. Ayatollahi, S. Doagou-rad, and S. Shadlou, "Nano- / Microscale Investigation of Tribological and Mechanical Properties of Epoxy / MWNT Nanocomposites," pp. 1–13, 2012.

[38] M. Meyer, "wI I," vol. 1, pp. 270–275, 1993.

[39] M. P. Manoharan, A. Sharma, A. V. Desai, M. A. Haque, C. E. Bakis, and K. W. Wang, "The interfacial strength of carbon nanofiber epoxy composite using single fiber pullout experiments," *Nanotechnology*, vol. 20, no. 29, 2009.

Chapter 4

Mechanical Properties of Epoxy/Clay Composite Coatings on an X65 Steel Substrate

Introduction

Epoxy/clay composites have attractive combinations of mechanical and interfacial properties [1] that have made them suitable for application in steel structures in oil and gas pipelines, storage tanks and structural applications [2]. They are also used extensively [3] [4] as coatings for the protection of steel. Furthermore, under service conditions, the durability of epoxy/montmorillonite clay composites depends on the mechanical and tribological properties of the montmorillonite clay fillers [5] in epoxy composites coatings. Clay fillers have been used due to their high availability and good thermal stability, in addition to the improved mechanical and fillers properties of their composites [6] and [7]. However, epoxy coatings are prone to damage by surface stresses and indentation/wear phenomena that can occur during service [8], [9]. Coating materials can also result due to abrasive wear phenomena [10]. Nano-indentation testing can, therefore, be used to evaluate the coating resistance and durability of clay-reinforced epoxy coatings. Furthermore, since most epoxy/clay composite-coated or epoxy/clay composites-bonded steel structures are subjected to multi-axial loading conditions [4], there is therefore a need for interfacial fracture studies for interfaces between steels and epoxy/clay composites-base coatings.

Several interfacial fracture mechanics specimen geometries have been used to study the mode mixity dependence of interfacial fracture toughness [5]. These include double cantilever beam specimen; four-point bend test specimen, Brazil-nut specimen, and indentation testing techniques [5]. These studies have shown that the interfacial fracture toughness depends strongly on the mode mixity [11]. The crack path criteria have also been shown to depend strongly on the mode mixity [11], while the crack/microstructure interactions depend on the mechanical properties of the reinforcements that are often incorporated into epoxy adhesive coatings [12]. Unlike most interfacial fracture mechanics specimen geometries, which are often only applicable to limited ranges of mode mixity [13], Brazil disk specimen geometries can be used to study the mode mixity dependence of interfacial fracture toughness over the complete range of mode mixity between pure mode I and pure mode II fracture [14] . This can be achieved by controlling the

angular orientations of the notches (**Figure 4.1d**) (relative to the vertical axis). Brazil disk specimens can also be loaded simply by applying compressive vertical loads to the oriented samples with simple loading fixtures [14]. The effects of negative mode mixities may also be studied using Brazil disk specimen geometries with appropriate mode mixity mismatch [13].

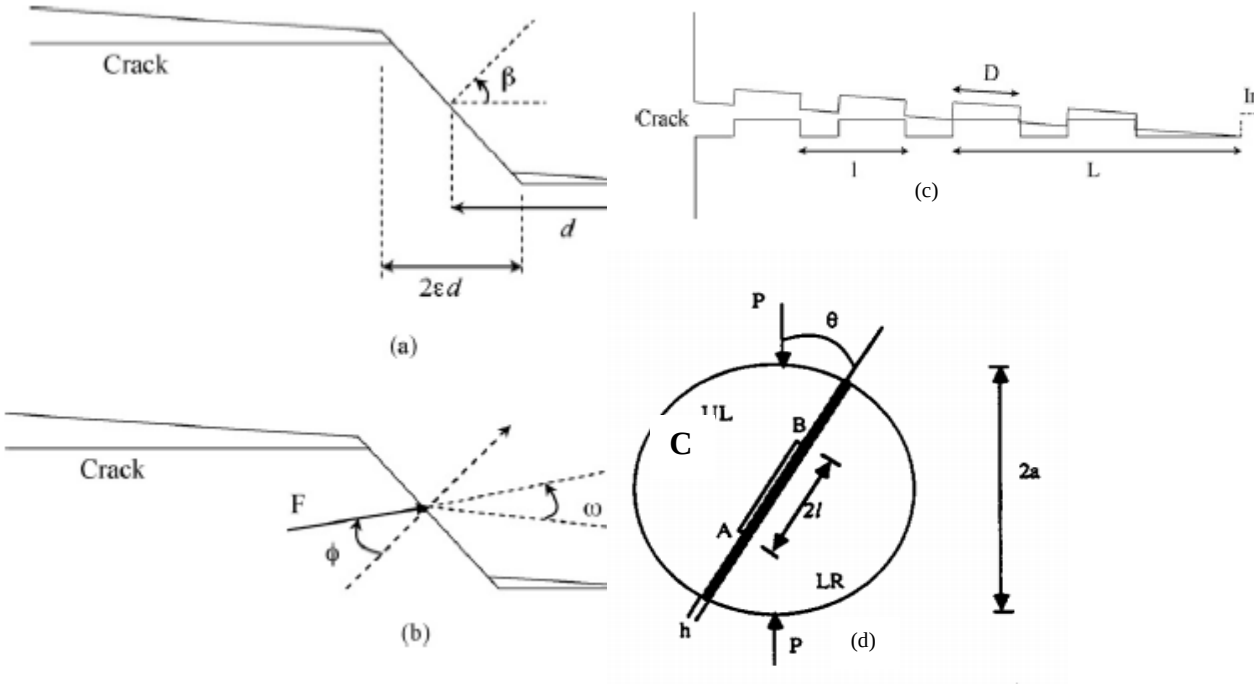

Figure 4.1: Schematics of Row model (a&b), Zone Model (c) and Brazil disk specimen (d). (Adapted from [15] **[19] with permission from Elsevier)**

Prior work on interfacial fracture between bi-material interfaces has explored ceramic/epoxy interfaces [14] for applications in dentistry and medicine [16] [17], and electronics packaging [16]. These have shown that the crack paths depend strongly on the ratio of the interfacial fracture toughness, to the interfacial energy release rate to the substrate fracture toughness, the substrate energy release rate (G_s) and the mode mixity/phase angle, ψ.

Rahbar et al. [14] have shown that the crack path selection criteria depend on crack interactions with ceramic particles that are present in epoxy composites often used as coatings. Rahbar et al. [14] and Tong et al. [16] have also shown that cracks can kink in and out of interfaces,

depending on the nature of the interactions between the crack-tip plastic zones and deformation fields around the nanoparticles. These result in deflected crack profiles that leave behind regions of crack bridging ligaments and distributed micro cracks. The shielding contributions from the cracking configurations have been estimated by Rahbar et al. [14] and Tong et al. [16] using zone and row models developed by Hutchinson et al. [18]. The zone and row models have also been used to explain the mode mixity dependence of the interfacial fracture toughness of organic electronic structures and ceramic/epoxy composite interfaces that are used in dentistry. This paper presents the results of a combined experimental and theoretical study of the interfacial and coating mechanical properties of epoxy/clay composites coatings on a mild steel substrate. The mechanical and interfacial properties of epoxy composites coatings (reinforced with montmorillonite clay particles) are studied using nano-indentation and Brazil disk techniques which are used to determine the Young's moduli, hardness values and the nano-wear characteristics of the composite coatings. The measured mechanical and interfacial properties are then compared with predictions from composite theories and performance criteria. The mode mixity dependence of the interfacial fracture toughness (between the epoxy/clay composite coatings and mild steel substrate) is also elucidated before discussing the implications of the current work for the design of epoxy/clay-composite coated or bonded steel structures.

1. THEORY

Atkinson [19] has shown that the mode I and mode II stress intensity factors, K_I and K_{II}, for the Brazil disk specimen are given by:

$$K_I = f_I \frac{F}{\pi t r}\sqrt{\pi a} \tag{4.1}$$

$$K_{II} = \mp f_{II} \frac{F}{\pi t r}\sqrt{\pi a} \tag{4.2}$$

where a is half of the crack length, the positive and negative signs correspond to the two tips, F is the applied load, t is the specimen thickness and r is the radius of the disk, while $f_I \; and \; f_{II}$ are the respective dimensionless factors for mode I and mode II. It is important to note here that the two dimensionless factors are functions of loading angle and crack size ($\frac{a}{r}$) [20]. The mode mixity/phase angle is given by [21]:

$$\Psi = \left(\frac{K_I}{K_{II}}\right) + \omega + \in ln\, ln\, \left(\frac{L}{h}\right) \tag{4.3}$$

where L is the length for the loading mode, h is the combined thickness of the sandwich materials, ω is the phase shift due to elastic mismatch and ∈ is the Dundurs parameter. The phase shift, ω, is a function of the Dundurs parameters α, β, and ∈, which are given in Table 1, [21]:

Table 4.1: Elastic mismatched parameters as adapted from [15]

Bimaterial	α	β	ϵ
Aluminum/epoxy	0.90	0.218	-0.071
Brass/epoxy	0.94	0.228	-0.074
Steel/epoxy	0.96	0.232	-0.075
Plexiglass/epoxy	-0.15	-0.029	0.009

$$\alpha = \frac{\frac{1-\vartheta_2}{\mu_2} - \frac{1-\vartheta_1}{\mu_1}}{\frac{1-\vartheta_2}{\mu_2} + \frac{1-\vartheta_1}{\mu_1}} \tag{4.4}$$

$$\beta = \frac{1}{2}\frac{\frac{1-2\vartheta_2}{\mu_2} - \frac{1-2\vartheta_1}{\mu_1}}{\frac{1-\vartheta_2}{\mu_2} + \frac{1-\vartheta_1}{\mu_1}} \tag{4.5}$$

$$\in = \frac{1}{2\pi} ln \frac{1-\beta}{1+\beta} \tag{4.6}$$

where μ_1 and μ_2 are the shear moduli of materials 1 and 2 respectfully. Note that in the case of the epoxy/steel system, $\omega = -13^0$ which falls within the range of $\omega = -14^0$ to -8^0 expected for metal/epoxy systems [15].

The interfacial fracture toughness between the two dissimilar materials can be estimated as the energy release rate at the tip of the interfacial crack between the bilayers. The mode I and mode II energy release rates are given by [17]:

$$G_I = \frac{K_I^2}{E^*} \tag{4.7}$$

$$G_{II} = \frac{K_{II}^2}{E^*} \tag{4.8}$$

where the total energy release rate (G_T) is given by:

$$G_T = G_I + G_{II} = \frac{1}{E^*}(K_I^2 + K_{II}^2) \quad (4.9)$$

where E^* is the Young's modulus, E, for plane stress conditions. In the case of plane strain, E^* is given by:

$$E^* = \frac{E}{1-\vartheta^2} \quad (4.10)$$

Finally, an effective E^* can be determined relative to the thickness of the bilayer material structure. This is given by [14];

$$\frac{1}{E^*} = \frac{\Gamma_1}{E_1} + \frac{\Gamma_2}{E_2} \quad (4.11)$$

where

$$\Gamma_1 = \frac{t_1}{t_1+t_2}, \text{ and } \Gamma_2 = \frac{t_2}{t_2+t_2} \quad (4.12)$$

2. Materials and Experimental Methods `

API X65 steel pipe materials were obtained from a pipeline factory (Schebite Construction Company, Bwari, Abuja, Nigeria). Both the epoxy base and the hardener were purchased from Sigma Coatings, Amsterdamseweg, Netherlands. The Cloisite 30B (C30 B) clay particles were procured from Southern Clay Products Inc. Texas, USA. They were mixed with epoxy to obtain epoxy/clay composites with clay particle volume fractions of 1 wt.%, 3 wt.% and 5 wt.%. These mixtures were then stirred with a magnetic stirrer for 2.5 hours at a rate of 1500 rpm. This was done at 50 ^{0}C to enable complete particle dispersion to occur. The resulting composites were

then degassed in a vacuum oven for 2 minutes. The curing agent was also added and mixed with a spatula prior to degassing in the vacuum oven for 30 seconds. Pure epoxy, without the clay reinforcement, was also prepared and studied as a control. The coating was formulated at a stoichiometric mixture of 2:1 base to hardener.

3.1 **Nano-indentation Testing**

Nano-indentation techniques were used to determine the Young's moduli and hardness values of the coatings. Details of the techniques are summarized in [22]. In these experiments, the Triboindenter T950 indentation system (Bruker, Minneapolis, MN, USA) was used. The indentation system was instrumented with a 3 sided pyramidal diamond Berkovic indenter tip with a triangular tip radius of 20 nm and an included angle of 142.3^0. The loading rate was fixed to minimize the possible strain hardening strain hardening effects on the measurements [22]. Furthermore, to minimize the possible creep effects, a total holding time of 2 seconds was applied. The indenter was calibrated prior to the indentation experiments, which were performed at a constant normal load of 8000 μN. The coating thickness on the X65 mild steel substrate was about 0.5 mm. The indentation tests were carried out at African University of Science and Technology, Abuja, Federal Capital Territory (FCT), Nigeria. For each sample, at least four indents were performed at different points on the surface.

The hardness values were calculated from the load–displacement curves using a method developed by Oliver and Pharr [23]. This gives:

$$H = \frac{F_{max}}{A} \tag{4.13}$$

F_{max} is the indentation load and A is the contact area.

$$A = 24.5h_f^2 \quad (4.14)$$

h_f is the contact depth of the indenter.

$$h_f = h_{max} - \varepsilon \frac{F_{max}}{S} \quad (4.15)$$

ε is the geometric constant for a pyramidal indenter and S is the contact stiffness of the material which can be considered as the slope of the unloading curve at the instant of peak load [22].

$$S = 2\beta\sqrt{\frac{A}{\pi}E_r} \quad (4.16)$$

β is the constant depending on the geometry of the indenter and E_r is the reduced Young's modulus.

$$\frac{1}{E_r} = \frac{1-\vartheta_s{}^2}{E_s} + \frac{1-\vartheta_i{}^2}{E_i} \quad (4.17)$$

E_i is given as 1140 GPa and ϑ_i as 0.07 are the respective Young's modulus and Poisson's ratio of the indenter. E and ϑ are the Young's modulus and Poisson's ratio of the sample. ϑ_s is estimated as 0.35 for polymeric materials [22].

3.2 Interfacial Fracture Testing

The halves of the Brazil disk geometry **(Table 4.2)** were machined using a Computer Aided Machine (CAM HAAS, Worcester, Massachusetts, USA) at Worcester Polytechnic Institute, Worcester, MA, USA. The resulting Brazil half disks had diameters of ~16 mm, thicknesses of ~5 mm and notch length of 1mm. The notch tip radii were ~0.5 mm. The rectangular diametral surface of the Brazil disk halves were ground with silicon carbide paper with grit sizes between 60 and 240 μm. The ground surfaces were then cleaned with acetone. A 3 wt.% formulation of the resulting epoxy composites was used for interfacial fracture testing. This has been found in literature (for clay-reinforced composites) to give 'optimum' properties in terms of the

combination of high hardness, high Young's moduli, and high strength [24] [25] [26] [27]. The degassed epoxy composite was dispensed onto the ground surfaces of two halves of the Brazil disks.

Table 4.2: Brazil Disk Specimen Geometry

Notch radius (l)[mm]	Disc radius (a)[mm]	Disc thickness (t)[mm]
1	8	5

The interfacial fracture toughness measurements were carried at WPI using an Instron Model 5848 servo-hydraulic mechanical testing machine (Instron, Canton, MA, USA) that was equipped with a 5 kN load cell. The notches in the Brazil nut specimens were oriented at different angles to the vertical axis, prior to compressive loading to failure under displacement control at a ramp rate of 0.001 mm/s. Both the load and displacement data were recorded during the tests that were controlled using the Bluehill Software Package (Instron, Canton, MA, USA). In this way, interfacial fracture toughness measurements were obtained for loading angles between 3^0 and 18^0. In selected cases, the loading of the Brazil disk specimens was stopped prior to complete interfacial fracture. This was done to enable the examination of the crack/microstructure interactions prior to the onset of catastrophic failure using a Scanning Electron Microscope (SEM) (EVO LS10, ZEISS, Massachusetts, USA.) at WPI. The sides of the specimens were coated with gold to enhance their conductivities and enable imaging in the SEM. The key features of the crack patterns were thus observed and measured, prior to incorporation into expressions for the estimation of crack-tip shielding levels from row and zone models [16].
After fracturing the specimens into two halves, via Scanning Electron Microscope (SEM) and EDS analysis. The insights from the SEM and EDS analysis were used to determine the crack paths that were associated with the measured mode mixity dependence on the interfacial toughness.

3. Modeling

4.1 Rule of Mixtures and Shear Lag Models

The effect of clay particles on the Young's moduli and strength of the epoxy/clay composites can be estimated using simple rule-of-mixture and shear lag models. The simple rule of mixture gives [28];

$$E_c = E_m V_m + \eta_{1e} E_f V_f; \quad (4.18a)$$

and

$$\sigma_c = \sigma_m V_m + \eta_{1s} \sigma_f V_f; \quad (4.18b)$$

where E is the Young's modulus, V is the volume fraction, and subscripts c, m and f correspond to the composite, matrix and clay reinforcement. The parameter η_f corresponds to the length efficiency factor. Furthermore, the shear lag model [28] gives:

$$\frac{E_c}{E_m} = V_m + V_f \left(\frac{E_f}{E_m}\right); \quad (4.19a)$$

$$\frac{\sigma_c}{\sigma_m} = 0.5 V_f \left(2 + \frac{1}{d}\right) + \left(1 - V_f\right); \quad (4.19b)$$

where X is given by:

$$x = \frac{1}{d}\left[(1 + V_m)\frac{E_f}{E_m}\, ln\, ln\, \left(V_f\right)^{\frac{-1}{2}}\right]^{\frac{-1}{2}}; \quad (4.19c)$$

where E_c, E_m and E_f are the respective Young's moduli of the composite, matrix and fillers; V_m and V_f are the respective volume fractions of matrix and fillers; and σ_c, σ_m and σ_f are the respective compressive strengths of the composite, matrix and filler; $\frac{l}{d}$ is the filler aspect ratio; n_{le}, n_{ls} are fillers efficiency factor for stiffness and strength, and υ_m is Poisson's ratio of the matrix. The aspect ratio is defined as the ratio of the dimension of the face of the platelet to its thickness.

The high aspect ratio makes the clays particles superior to all other conventional fillers or short glass fibers [29]. The mechanical properties that were used to determine the parameters in equations 4.18 and 4.19 are summarized in **Table 4.3**.

4.2 Indentation Models

The indentation stress is given by the following expression [30] [31]:

where P is the indentation load and a is the contact radius. The indentation stress is also defined as the ratio of the contact radius and effective tip radius [31] [32]. This is given by:

$$\sigma = \frac{P}{\pi a^2}, \quad (4.20)$$

Where the effective tip radius is given by:

$$a = \sqrt{\frac{contactarea}{\pi}} \quad (4.20a)$$

and

$$\varepsilon = \frac{a}{} \quad (4.20b)$$

where P is the indentation load, and h is the indentation depth, R_{eff} is the radius of the indenter, and $\sigma\ and\ \varepsilon$ are the stress and strain, respectively. Since the radius varies with normal load; there is a corresponding stress for each load value. Hence, the measured values of P and h correspond to points on stress-strain curves that are associated with the indentation experiments.

Table 4.3: Mechanical Properties of Clay and Epoxy Used in the Analytical Modeling

Properties	**Clay**	**Epoxy**
Compressive Strength ($\sigma\ (GP_a)$)	14.6	87
Young's Modulus ($\varepsilon\ GP_a$)	2.4	3 - 2
Poisson Ratio [33], [34]	0.41	0.35

4.3 **Interfacial Fracture Toughening Models and Crack Path Selection**

4.3.1 Row and Zone Models

Row and zone models [35] were used to estimate the cracked-tip shielding levels that were associated with the measured cracked profiles. The models assumed that, as the cracks reach an

obstacle, they deflect around it [16], [17], [35]. Hence the shielding in the row model is influenced by the shear resistance that arises from the interactions between the two materials (friction angle, Ø), the angle of deflection, β, and the loading angle, θ. These were determined along with the applied forces associated with mode I and mode II, and used to estimate the crack-tip shielding, as shown in **Figure 4.1a and 4.1c**. If energy release rate is represented by G, the interfacial fracture resistance (shielding) can be expressed as [35]:

$$\frac{\Delta G}{G_o} = \sum \quad (\phi, \beta, \varphi, \in) = 2h \frac{[(sinsin\ \beta + coscos\ \beta\ tantan\ \varphi)(sinsin\ (\beta-\varphi)) + coscos\ (\beta-\phi)\ tantan\ \varphi]}{coscos\ \phi\ (1+\varphi)} - \frac{h^2(sinsin\ \beta + coscos\ \beta\ tantan\ \varphi)^2}{\phi\ (1+\varphi)} \tag{4.21}$$

The zone model was explored as a second model [35]. This utilized a simplified idealization of the crack profile that is shown in **Figure 4.1c**. Note that the zone model does not account for friction, as β=0 and Ø=0 [14] [16]. The shear stresses and displacements are also assumed to be elastic and similar to those associated with a linear array of micro-cracks. From **equation 22** and equation 23, E is the Young's modulus, L is the zone length, H is the height of the interface step, D is the facet length and values of l are the spacing between the facet (micro-cracks) centers. The zone model gives the toughening increment ratio as:

$$\frac{\Delta G}{G_o} = \frac{\varphi\left[1-k\left[\alpha_o(1+\varphi)\left(\frac{\Delta G}{G_o+1}\right)\right]\right]}{1+\varphi}; \tag{4.22}$$

where α_o is a material factor that can be estimated from the following expression [35]:

$$\alpha_o \approx 0.1 \frac{\frac{EH}{G_o}}{(1-\upsilon^2)} \tag{4.23}$$

$$\frac{D}{I} = \frac{1}{2}, \frac{H}{I} = \frac{1}{2} \tag{4.24}$$

For cases in which $\alpha_o \gg 1$, the mode mixity dependence of toughening can be estimated from Ref.[35]. This gives:

$$G = G_o(1 + \varphi) \quad (4.25)$$

$where\ k$ is determined by the value of α_o as determined by Budianski et al.[36].

Results and Discussion

5.1 Nano-indentation Measurements of Reduced Young's Modulus and Hardness

A typical three-dimensional topographical SPM image (obtained from an epoxy/clay composite coated sample) is presented in **Figure 4.2,** which also includes load displacement curves for pristine epoxy and epoxy composite coatings that were subjected to indentation loading up to a maximum load of 8000 μN. The load-displacement curves were used to determine the hardness (H) and the reduced elastic Young's moduli (Er) of the tested samples. Under the same loading conditions, pristine epoxy had the lowest resistance to penetration by an indentation force (hardness) and the highest maximum indentation depth at that force. The hardness values and the reduced elastic moduli are summarized in **Table 4.4**. The results show that, for clay weight fractions of 1, 3, and 5 %, the hardness (H) increased, respectively, by 46 %, 80 % and 88 %. Furthermore, for the same range of clay particle reinforcement, the respective reduced Young's moduli were 23 %, 58.5 % and 50 % greater. These suggest that the increase in clay content in the composite coatings increased the hardness and elastic modulus of the material. This is consistent with work done by Ayatolah et al. 2012 [37] and Ghader et al. 2007 [26]. Inclusion of high strength clay particles into the structure of the epoxy coatings made them more resistant to deformation compared with the pristine epoxy hence produced a much higher hardness value.

Figure 4.3 presents a summary of the effect of clay content on the hardness and Young's moduli. It shows that there is a progressive increase in the hardness and reduced moduli of the composite coatings with increasing clay reinforcement weight fraction. Typical values of H/Er are presented in **Table 4.4** as measures of plastic indentation resistance. The plastic indentation resistance decreases with increasing clay content. These results suggest that controlled reinforcement with the clay particles may be used to control the hardness plastic indentation resistance of clay reinforced composites.

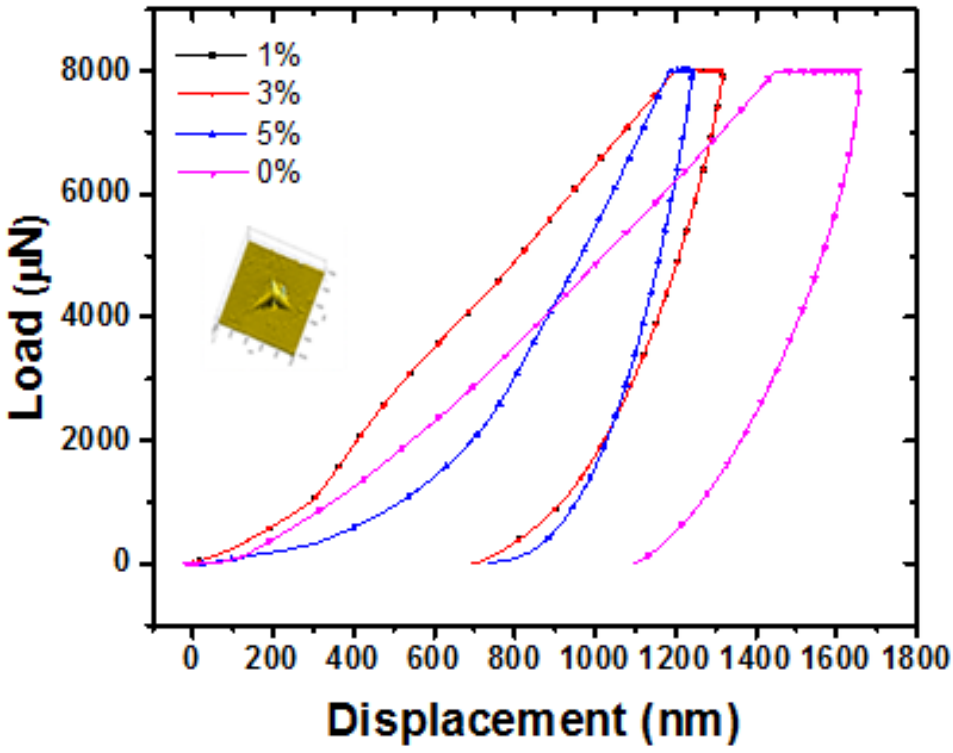

Figure 4.2: The load - displacement plots of pristine epoxy and the different composites coatings

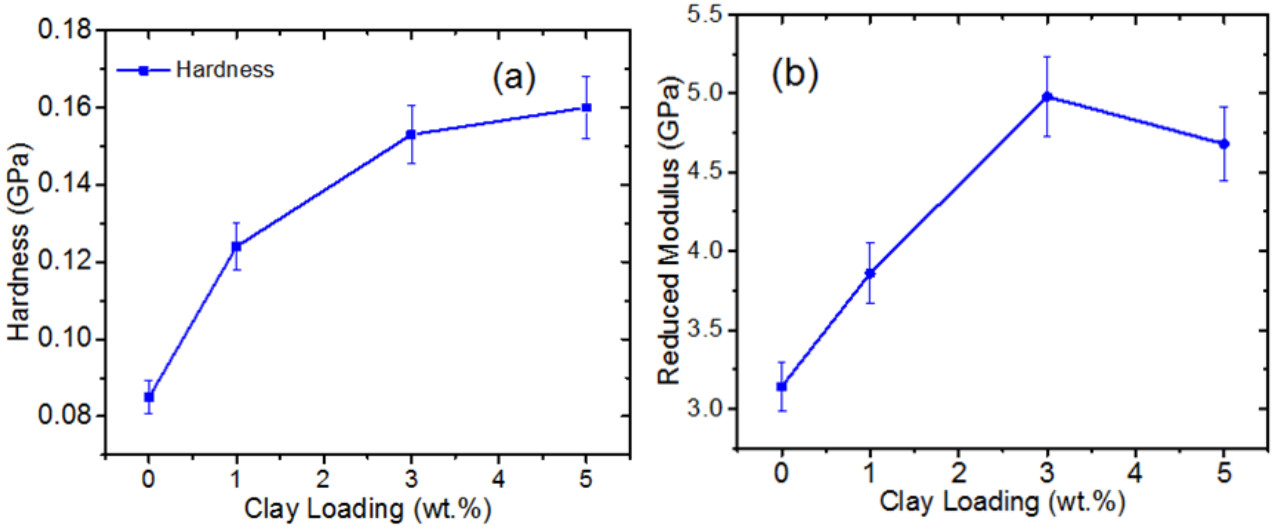

Figure 4.3: Hardness as a function of clay loading (a) and reduced modulus as a function of depth (b) of pristine epoxy and its nanocomposite.

Table 4.4: Summary of Mechanical Properties of Indented Samples

Sample	Hardness, $H(GPa)$	Reduced Young Modulus, $E_r(GPa)$	Resistance to Indentation, H/E_r^2
Neat Epoxy	0.085 ± 0.04	3.14 ± 2.01	0.0086
Epoxy Composite (1%)	0.124 ± 0.07	3.86 ± 1.75	0.0083
Epoxy Composite (3%)	0.153 ± 0.06	4.98 ± 1.35	0.0062
Epoxy Composite (5%)	0.160 ± 0.00	4.68 ± 0.00	0.0073

5.2 Rule of Mixtures and Shear Lag Models

The predictions of strength and Young's moduli obtained from the rule of mixtures and shear lag models are compared with the experimental measurements in **Table 4.5.** There was variation in the prediction results of the different composites as seen in table 5. This may be due to a huge influence of clay particles in the epoxy matrix which became more evident with increase in reinforcement. Previous studies have shown that reinforcements give a better opportunity for stress to be distributed well in the epoxy matrix and the reinforced particles [39]. This might also be associated with a reduction in dislocation movement as a result of increased grain boundary density from the reinforcement [37]. It can therefore be suggested that the composite strength can be engineered by controlling the fiber and interfacial strengths, and the aspect ratios of the particles.

They were obtained using epoxy and clay particle properties that are summarized in **Table 4.**2.

Table 4.5: Comparison of ROM and Shear Lag Predictions and Experimental Results

	Mechanical Properties	Experimental	Simple ROM	Shear Lag
Epoxy	Modulus (E) (GPa)	3.14	3.14	3.14
	Strength (σ) (MPa)	87.08	87.08	87.08
1 wt.%	Modulus (E) (GPa)	3.86	3.2	3.00
	Strength (σ) (Mpa)	97.15	110.2	108
3 wt.%	Modulus (E) (GPa)	4.98	3.40	3.00
	Strength (σ) (Mpa)	158	156.40	152.39
5 wt.%	Modulus (E) (GPa)	4.31	3.60	2.97

Strength (σ) (MPa)	170	202	195

5.3 **Mode Mixity Dependence of Interfacial Fracture Toughness**

The interfacial fracture toughness values were obtained from four sets of experiments that are presented in **Figure 4.4** for interfaces between the X65 steel and the epoxy/clay composite coatings. The results were considered valid when the initial crack extension occurred along the steel/coating interface. As in earlier studies on other steel/epoxy interfaces [15] [17], the measured interfacial fracture toughness values increase with increasing mode mixity (**Figure 4. 4**). The interfaces between the X65 steel and the clay composites also had higher interfacial fracture toughness values than those between the epoxy and the X65 Steel.

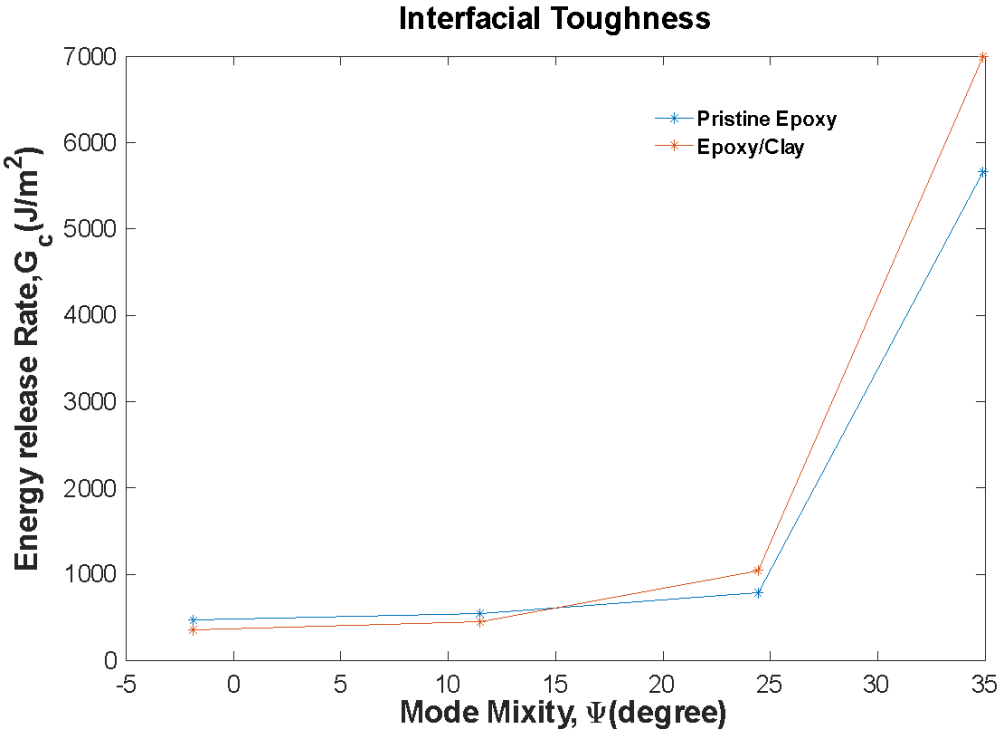

Figure 4.4: Fracture Toughness of Epoxy and Epoxy/Clay as a Function of Loading Phase, ψ.

SEM images of fractured halves of the Brazil disk fracture toughness specimens are presented in **Figure 4.5 (A and C)** for epoxy/steel interfaces, and **Figures 4.5 (**B **and D)** for epoxy/clay

composite/steel interfaces. At 3^0 and 12^0, loading inclination angles for the epoxy/steel interface, the crack kinked in and out of the interface. However, in the case of epoxy/clay composite/steel interfaces, bridging elements were observed along the crack profile, along with evidence with kinking in and out of the crack from the interfaces (**Figure 4.5B and 4.5D, Figure 4.6).** This suggest that toughening in the interfacial fracture experiments can be attributed largely to crack bridging and crack deflection[14], [15] as shown in **Figures 4.6.** Hence, the toughening mechanisms were idealized and modeled using simplified zone and zone models presented in **Figure 4.7.**

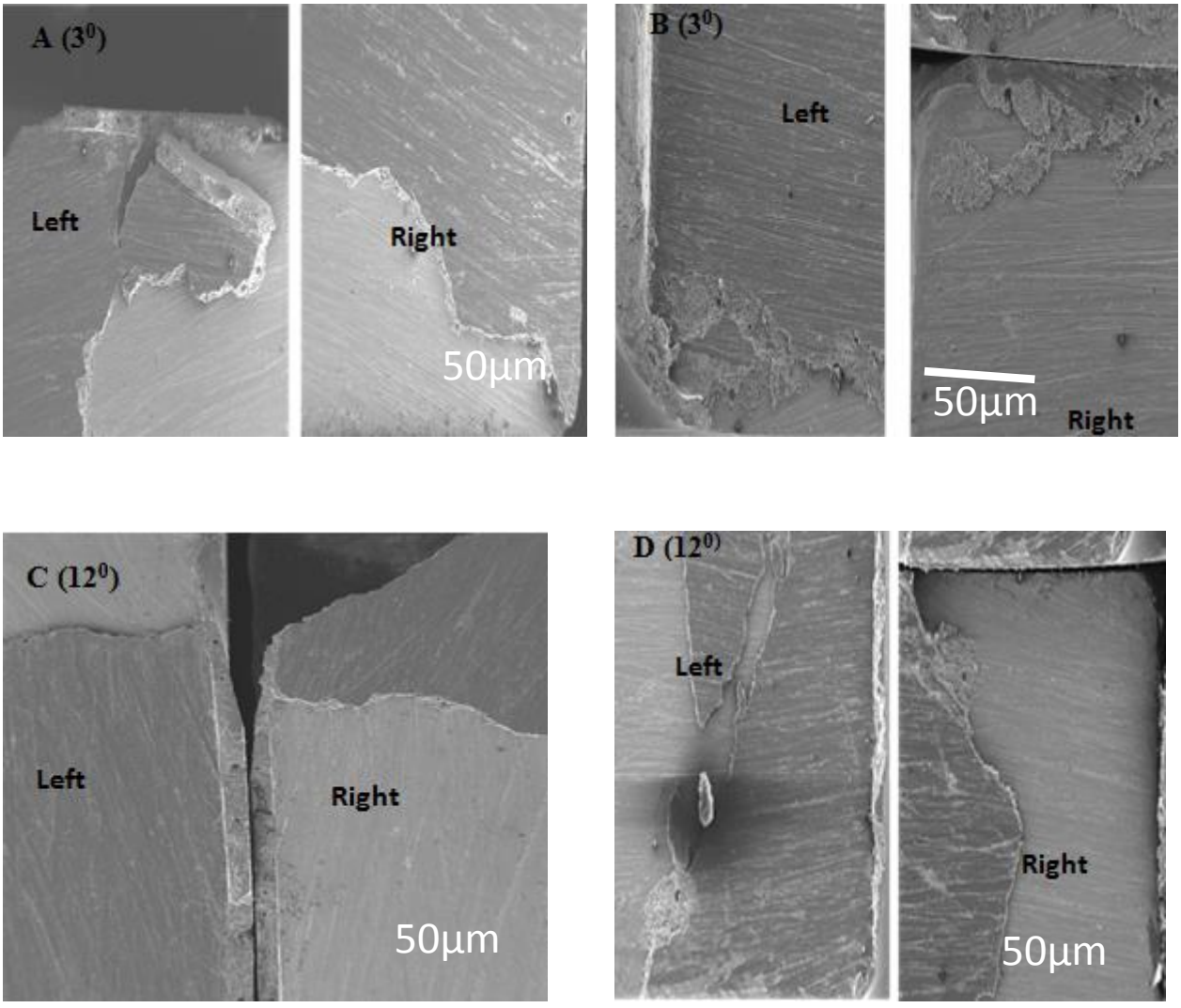

Figure 4.5: SEM Images of Fractured Brazil Disc Specimenat ψ=3^0 for Epoxy (a) and Epoxy/Clay Composite (b) and at ψ=12^0 for Epoxy (C) and Epoxy/Clay Composite (d)

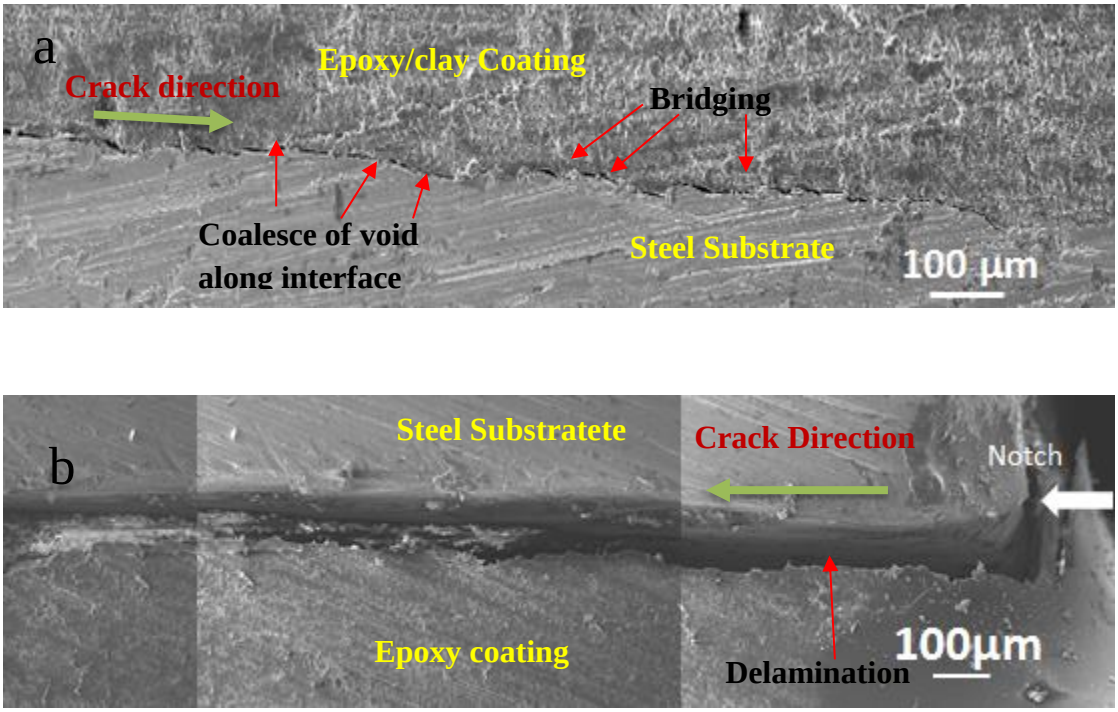

Figure 4.6: SEM Images Showing the Incomplete Fractured Discs at $\psi=3^0$ for Epoxy/Clay Steel interface (a) and for epoxy/steel interface (b)

5.4 Toughening Models

For each Brazil disk crack, the energy release rate, G, was calculated using the mechanical properties of the epoxy and epoxy composites obtained from indentation measurements on the layers in Brazil disks that were tested at loading angles of $\theta = 3^0, 7^0, 12^0 \; and \; 17^0$. The corresponding mode mixity values, ψ, were found to be $\psi = 1.81^0, 11.47^0, 24.42^0 \; and \; 34.88^0$ respectively. There were four different sets of experiments and averages taken for each experiment. These results were consistent with similar work done by Rahbar et al. and Tiffany et al. [14], [16], [17]. This work was restricted to $\beta = 0$ as the influence of β on ψ is negligibly small in this case [38]. The toughening estimates obtained using the above data are summarized in **Table 1.** These were incorporated into the expressions presented in **Section 2** to obtain predictions of toughening from Row, zone to simplified zone models. The predictions are presented in **Figure 7 and Table 6** along with the experimental measurements of the mode mixity dependence of the interfacial fracture toughness values. The trends in the predicted

interfacial fracture toughness were generally in good agreement with predictions from the zone and row models, as well as the simplified zone models, at lower mode mixities which was similar work done by Tiffany et al [16]. However, larger differences were observed between the predictions and the measurements of the interfacial fracture toughness at higher mode mixities. The lower energy release rate obtained from the predictions relative to the higher one from experiments may have been due to higher shearing forces overriding mode I opening that eventually encouraged kinking into the substrate which is not evaluated by the model presented in this study.

Table 4.6: Comparison of Experimental and Predicted Fracture Toughness G[J/m^2]

Model	Ψ= -1.87^0	Ψ=11.47^0	Ψ=24.42^0	Ψ=34.88^0
Simplified Zone	411.64	428.14	496.02	1307.10
Zone	411.64	427.17	476.16	1024.50
Row	412.07	443.74	551.83	2010.14
Experiment	410	494.49	702.70	5007.44

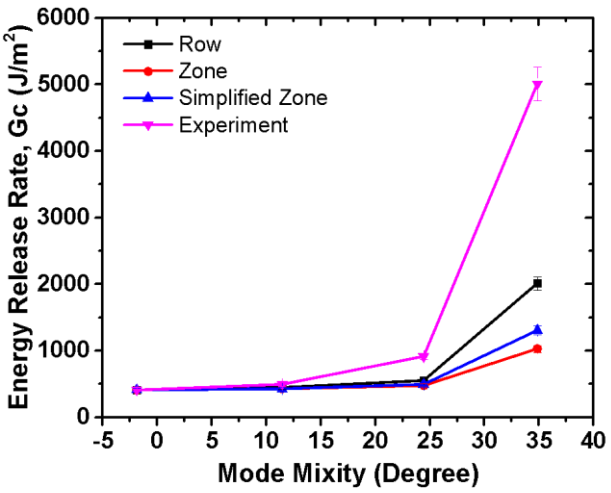

Figure 4.7: Experimental and Predicted Fracture Toughness

Implications

The current work suggests that epoxy/clay composites can ψ be designed to have attractive combinations of strength, Young's moduli and interfacial fracture toughness between steels and epoxy/clay composite coatings. This can be achieved by the reinforcement of the epoxy matrices with clay particles with weight percentages up to about 3 percent. However, above this, the elastic moduli and hardness may decrease, perhaps due to the clustering of the particles, which may result in stress concentration effects, and the reduction of composite mechanical properties. In any case, the measured Young's moduli and strength estimates obtained from hardness values are comparable to estimates obtained from rule-of-mixture and shear lag models. The models are also generally found to capture the trends in the measured Young's moduli and hardness/strength data for the different composites that were examined in this study. Furthermore, the current work suggests that controlled reinforcement with the clay particles may be used to control the hardness plastic indentation resistance (**Table 4.**5). In general, the plastic indentation resistance decreases with increasing clay particle loading.

Finally, it is of interest to note that the interfacial fracture toughness values (between the X65 steel and the epoxy or epoxy/clay composite coatings) increased with increasing mode mixity for 3 wt. %. Interfacial fracture was also associated largely with the kinking of cracks in and out of interfaces, with some bridging elements and crack deflection. These result in crack-tip shielding that explains much of the toughening that is observed at lower mode mixities. However, at higher mode mixities, there are discrepancies between the predicted and the measured toughening levels. These might be due to the shear-induced interlocking of asperities at higher mode mixities where the mode II components of the crack driving forces are much greater. Further work is needed to develop more robust models for the prediction of the mode mixity dependence of the interfacial fracture toughness at higher mode mixities. In any case, we hope that the ideas presented in this paper will be useful in the design of structural integrity in the oil and gas industry, as well as in the design and fabrication of steel structures that are bonded or coated with epoxy/clay mixtures.

Conclusions

1. The incorporation of 1, 3 and 5 wt. % of clay particle fillers (into epoxy) increases the hardness by 46 %, 80 % and 88 % and increases Young's moduli by 23 %, 58.5 % and 50 %, respectively. The improvements are associated with the deformation restraint provided by the clay particles.

3. The interfacial toughness between X65 steel and the epoxy/clay coatings (of the composite reinforced with 3 wt. % of clay) increases with increasing mode mixity. This increase is associated with crack-tip shielding by crack deflection and crack bridging.

4. The trends in the measured mode-mixity dependence of the interfacial fracture toughness values are consistent with predictions from the simplified zone, normal zone and row models at lower mode mixity.

References

[1] Z. T. Khodair, A. A. Khadom, and H. A. Jasim, "Corrosion protection of mild steel in different aqueous media via epoxy/nanomaterial coating: Preparation, characterization and mathematical views," *J. Mater. Res. Technol.*, no. x x, pp. 1–12, 2018.

[2] "The Evolution of Pipeline Coatings [Gas Exploration]KTA University." [Online]. Available: https://ktauniversity.com/evolution-pipeline-coatings/. [Accessed: 19-Jun-2019].

[3] "Epoxy Resin Market Analysis and Industry Forecast 2022." [Online]. Available: https://www.alliedmarketresearch.com/epoxy-resins-market. [Accessed: 19-Jun-2019].

[4] A. U. Malik, S. Ahmad, I. Andijani, F. Al-muaili, T. L. Prakash, and J. O. Hara, "Corrosion Protection Evaluation of Some Organic Coatings in Water Transmission Lines 1," no. November 1999, pp. 1966–1827, 1999.

[5] Z. Chen, K. Zhou, X. Lu, and Y. C. Lam, "A review on the mechanical methods for evaluating coating adhesion," *Acta Mech.*, vol. 225, no. 2, pp. 431–452, 2014.

[6] A. Jumahat, C. Soutis, N. Ahmad, and W. M. Wan Mohamed, “Fracture toughness of nanomodified-epoxy systems,” *Appl. Mech. Mater.*, vol. 393, pp. 206–211, 2013.

[7] A. Jumahat, C. Soutis, F. R. Jones, and A. Hodzic, “Compressive behaviour of nanoclay modified aerospace grade epoxy polymer,” *Plast. Rubber Compos.*, vol. 41, no. 6, pp. 225–232, 2012.

[8] N. Saba, M. Jawaid, and M. T. H. Sultan, *An overview of mechanical and physical testing of composite materials*. Elsevier Ltd, 2019.

[9] R. S. R. Kalidindi and R. Subasri, *Sol-gel nanocomposite hard coatings*. Elsevier Ltd, 2014.

[10] O. F. Ngasoh, V. C. Anye, B. Agyei-Tuffour, O. K. Oyewole, P. A. Onwualu, and W. O. Soboyejo, “Corrosion behavior of 5-hydroxytryptophan (HTP)/epoxy and clay particle-reinforced epoxy composite steel coatings,” *Cogent Eng.*, vol. 7, no. 1, 2020.

[11] R. A. Gledhill, A. J. Kinloch, S. Yamini, and R. J. Young, “Relationship between mechanical properties of and crack progogation in epoxy resin adhesives,” *Polymer (Guildf).*, vol. 19, no. 5, pp. 574–582, 1978.

[12] S.-R. Kim and J. A. Nairn, “Fracture mechanics analysis of coating/substrate systems: Part II: Experiments in bending,” *Eng. Fract. Mech.*, vol. 65, no. 5, pp. 595–607, 2000.

[13] L. Banks-sills and J. Schwartz, “Crack paths in adhesive bonds,” pp. 225–234, 2002.

[14] N. Rahbar *et al.*, “Adhesion and interfacial fracture toughness between hard and soft materials,” *J. Appl. Phys.*, vol. 104, no. 10, 2008.

[15] J. S. Wang and Z. Suo, “Experimental determination of interfacial toughness curves using Brazil-nut-sandwiches,” *Acta Metall. Mater.*, vol. 38, no. 7, pp. 1279–1290, 1990.

[16] T. M. Tong, T. Tan, N. Rahbar, and W. O. Soboyejo, “Mode Mixity Dependence of Interfacial Fracture Toughness in Organic Electronic Structures (September 2012),” vol. 14, no. September 2012, pp. 291–299, 2013.

[17] N. Rahbar, Y. Yang, and W. Soboyejo, “Mixed mode fracture of dental interfaces,” vol.

488, pp. 381–388, 2008.

[18] J. W. Hutchinson, *Mixed Mode Cracking in Layered Materials*, vol. 29. 1992.

[19] Atkinson. C, Smelser. R.E et al. “Combined Mode Fracture Via the cracked Brazillian Disk Test, Vol. 18, No. 4, pp. 279-2921, April 1982.

[20] M. Hoerantner, T. Leijtens, G. Eperon, N. Renewable, and M. D. Mcgehee, “The Potential of Multijunction Perovskite Solar,” no. October, 2017.

[21] E. D. Orthogonal, E. Wedges, U. Normal, and S. Loading, “1 B | I discussion,” vol. 31, pp. 650–652, 2016.

[22] L. Shen, L. Wang, T. Liu, and C. He, “Nanoindentation and Morphological Studies of Epoxy Nanocomposites,” pp. 1358–1366, 2006.

[23] W. C. Oliver and G. M. Pharr, “An Improved Technique for Determining Hardness and Elastic Modulus Using Load and Displacement Sensing Indentation Experiments,” Journal of Biomedical Meterials Research, Vol. 7, No. 6, 1992, pp. 1564-1583. doi:10.1557/JMR.1992.1564

[24] C. P. Systems, F. Corrosion, and F. Perspectives, “Corrosion Protection Systems and Fatigue Corrosion Future Perspectives,” pp. 1–51, 2017.

[25] Kusmono, M. W. Wildan, and Z. A. Mohd Ishak, “Preparation and properties of clay-reinforced epoxy nanocomposites,” *Int. J. Polym. Sci.*, vol. 2013, 2013.

[26] G. Khanbabaei, J. Aalaie, A. Rahmatpour, A. Khoshniyat, and M. A. Gharabadian, “Preparation and properties of epoxy-clay nanocomposites,” *J. Macromol. Sci. Part B Phys.*, vol. 46, no. 5, pp. 975–986, 2007.

[27] A. A. Azeez, K. Y. Rhee, S. J. Park, and D. Hui, “Epoxy clay nanocomposites - Processing, properties and applications: A review,” *Compos. Part B Eng.*, vol. 45, no. 1, pp. 308–320, 2013.

[28] W. O. Soboyejo, R. J. Lederich, and S. M. L. Sastry, “Mechanical behavior of damage tolerant TiB whisker-reinforced in situ titanium matrix composites,” *Acta Metall. Mater.*,

vol. 42, no. 8, pp. 2579–2591, 1994.

[29] BYK Additives &Instruments, “Technical Information B-RI 10 Cloisite Nanocomposite Additive for Halogan free Flame Retardants,” pp. 1–4, 2013.

[30] D. Brabazon, *Chapter 16. Nanocharacterization techniques for dental implant development*. Elsevier Inc., 2018.

[31] F. O. Square, “Determination of Stress-Strain Curve through Berkovich Indentation Testing A.M.S. Dias, 1,” vol. 637, pp. 1186–1193, 2010.

[32] “Strong Adhesives for Bonding Metal, Glass & Plastic | Permabond.” .

[33] A. Kepstan and S. A. Polymers, *10 High-Temperature Polymers*. 2015.

[34] A. Arciniegas and L. E. Amaya, “Poisson’s ratio,” *New Trends in Ophthalmology*, vol. 4, no. 1. pp. 25–46, 1989.

[35] A. G. Evans, “Effects of Non-Planarity on the Mixed Mode Fracture Resistance of Bimaterial Interfaces,” vol. 37, no. 3, pp. 909–916, 1989.

[36] Bernard Budiansky, John C. Amazigo and Anthony G. Evans, “Small-Scale Bridging and the Fracture Toughness of Particulate-Reinforced Ceramics, Journal of the Mechanics and Physics of Solids, vol. 36, no. 2, 167-187, 1988.

[37] M. R. Ayatollahi, S. Doagou-rad, and S. Shadlou, “Nano- / Microscale Investigation of Tribological and Mechanical Properties of Epoxy / MWNT Nanocomposites,” pp. 1–13, 2012.

[38] M. Meyer, “wI I,” vol. 1, pp. 270–275, 1993.

Chapter 5

Tribological properties of epoxy/clay composites coatings on a mild steel substrate

5.1 Introduction

Tribology is the science and engineering of interacting surfaces in relative motion. It includes the study and application of the principles of friction, lubrication and wear. Epoxy coatings are thermosetting resin that provides good adhesion to metal surface, chemical as well as corrosion resistance. As one of the major classes of polymeric materials, various types of epoxies are used extensively in different tribo-engineering applications such as automotive electronic, storage tanks and the oil and gas industries [1] this is because of their attractive mechanical and tribological properties [2]. Epoxy-based composite materials have become proper substitutes for traditional materials like metals, metal alloys, wood, etc. due to their prominent properties such as lightness, ease of processing, and relatively low cost. However, one of the major drawbacks in their increasing applications is their poor surface properties. Composites of Epoxy/clay are suitable for applications in steel structures in oil and gas pipelines, storage tanks and structural applications [1]. The coatings used for the protection of steel structures can result in material loss due to abrasive wear phenomena [3]. Furthermore, under service conditions, the durability of epoxy/clay composites depends on the mechanical and tribological properties of the clay fillers [4] in epoxy composites coatings. Clay fillers have been used due to their high availability and good thermal stability, in addition to the improved mechanical and tribological properties of their composites [5] and [6].

Basically, epoxy coatings are prone to damage by surface stresses and indentation/wear phenomena that can occur during service [7] [8]. Nano-indentation and nano-scratch testing can, therefore, be used to evaluate the coating resistance and durability of clay-reinforced epoxy coatings. Scratch testing can either be done under constant load or under progressive loading [7],

[8], nano-scratch testing can be used to study the interfacial and surface properties of coating materials. Scratch testing can also be used to study resistance to surface coatings to abrasion and wear [9]. Research done by Kato et al [10] and Aradhya et al [11] explain that tribocorrosion of passive metals and coatings is generated as the result of the combined effects of friction and wear. They later on discovered that plastic deformation of the contact asperity under the combined stresses of compression and shear is as a result of increased coefficient of friction generated by the growth of the contact areas. According to Kato et al [10]a friction coefficient in the order of 0.1 is common for metals, ceramics and polymers in air without liquid films, and the corresponding specific wear rate varies in the wide range from about 10^{-6} to about 10^{-2} mm3/N m. These values of friction coefficient and specific wear rate are generated by the strong effects of adsorbed gas molecules and/or surface films of oxides. Fillers can play a major role in enhancing the mechanical properties of nanocomposites. As a result, using this method enhances our perception of the nanostructure of nanocomposites. Prior work on the wear behavior of epoxy/clay composites has focused largely on micron-scale wear phenomena that were studied using pin-on-disk experiments [12]. While several researchers have focused on the tribological properties of polymeric nanocomposites, detailed nano- micro-understanding of surface characteristics of these materials is vital for their commercialization especially by means of nanoscratch tests [13]. Current development in the application of polymeric materials for nano-technology applications shows that very small force is applied in nanofabrication and nano machining hence more work needs to be done on their nanoscratch behavior.

Nanoscale indentation and scratch tests are two powerful tools in dealing with tribological and mechanical properties especially in the realm of advanced materials where less consumption of the material is preferable [14]. Moreover, these nanoscale tests have prominent advantages

relative to other characterization tests, such as better control in the normal load as well as the scan size and the absence of chemical and electrical fields [13]. Polymers are susceptible to deformation and damage even under low contact loads. Therefore, the polymer-based nanocomposites suffer too. Despite the enhancement in other mechanical properties, fillers may not always improve the friction and wear/scratch properties; hence, deeper investigations into the scratch response of epoxy based nanocomposites seem to be necessary. However, very few papers are available on the details on scratching in the nanoscale.

This paper presents the results of a combined experimental and theoretical study of the interfacial and coating mechanical properties of epoxy/clay composites coatings on a mild steel substrate. The mechanical and tribological properties of epoxy composites coatings (reinforced with montmorillonite clay particles) are studied using nano-indentation and nano-scratch techniques. These are used to determine the Young's moduli, hardness values and the nano-wear characteristics of the composite coatings. The measured mechanical and tribological properties are then compared with predictions from composite theories and wear performance criteria. In order to determine the dispersion of the nano-fillers, the scanning electron microscope was used.

5.2 Materials and Experimental Methods

API X65 steel pipe materials were obtained from a pipeline factory (Schebite Construction Company, Bwari, Abuja, Nigeria). Both the epoxy base and hardener were purchased from Sigma Coatings, Amsterdamseweg, Netherlands. The Cloisite 30B (C30 B) clay particles were procured from Southern Clay Products Inc Texas, USA. They were mixed with epoxy to obtain epoxy/clay composites with clay particle volume fractions of 1 wt.% and 3 wt.% . These were then stirred with a magnetic stirrer for 2 h and 30 minutes at the rate of 1500 rpm. This was done at 50 ^{o}C to enable complete particle dispersion to occur. The resulting composites were then

degassed in a vacuum oven for 2 minutes. The curing agent was added and mixed with a spatula prior to degassing in the vacuum oven for 30 seconds. Pure epoxy, without the clay reinforcement, was prepared and studied as a control. The coating was formulated at a stoichiometric mixture of 2:1 base to hardener.

5.2.1 Nano-Scratching and Scanning Wear Testing of Epoxy/clay Composites on Mild Steel Substrate

Scratch testing was carried out in accordance with ASTM 7027/ISO19252 conditions [9] [15]. This was done using a Triboindenter T950 system (Bruker, Minneapolis, MN, USA) that was instrumented with a 3 sided pyramidal diamond Berkovic indenter tip with a triangular tip radius of 100 nm. Scratch testing was carried out at the African University of Science and Technology (AUST), Abuja, Federal Capital Territory (FCT), Nigeria. Scratch test was used to simulate the possible effects of abrasive hard particles that can abrade the coated steel surfaces under service conditions [16]. For example, in the case of steel pipeline materials can result in material loss due to abrasive wear phenomena [3]. Hard sand particles can also abrade the exterior surfaces of exposed pipelines in desert conditions. In any case, such abrasion wear phenomena may be simulated by nano-scratch experiments. The nano-scratch testing was used to evaluate the abrasive and scratch performance of the composite coating under constant load.

Prior to scratch testing, the X65 steel samples were polished using different grades of grinding paper from coarse to fine SiC grit paper. The ground surfaces were then fine polished using 0.05 µm diamond paste to obtain ultra-smooth surfaces [17]. This was done to avoid possible effect of the surface roughness on the indentation and scratch behavior of the coated surface. After polishing, the indenter was drawn across the different specimens up to the point of failure. The load at the point of failure is the critical load and it gives information about the abrasive strength

of the polymer coating. This failure which also signifies the damage of the coating represents the onset of cracking around the crack tip. It involves the spalling of the coatings or the formation of interfacial cracks, which involve loss of the coating in that area from the substrate. The scratch tests were also used to determine the coefficients of friction, which was defined as the ratio of sliding load (required to overcome friction) and the normal load (frictional force divided by normal load). Damage was found to occur when there was a sudden rise in the coefficient of friction.

In order to determine the scratch resistance, a scratch duration of about 3 minutes was adopted. SPM images of samples were also obtained before and after the friction and wear experiments. It is worth noting that the scratch depth was calculated from the difference between the SPM images taken before and after the experiments (following exposure of the maximum load). The specific wear rate was calculated using the measured average depth obtained during each scratch. The wear rate was thus reported as the volume of material removed per unit normal force per unit sliding distance. The following expressions were used to characterize the material removal due to sliding wear [18]:

$$Wear\ Rate = \frac{Wear\ Volume, V\ (m^3)}{Sliding\ Distance, S\ (m)} \quad (18a)$$

The volume, V, of the material removed is given by:

$$V = K_a F_n S \quad (18b)$$

where V is volume of material removed/displaced,

K_a is the Wear Rate Constant/Coefficient,

F_n is the Normal Contact Force,

S is the Sliding Distance, and

Specific Wear Rate is given by:

$$Specific\ Wear, K = \frac{V(Wear\ Volum\ (m^3))}{P((Normal\ Load, (N)) \times L(Sliding\ Distance\ (m)))} - - - - - - - - - (19)$$

where P is the normal force (in Newtons) and L is sliding distance (in meters).

Table 5.1 Nano-Scratch Test parameters

Parameters	**Nano-Scratch**
Test Prop[19][20], [21][22]	3 sided Berkovich indenter tip
Scan size	20μm
Scratch distance	4 nm
Scratch Constant Load	1000 μN
Indenter's radius	100 nm

5.2.2 Imaging

The scanning electron microscope was used to investigate the state of clay filler dispersion in the epoxy coating.

5.2.3 Grid Nano-indentation

Grid nano-indentation arrays consist of a large number of indentations that are introduced at random locations. For heterogeneous materials composed of N different phases, this technique can provide both quantitative and qualitative data on the mechanical properties of the phases

(hardness and reduced elastic modulus) [23]. Prior to indentation testing, the X65 coated steel samples were polished using different grades of grinding paper from coarse to fine SiC grit paper. The ground surfaces were then fine polished using 0.05 μm diamond paste to obtain ultra-smooth surfaces [17]. This was done to avoid possible effects of the surface roughness on the indentation and scratch behavior of the coated surface. The experiment was performed using the Triboindenter T950 indentation system (Bruker, Minneapolis, MN, USA) was used. The indentation system was instrumented with a 3 sided pyramidal diamond Berkovic indenter tip with a triangular tip radius of 20 nm and an included angle of 142.3^0. The loading rate was fixed to minimize the possible strain hardening strain hardening effects on the measurements [24].

Indentation load-displacement data was obtained from 100 indents covering a representative area of 70×70 μm^2 At least three sets of grid indentation were performed on each sample at different locations in the samples resulting in a total of 300 indentation points per sample. This was done to ensure that the results were representative of the sample microstructure. Elastic properties were evaluated from the load-displacement curves using Oliver and Pharr method [25].

5.3.3 Statistical Deconvolution

Statistical deconvolution of the grid nanoindentation measurements was used to estimate the mean and standard deviation of the indentation hardness (Hi) and elastic modulus (Ei) as well as the volume fraction of filler phase of the coating. This is applied to histograms of the hardness and moduli that were extracted from the indentation experiment. This method is analytically more convenient to generate an experimental cumulative distribution function (CDF) rather than a probability density function (PDF) as the generation of experimental PDFs requires a choice of bin size for the construction of histograms which is user-dependent [23], [26]. However, with a satisfactory bin size, histograms are more physically intuitive and give a better visual

representation of distinct phases. Consequently, using a bin size of 1 GPa, which is reasonable for structural materials, histograms were plotted against frequency density in this study. Deconvolution into phases was conducted under the assumption that values of $E \geq 20$ GPa could be attributed to impurities, and were not considered due to their random occurrence in different grids.

5.3 Result and Discussion

5.3.1 Nano-Scratching and Scanning Wear Testing of Epoxy/clay Composites on Mild Steel Substrate

The surface morphologies of the scratched surfaces are presented in **Figure 5.1** using SPM images obtained for pristine epoxy and clay-reinforced epoxy composite. The residual scratch depth/area and the distance slid were used to determine the volume of material removed during the nano-scratch test. Atleast 5 measurements of scratch widths and depth were obtained for each scratch that was used to determine the nanoscratch volume.

The efficiency of the reinforcement significantly depends on the quality of the dispersion and formation of strong interfacial bond as seen in scanning electron microscopic images seen in figure 4

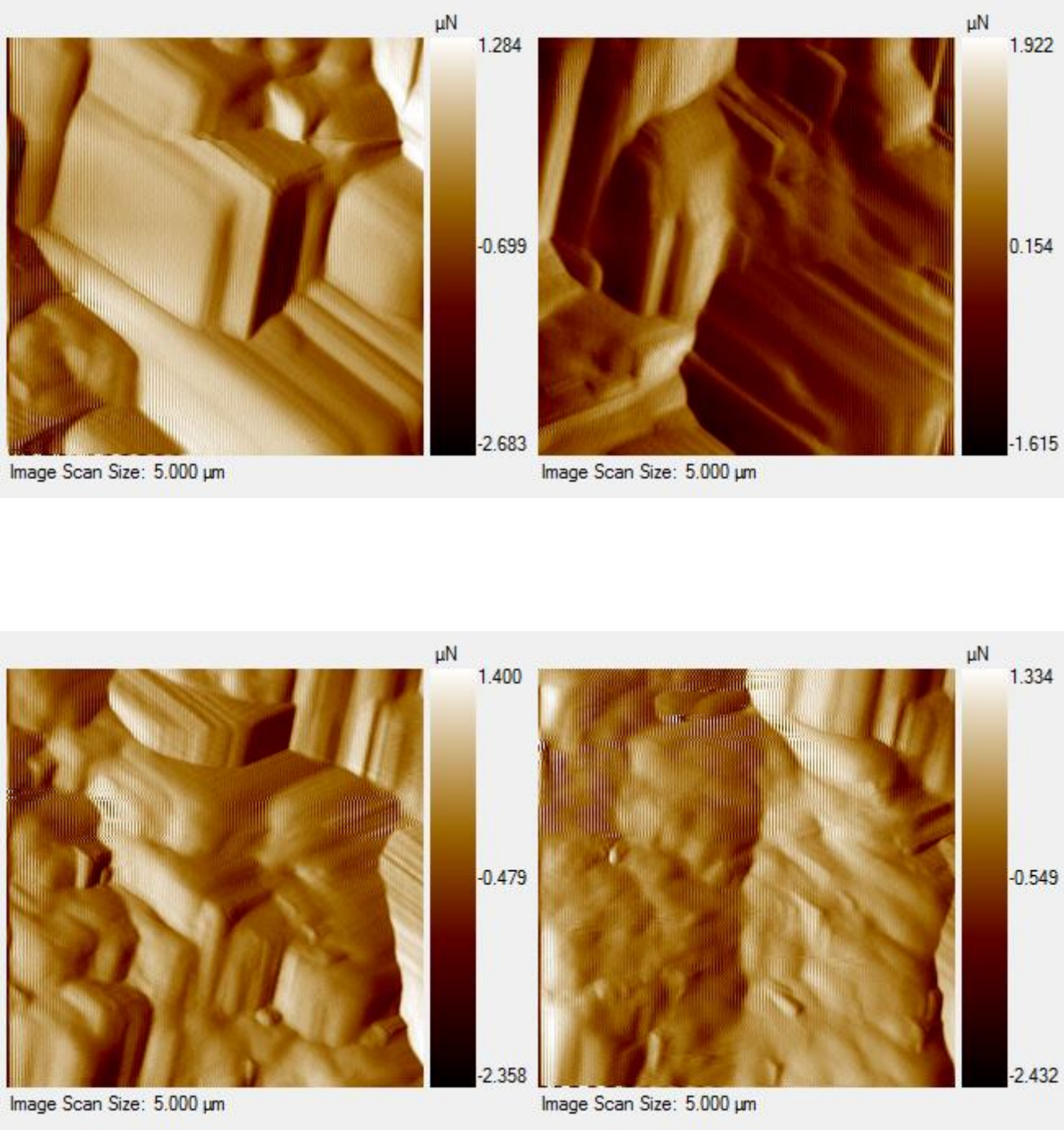

Figure 5.1 SPM Scratch Images Obtained for 1 wt. % Reinforcement (a) and 3 wt. % Reinforcement (b)

The friction coefficient and critical sliding load obtained for the coatings that were examined in this study are summarized in **Table 5.2.** Note that an instantaneous increase in friction

coefficient occurs at a critical load. This rise in friction may also be due to the accumulation of debris. However, the subsequent drop in the friction coefficient may be associated with the onset of damage in coating or interface. After the first drop in the coefficient of friction observed, no significant changes were observed in the friction coefficient until the critical normal load was reached at a load of about 1000 µN. Furthermore, as the reinforcement increased from 0 to 3 %, there was a general decrease in the coefficient of friction, as shown in **Figure 2b.** The highest friction coefficient was obtained for pristine epoxy, in which the most severe evidence of surface damage. Following an initial increase to peak value, the coefficient of friction decreases in two stages (first to a value corresponding to a peak load of 500 µN, and then to a critical load of about 1000 µN at which a sudden increase in scratch depth was observed (**Figure 2band Table 2**). The wear rates obtained for the clay-reinforced epoxy composites are presented in **Figure 2a & b,** showing that the wear rates decreased with increasing clay weight percentage.

Table 5.2: **Summary of the Friction coefficients and Critical Loads**

Material Type	Critical Load (µN)	Critical Coefficient of Friction	Coefficient of Friction	
			Onset	End
0% Reinforcement	0	0.63	0.19	0.3
1% Reinforcement	0	0.32	0.05	0.27
3% Reinforcement	0	0.25	0.06	0.36

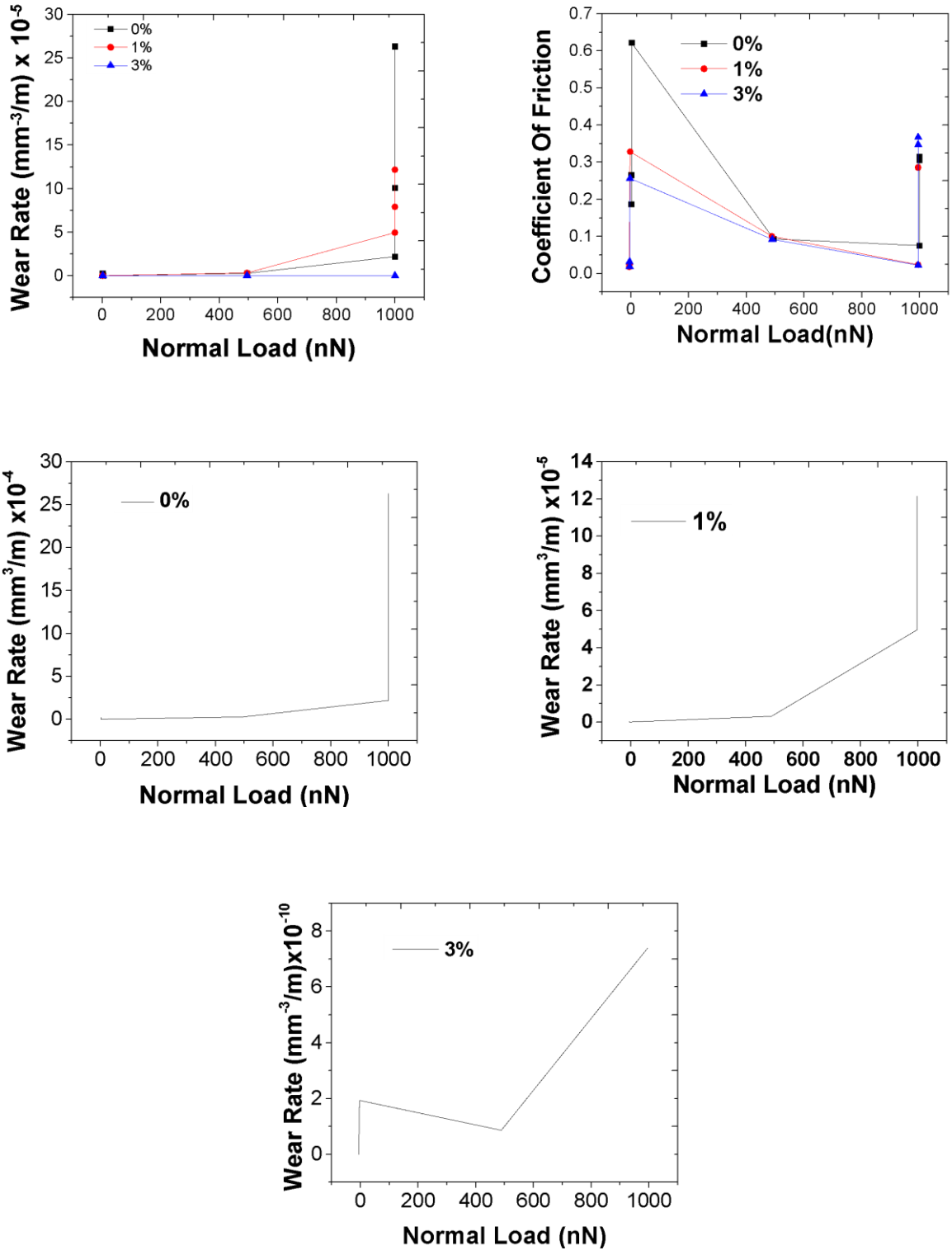

Figure 5.2 Wear Rate (C & A) and Friction Coefficient (B) as a Function of Normal Load

Table 5.3: Specific Wear Rate, Scratch Volume and Hardness of Pristine Epoxy and Reinforced composite Coating

Sample	**Specific Wear Rate (mm^3/mN) (Wear Coefficient, k)**	Reduced Young Modulus, $E_r(GPa)$	Wear Resistance ,H/E_r	**Scratch Volume (mm^3)**	**Hardness (GP_a)**
Pristine Epoxy (0% Reinforcement)	0.26	3.14 ± 2.01	0.027	$1.0x10^{-9}$	0.085
1% Clay Reinforcement	0.12	3.86 ± 1.75	0.032	$4.82x10^{-10}$	0.124
3% Clay Reinforcement	$5.6x10^{-5}$	4.98 ± 1.35	0.031	$3.16x10^{-15}$	0.153

The specific wear rate for any material can be calculated using the measured average depth during each scratch. This shows the loss of material due to wear. Values of k vary from 10^{-2} to 10^{-7}, with anything typically above 10^{-5} being considered not very resistant to wear [18]. **Figure 5.3** presents the specific wear rate obtained for pristine epoxy and the clay-reinforced epoxy with with clay weight percentages of 1 and 3 wt.%.

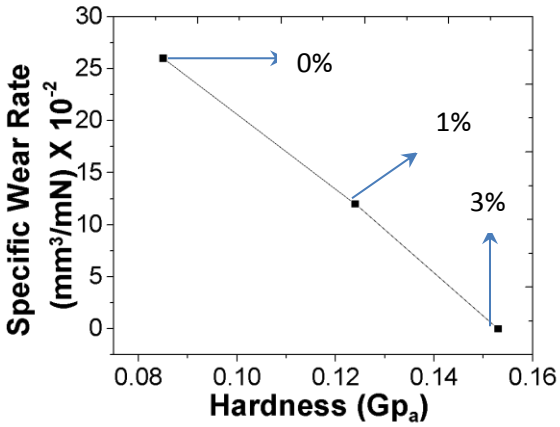

Figure 5.3: Specific Wear Rate as a Function of Hardness of Pristine Epoxy and Reinforced Epoxy

5.3.2 Section groove profile

The section grove profile for each sample shows that, under the same scratch load and duration, the scratch depth reduced as the clay reinforcement increased (**Figure 5.4)**. The residual depth decreased about 40.% by adding 1. Wt% and 50.% by adding 3 wt% of cloisite 30C into the polymer. The pile-ups and residual depths are important criteria that one can use for understanding the mechanism involved in the nanoscratch behavior of materials. The height of pile-ups and the depth of residual grooves showed greater reduction in nanocomposite specimens containing more nanofiller. These results correlate with finding of research works on epoxy nanocomposites reinforcing with MWCNTs [13]. The scratch volumes of the reinforced epoxy samples were also less than those of the pristine epoxy, as shown in **Figure 5.3.** This is attributed to the higher intrinsic scratch resistance of the clay particles. **Figure 5.4** shows typical plots of the residual depth profiles that were obtained for some of the tested samples. These were obtained for the same applied load of 1000 μN.

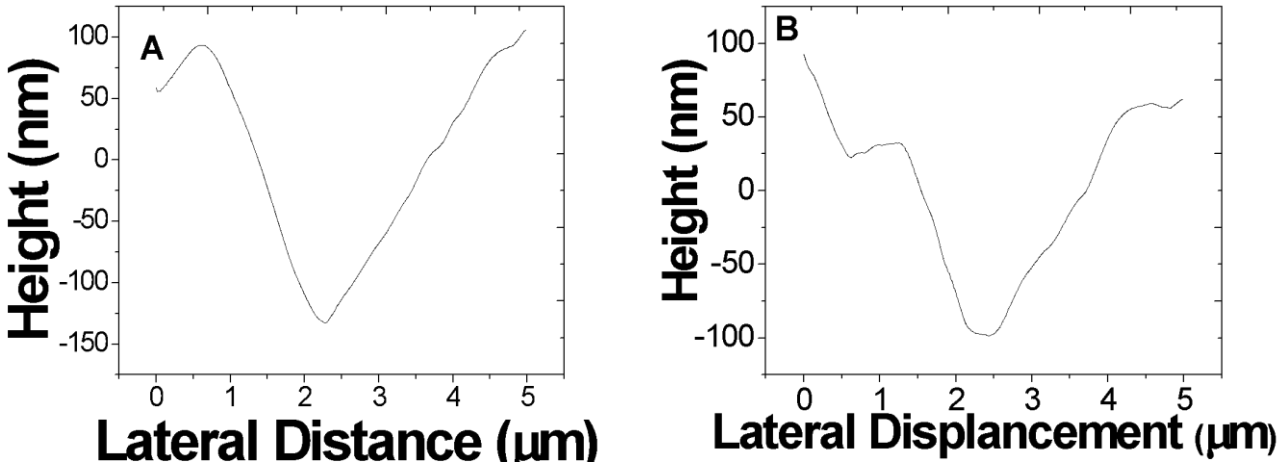

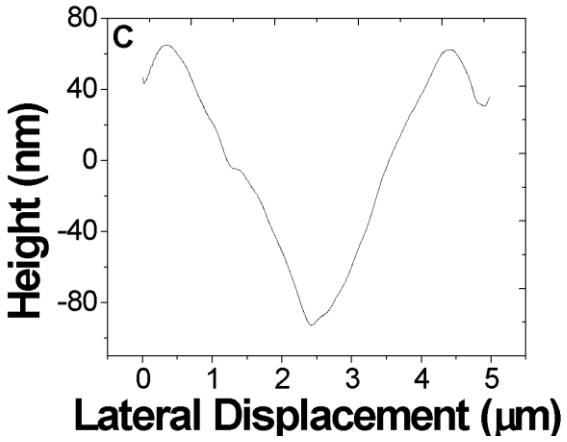

Figure 5.4 Sections of Grooves/Wear tracks for Pristine Epoxy (a), 1 wt. % (b) and 3 wt. %(c) Clay Reinforced Epoxy Clay Composites Coatings .

5.3.3 Statistical Deconvolution

The statistical deconvolution was used to extract the Young's moduli and hardness values obtained from multiple indentation measurements within different grids. The frequency plots of indentation modulus obtained from the nano-indentation experiments (using a fixed bin size of 1 GPa), are presented in **Figure 5.5.** The deconvolution algorithm was applied to the experimental histograms of elastic moduli with the assumption of a 2-phase system in which the clay is the reinforced phase and the epoxy is the matrix material. Frequency plots (histograms) obtained for unreinforced coating exhibited a single modal peak that corresponded to a larger proportion of matrix (**Figure 5.5a)**. On the other hand, the presence of clay reinforcements resulted in development of a second peak as the clay weight fraction was increased (**Figure 5.5b-5.5d)**. The result suggests that one distribution corresponds to the properties of the epoxy matrix, while the second corresponds to the properties of the reinforcement. They also suggest that higher weight fractions of the clay reinforcement should result in improved mechanical properties (higher Young's moduli). **Table 5.4** gives the Hardness and Elastic modulus of epoxy resin and clay reinforcement found in the composite coatings.

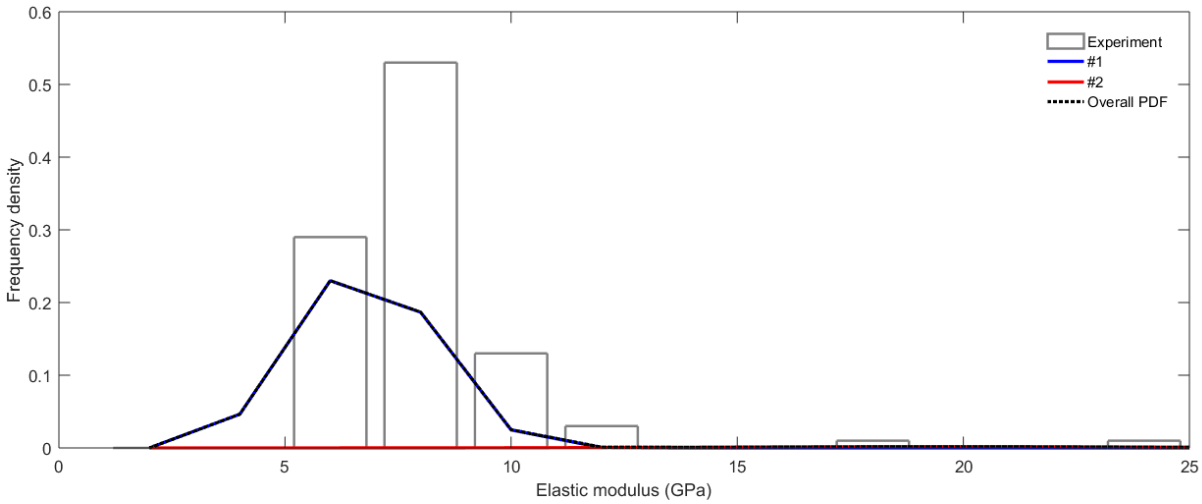

A. Epoxy Matrix (0% Clay Particles)

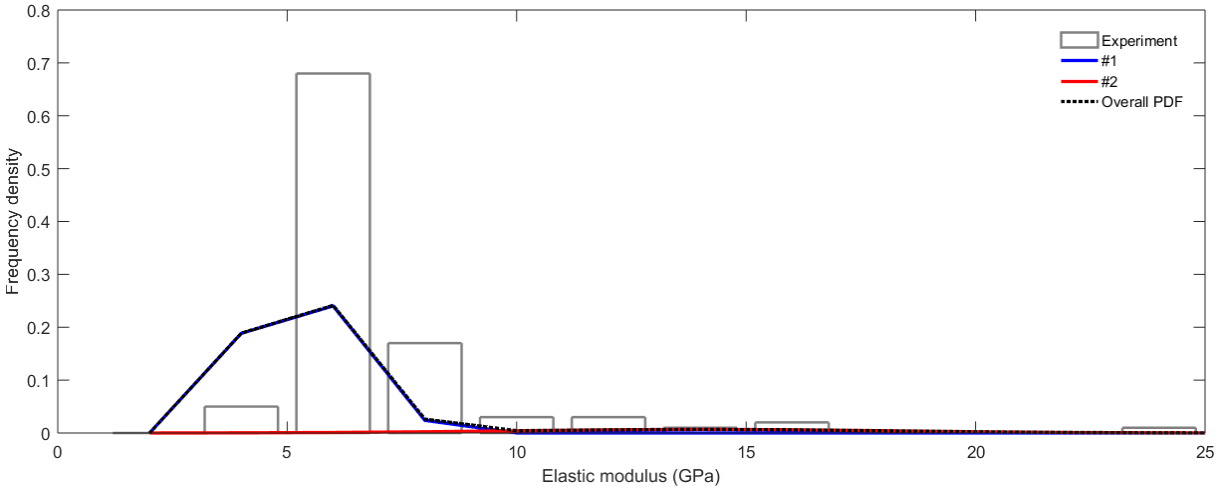

B. Epoxy Reinforced With 1 wt.% Clay

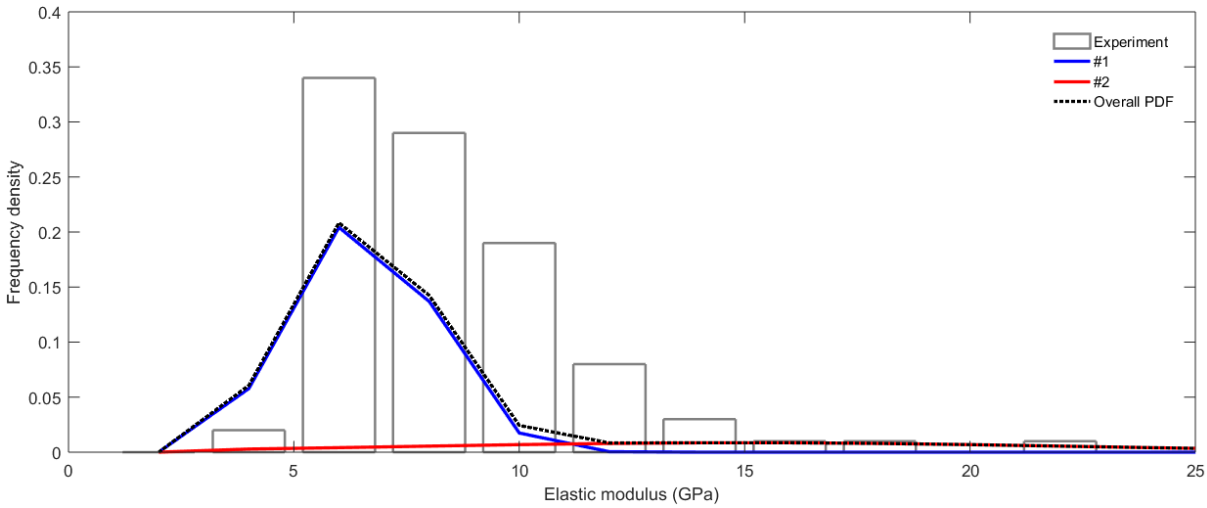

C. Epoxy Reinforced with 3 wt.% Clay

Figure 5.5 Experimental PDF and Deconvolution Results obtained for (a) Pristine Epoxy; (b) 1 wt. % Reinforcement, and (c) 3 wt. % Reinforcement, Conclusions

Table 5.4 Hardness and Elastic modulus of the various filler fraction present in the indented area

Mineral	**Hi (GPa)**	**Vol. (%)**	**Ei (GPa)**	**Vol. (%)**
O%				
Epoxy Resin	0.205± 0.61	92	4.372 ± 1.295	98
Clay Filler	0.920 ± 0.596	8	19.6 ± 4.666	2
1% **Epoxy Resin**	0.225 ± 0.14	96	5.190 ± 1.143	93
Clay Filler	2.257 ± 1.143	4	14.07 ± 4.06	7

3% **Epoxy Resin**	0.212± 0.193	98	6.603 ± 1.63	86
Clay Filler	2.648± 1.097	2	15.698 ± 7.194	14

5.4 Implication

The current work suggests that epoxy/clay composites can be designed to have attractive combinations of a good abrasive and adhesive resistance between steels and epoxy/clay composite coatings. This can be achieved by the reinforcement of the epoxy matrices with clay particles with weight percentages up to about 3 percent. However, the elastic moduli and hardness may decrease, perhaps due to the clustering of the particles, which may result in stress concentration effects, and the reduction of composite mechanical properties. However, the nano-wear characteristic and statistical deconvolution of the composite coating gives a unique way of evaluating composite coating. This study also suggested that statistical deconvolution can be used to obtain the mechanical properties of the epoxy matrix and clay particles found in the epoxy composite. The section grooves gives a nano-scratch characteristic that was unique to each composite, that is the groove depth was seen to reduce with reinforcement. Furthermore, the current work suggests that controlled reinforcement with the clay particles may be used to control the hardness plastic indentation resistance and the wear rates. In general, the plastic indentation resistance decreases with increasing clay particle loading, while the wear rates in the

different epoxy/clay composites decreases with increasing clay loading up to 3 % reinforcement. This again suggests that intermediate particle loading is needed for the design of a balance of wear resistance and indentation resistance.

5.6 Conclusions

This paper presents the results of a combined experimental and analytical study of the tribological properties of epoxy/clay composites coatings on mild steel substrate. The mechanical and tribological properties of pristine epoxy and its composites were investigated using a combination of experiments and models. At the nanoscale, load, time, and volume fraction has a significant contribution to wear because surfaces may not have enough contact with each other. This is not the case at the macroscale because there is maximum contact between surfaces hence load or time is not a contributing factor. Salient conclusions arising from this study are summarized below.

1. The plastic indentation resistance of the composites decreases with increasing particle loading, while the wear rates also drops with increasing particle loading between 1 and 3 wt.%. This suggests that there is a need for a balanced approach to the engineering of wear and indentation resistance. Such balance may be achieved by the use of lower clay loadings between 1 and 3 wt.%.
2. The section groove profile of each sample showed that the scratch depth reduced as clay reinforcement increased. The scratch depth of pristine epoxy was the highest ~ 150 nm followed by a depth of 100 nm for the 1% clay reinforced epoxy and 90 nm depth for 3% reinforced epoxy and lastly 85 nm depth for 5% clay reinforced epoxy.

3. The scratching experiments revealed a slight decrease in the surface damage of the coating with increasing clay loading. However, in all of the composites, the friction coefficients varied from 0.63 to 0.015.
4. The friction, indentation and wear properties of clay-reinforced epoxy composites decreased with increasing particle loading (weight percentage), for particle reinforcement between 1 and 3 wt. %. This is attributed to the higher intrinsic and wear characteristics of about 3 wt. %.

5.7 References

[1] "The Evolution of Pipeline Coatings [Gas Exploration]KTA University." [Online]. Available: https://ktauniversity.com/evolution-pipeline-coatings/. [Accessed: 19-Jun-2019].

[2] Z. T. Khodair, A. A. Khadom, and H. A. Jasim, "Corrosion protection of mild steel in different aqueous media via epoxy/nanomaterial coating: Preparation, characterization and mathematical views," J. Mater. Res. Technol., no. x x, pp. 1–12, 2018.

[3] O. F. Ngasoh, V. C. Anye, B. Agyei-Tuffour, O. K. Oyewole, P. A. Onwualu, and W. O. Soboyejo, "Corrosion behavior of 5-hydroxytryptophan (HTP)/epoxy and clay particle-reinforced epoxy composite steel coatings," Cogent Eng., vol. 7, no. 1, 2020.

[4] Z. Chen, K. Zhou, X. Lu, and Y. C. Lam, "A review on the mechanical methods for evaluating coating adhesion," Acta Mech., vol. 225, no. 2, pp. 431–452, 2014.

[5] A. Jumahat, C. Soutis, N. Ahmad, and W. M. Wan Mohamed, "Fracture toughness of nanomodified-epoxy systems," Appl. Mech. Mater., vol. 393, pp. 206–211, 2013.

[6] A. Jumahat, C. Soutis, F. R. Jones, and A. Hodzic, "Compressive behaviour of nanoclay

modified aerospace grade epoxy polymer," Plast. Rubber Compos., vol. 41, no. 6, pp. 225–232, 2012.

[7] N. Saba, M. Jawaid, and M. T. H. Sultan, An overview of mechanical and physical testing of composite materials. Elsevier Ltd, 2019.

[8] R. S. R. Kalidindi and R. Subasri, Sol-gel nanocomposite hard coatings. Elsevier Ltd, 2014.

[9] G. Wypych, "Scratch and Mar Resistance," Handb. Surf. Improv. Modif., pp. 3–41, 2018.

[10] "Friction and wear of passive metals and coatings," 2011.

[11] R. Aradhya and N. M. Renukappa, "Mechanical and Tribological Properties of Epoxy Nano Composites for High Voltage Applications."

[12] Rashmi, N. M. Renukappa, B. Suresha, R. M. Devarajaiah, and K. N. Shivakumar, "Dry sliding wear behaviour of organo-modified montmorillonite filled epoxy nanocomposites using Taguchi's techniques," Mater. Des., vol. 32, no. 8–9, pp. 4528–4536, 2011.

[13] M. R. Ayatollahi, S. Doagou-rad, and S. Shadlou, "Nano- / Microscale Investigation of Tribological and Mechanical Properties of Epoxy / MWNT Nanocomposites," pp. 1–13, 2012.

[14] M. M. Shokrieh, M. R. Hosseinkhani, M. R. Naimi-jamal, and H. Tourani, "Nanoindentation and nanoscratch investigations on graphene-based nanocomposites," Polym. Test., vol. 32, no. 1, pp. 45–51, 2013.

[15] S. Du, M. Hamdi, and H. Sue, "Experimental and FEM analysis of mar behavior on

amorphous polymers," Wear, p. 203155, 2020.

[16] O. F. Ngasoh, V. C. Anye, B. Agyei-tuffour, O. K. Oyewole, P. A. Onwualu, and W. O. Soboyejo, "Corrosion behavior of 5-hydroxytryptophan (HTP)/ epoxy and clay particle-reinforced epoxy composite steel coatings Corrosion behavior of 5-hydroxytryptophan (HTP)/ epoxy and clay particle-reinforced epoxy," Cogent Eng., vol. 7, no. 1, 2020.

[17] S. Das, S. Halder, A. Sinha, M. Imam, and N. I. Khan, "Assessing Nano Scratch Behavior of Epoxy Nanocomposite Toughened with Silanized Fullerene Assessing Nanoscratch Behavior of Epoxy Nanocomposite Toughened with Silanized Fullerene," 2018.

[18] J. F. Archard and W. Hirst, "The Wear of Metals under Unlubricated Conditions," pp. 397–410, 1956.

[19] H. Wang, J. Feng, X. Hu, and K. M. Ng, "Tribological Behaviors of Aligned Carbon Nanotube / Fullerene-Epoxy Nanocomposites," 2008.

[20] E. K. Arthur et al., "Nano- and Macro-wear of Bio-carbo-nitrided AISI 8620 Steel Surfaces," Metall. Mater. Trans. A, 2015.

[21] E. K. Arthur et al., "Materials Science & Engineering A Indentation size effects in pack carbo-nitrided AISI 8620 steels," Mater. Sci. Eng. A, vol. 644, pp. 347–357, 2015.

[22] Z. Wang, P. Gu, X. Wu, H. Zhang, Z. Zhang, and M. Y. M. Chiang, "Micro / nano-wear studies on epoxy / silica nanocomposites," Compos. Sci. Technol., vol. 79, pp. 49–57, 2013.

[23] G. Constantinides, K. S. R. Chandran, F. Ulm, and K. J. Van Vliet, "Grid indentation analysis of composite microstructure and mechanics : Principles and validation," vol.

430, pp. 189–202, 2006.

[24] L. Shen, L. Wang, T. Liu, and C. He, “Nanoindentation and Morphological Studies of Epoxy Nanocomposites,” pp. 1358–1366, 2006.

[25] W. C. Oliver and G. M. Pharr, “An improved technique for determining hardness and elastic modulus using load and displacement sensing indentation experiments,” J. Mater. Res., vol. 7, no. 6, pp. 1564–1583, 1992.

[26] F. J. Ulm, M. Vandamme, C. Bobko, J. Alberto Ortega, K. Tai, and C. Ortiz, “Statistical indentation techniques for hydrated nanocomposites: Concrete, bone, and shale,” J. Am. Ceram. Soc., vol. 90, no. 9, pp. 2677–2692, 2007.

Chapter 7

7.1 Implications

The implications of the current work are quite significant. This is because it gives a balance between the corrosion and fracture mechanics framework approach in the study of epoxy composite coating.

1. Firstly, the results showed that fillers such as 5-HTP and cloisite clay particles can be used to enhance the corrosion resistance of epoxy-based coatings in acidic or neutral environments. However, the enhancements depend on the pH, as shown in the current work. Similar improvements have been reported by other researchers [10] that have used fillers to enhance the corrosion resistance of epoxy-based coatings. The improvements are attributed to the interactions between the filler materials and aqueous species. In the case of the cloisite clay particles and the 5-HTP particles, the fillers behave in ways that can delay the transport of aqueous species to the steel substrate. *In-situ* reactions and chemisorption processes can also occur in ways that reduce the transport of aqueous species to the substrate.

2. Epoxy/clay composites can be designed to have attractive combinations of strength, Young's moduli and interfacial fracture toughness between steels and epoxy/clay composite coatings. This can be achieved by the reinforcement of the epoxy matrices with clay particles with weight percentages up to about 3 percent. However, above this, the elastic moduli and hardness may decrease, perhaps due to the clustering of the particles, which may result in stress concentration effects, and the reduction of composite mechanical properties.In any case, the measured Young's moduli and strength estimates obtained from hardness values are comparable to estimates obtained from rule-of-mixture and shear lag models. The models are also generally found to capture the trends in the measured Young's moduli and hardness/strength data for the different composites that were examined in this study. Furthermore, the current work suggests

that controlled reinforcement with the clay particles may be used to control the hardness plastic indentation resistance (**Table** 5 of chapter 4). In general, the plastic indentation resistance decreases with increasing clay particle loading. Finally, it is of interest to note that the interfacial fracture toughness values (between the X65 steel and the epoxy or epoxy/clay composite coatings) increased with increasing mode mixity for 3 wt. %. Interfacial fracture was also associated largely with the kinking of cracks in and out of interfaces, with some bridging elements and crack deflection. This resulted in zone shielding that was predicted at low mixities by the simplified zone, zone and row models.

3. Finally, epoxy/clay composites can be designed to have attractive combinations of abrasive and adhesive resistance between steels and epoxy/clay composite coatings. This can be achieved by the reinforcement of the epoxy matrices with clay particles with weight percentages up to about 3 percent. However, the elastic moduli and hardness may decrease, perhaps due to the clustering of the particles, which may result in stress concentration effects, and the reduction of composite mechanical properties. However, the nano-wear characteristic and statistical deconvolution of the composite coating gives a unique way of evaluating composite coating. This study also suggested that statistical deconvolution can be used to obtain the mechanical properties of the epoxy matrix and clay particles found in the epoxy composite. Furthermore, the current work suggests that controlled reinforcement with the clay particles may be used to control the hardness plastic indentation resistance and the wear rates.

7.2 Conclusions

This Thesis has presented a combined experimental and analytical approach to study the degradation of epoxy composite coatings on low carbon steel. The key issues discussed in this Thesis include: the corrosion behavior, debondment studies, electro-chemical Impedance studies, of epoxy composites coatings; adhesion of the different composites studies; nanoindentation

analysis of the different composites coatings; tribological studies of epoxy composite coatings. The results and salient conclusions of each of the key issues are summarized below:

1. The results of an experimental study of corrosion inhibition of mild steel that was coated with epoxy and epoxy composites that contained 5-HTP and cloisite 30B clay particles revealed that corrosion was largely pH- dependent as shown by the electrochemical impedance spectroscopy and the scribe test. Furthermore, less corrosion products were seen on the scribe areas of the HTP samples in the scribe test in the pH of 3 corroding environments. This signifies a better adhesion of coating in that environment for HTP/epoxy coatings. This was also confirmed by **Figure 6 of chapter 3**where just 1 mm size of blister was observed for epoxy sample exposed at pH of 3 while all the other sample blistered at different sizes ranging from 1mm, 2mm and 4mm in the corroding environment of pH=7 after 90 days of EIS experiments. The TGA results reveal that the HTP/epoxy samples had a better heat resistance than the clay/epoxy and pristine epoxy. The enhanced thermal stability of HTP/epoxy nanocomposites, in combination with the high corrosion protection, makes them attractive candidates for various coating applications. Hence, HTP could be a potential filler for epoxy coatings for use in coating steel pipes and tanks. The FTIR spectra reveal the presence of O-H bonds in HTP/epoxy which acts as the bonding site of the coating just like in clay/epoxy.

2. The incorporation of 1, 3 and 5 wt. % of clay particle fillers (into epoxy) increases the hardness by 46 %, 80 % and 88 % and increases Young's moduli by 23 %, 58.5 % and 50 %, respectively. The improvements are associated with the deformation restraint provided by the clay particles. There was variation in the prediction results of the different composites as seen in table 5. This may be due to a huge influence of clay particles in the epoxy matrix which became more evident with increase in reinforcement. Previous studies have shown that reinforcements

give a better opportunity for stress to be distributed well in the epoxy matrix and the reinforced particles [39]. This might also be associated with a reduction in dislocation movement as a result of increased grain boundary density from the reinforcement [37]. It can therefore be suggested that the composite strength can be engineered by controlling the fiber and interfacial strengths, and the aspect ratios of the particles.The interfacial toughness between X65 steel and the epoxy/clay coatings (of the composite reinforced with 3 wt. % of clay) increases with increasing mode mixity. This increase is associated with crack-tip shielding by crack deflection and crack bridging. The trends in the measured mode-mixity dependence of the interfacial fracture toughness values are consistent with predictions from the simplified zone, normal zone and row models at lower mode mixity.

3. The mechanical and tribological properties of pristine epoxy and its composites were investigated using a combination of experiments and models. At the nanoscale, load, time, and volume fraction has a significant contribution to wear because surfaces may not have enough contact with each other. This is not the case at the macroscale because there is maximum contact between surfaces hence load or time is not a contributing factor. The plastic indentation resistance of the composites decreases with increasing particle loading, while the wear rates also drops with increasing particle loading between 1 and 3 wt.%. This suggests that there is a need for a balanced approach to the engineering of wear and indentation resistance. The scratch depth of pristine epoxy was the highest ~ 150 nm followed by a depth of 100 nm for the 1% clay reinforced epoxy and 90 nm depth for 3% reinforced epoxy and lastly 85 nm depth for 5% clay reinforced epoxy. The scratching experiments revealed a slight decrease in the surface damage of the coating with increasing clay loading. However, in all of the composites, the friction coefficients varied from 0.63 to 0.015. The friction, indentation and wear properties of clay-

reinforced epoxy composites decreased with increasing particle loading (weight percentage), for particle reinforcement between 1 and 3 wt. %. This is attributed to the higher intrinsic and wear characteristics of about 3 wt. %.

7.3 Suggestions for future work

- In-situ reactions and chemisorption processes can also occur in ways that reduce the transport of aqueous species to the substrate. Further work is clearly needed to provide mechanistic insights into such phenomena.
- Further work is needed to develop more robust models for the prediction of the mode mixity dependence of the interfacial fracture toughness at higher mode mixities.
- One of the limitations of this work was that the TGA test was performed only in a nitrogen environment. Further work needs to be done to perform TGA in air for better comparisons.
- It is recommended that further work should be done on the char yield to determine the flame resistance of the HTP composite.